

**Politecnico di Torino**

---

DIPARTIMENTO DI INGEGNERIA MECCANICA E AEROSPAZIALE

Corso di Laurea Magistrale in Ingegneria Meccanica

## **Tesi di Laurea Magistrale**

Optimal design of thermal energy storage systems for  
renewable driven heat and power energy systems



**Relatore**

prof. Vittorio Verda

**Correlatore**

prof. Adriano Sciacovelli

**Candidato**

Bernardina Cicinelli

---

**Anno Accademico 2018/2019**



# POLITECNICO DI TORINO

Joint work with:



# UNIVERSITY OF BIRMINGHAM

# Abstract

---

Environmental pollution is becoming an urgent issue to fix. All contaminant emissions in the air, like sulphur and nitrate oxide as well as fine particulate matter, are the main causes of several serious illnesses, cancer, and premature deaths. Besides, the continuous releasing of carbon dioxide is making dangerous greenhouse effect, arousing terrible effects for surrounding and all planet inhabitants. To properly face this emergency, it is necessary to innovate some human activities, like power production, which is a very polluting sector. Solar energy is among the most interesting renewable sources employed by the human to generate electricity and with this aim many technologies have been undeveloped, especially Concentrated Solar Power (CSP) system.

Solar Thermal Brayton Cycle (STBC) is the technology chosen for this analysis. The plant uses a parabolic dish to collect and concentrate the solar beam onto a small area, where is placed a receiver. This thermal energy promotes the heating of the working fluid, which moves the turbine of power block, producing electricity. Furthermore, the system operates at low pressure, thanks to the regenerative cycle involved; a recuperator is placed after the compressor in order to pre-heat the incoming air using the exhaust gas from the turbine.

STBC technology is very promising among the CSP, thanks to the major peak efficiency, due to the higher operating temperature reachable and concentration ratio designed. Particularly, the small-scale plant (1-20kW) has been analysing, thought to provide electricity for the small villages and isolated communities, which aren't often linked to the main grid as the transmission line can't cross vast stretches of land. For all this reason, it has been analysed in this work.

In the first part, a model of the STBC plant has been built, considering the main governing equations valid for all components: recuperator, receiver, dish and turbocharger group. After the validation, it has been involved for quasi-steady state analysis, simulating the plant function over the time, following an actual irradiance profile. To do that, some control strategies have been proposed, in order to keep the operating temperature near the design value and to avoid the turbine overheating when the overload phase occurs. Among them, the TES introduction has shown great results as control strategy: it allows to keep constant the power generation as well as the turbine inlet temperature and leads to the best exploiting of surplus solar energy without any waste. This means increasing the STBC plant efficiency during the peak hours.

In the second part, the integration of the TES in the STBC system has been studied more deeply, underling the advantages in term of working hours, plant efficiency and economical convenience. Since the literature was quite lacking about this investigation, a preliminary study has been conducted, to find the best TES typology among all available possibilities. In this view, a passive TES with sensible material since it is the cheapest technology. On the other hand, it should be placed on the ground, distant from the other plant component which are supported by the tracking system. This displacement leads a greater heat loss but is necessary owing to the enormous weight predicted. Anyway, a plant layout has been conceptually designed in order to allow the air flow in two different direction, during the charging or discharging phase. Particularly a packed-bed configuration has been selected and its more detailed model has been built. At the end the functioning of a STBC plant with the TES integration has been simulated, showing and discussing the results.

# Table of Contents

---

<b>ABSTRACT .....</b>	<b>0</b>
<b><u>1. INTRODUCTION.....</u></b>	<b><u>3</u></b>
1.1 POLLUTION EMISSIONS AND THE GREENHOUSE EFFECT .....	4
1.2 RENEWABLE RESOURCES FOR POWER PRODUCTION .....	6
1.2.1 SOLAR POWER GENERATION: PV VS CSP .....	9
1.3 CONCENTRATED SOLAR POWER (CSP) PLANT .....	11
1.4 THERMAL ENERGY STORAGE (TES) .....	14
<b><u>2. THE SOLAR THERMAL BRAYTON CYCLE (STBC): SYSTEM, MODEL AND VALIDATION .....</u></b>	<b><u>17</u></b>
2.1 OVERVIEW: THE REGENERATIVE BRAYTON CYCLE .....	17
2.2 SYSTEM DESCRIPTION .....	19
2.2.1 ADVANTAGES OF THE STBC PLANT .....	20
2.3 MODELING METHODOLOGY.....	20
2.3.1 RECEIVER .....	21
2.3.2 PARABOLIC DISH.....	23
2.3.3 RECUPERATOR .....	24
2.3.4 TURBOCHARGER GROUP .....	26
2.4 MODEL VALIDATION .....	27
2.4.1 PLANT-LEVEL VALIDATION .....	27
2.4.2 RECEIVER SUB-MODEL .....	28
<b><u>3. ANALYSIS OF STBC PLANT.....</u></b>	<b><u>30</u></b>
3.1 FEATURE OF THE STBC PLANT .....	30
3.2 STEADY-STATE APPROACH: DESIGN CONDITIONS.....	31
3.3 QUASI-STEADY-STATE ANALYSIS APPROACH: OFF-DESIGN CONDITIONS.....	33
3.3.1 SHAVING DEVICE METHOD.....	35
3.3.2 AIR-FLOW RATE ADJUSTMENT .....	37
3.3.3 TES INTEGRATION.....	40
<b><u>4. PRELIMINARY STUDY FOR THE TES INTEGRATION.....</u></b>	<b><u>44</u></b>
4.1 TYPOLOGY OF TES .....	45
4.1.1 ACTIVE TES: INDIRECT SYSTEM.....	45
4.1.2 PASSIVE TES.....	47
4.1.3 TES PRELIMINARY SIZING .....	49
4.2 PLANT LAYOUT.....	52

<b>5.</b>	<b><u>SENSIBLE PACKED-BED TES ANALYSIS.....</u></b>	<b><u>54</u></b>
5.1	LITERATURE REVIEW .....	54
5.2	MAIN FEATURES .....	54
5.3	AIT-BAHA PILOT PLANT: .....	55
5.4	MODELLING METHODOLOGY .....	56
5.5	COMPUTATIONAL SETTINGS .....	58
5.6	RESULTS ABOUT VALIDATION OF TES MODEL .....	60
<b>6.</b>	<b><u>INTRODUCTION OF ROCKS PACKED-BED TES IN THE STBC PLANT .....</u></b>	<b><u>62</u></b>
6.1	STARTING HYPOTHESIS AND INPUTS FOR THE MODEL .....	62
6.2	RESULTS .....	65
6.2.1	1 <sup>ST</sup> SCENARIO: HEAT LOSSES NEGLECTED .....	66
6.2.2	2 <sup>ST</sup> SCENARIO: HEAT LOSSES CONSIDERED .....	72
<b>7.</b>	<b><u>CONCLUSIONS.....</u></b>	<b><u>77</u></b>
<b>8.</b>	<b><u>REFERENCES.....</u></b>	<b><u>78</u></b>
<b>9.</b>	<b><u>WEBOGRAPHY .....</u></b>	<b><u>80</u></b>

# 1. Introduction

---

Environmental pollution is becoming an urgent issue to fix. All contaminant emissions in the air, like sulphur and nitrate oxide as well as fine particulate matter, are the main causes of several serious illnesses, cancer, and premature deaths. Besides, the continuous releasing of carbon dioxide is making dangerous greenhouse effect, arousing terrible effects for surrounding and all planet inhabitants. To properly face this emergency, it is necessary to innovate some human activities making them “cleaner” and sustainable. A great impact is certainly due to power production, which is a very pollution sector, with industry and transports too. Therefore, solar energy is one of the most interesting renewable sources employed by the human to generate electricity and with his aim the technologies enveloped have been photovoltaic (PV) cell and Concentrated Solar Power System (CSP). In spite of the former have been the most common so far, currently CSP technologies are regaining a certain interest in the research community, thanks to the major advantage over PV: dispatchability which allow a shift of power production according to demand, becoming less dependent on the time and daily weather conditions.

Dispatchability of the CSP due to the TES integration has been the fundamental concept investigated in this research, since it is becoming a promising idea in the “green” power production, exploiting solar energy in the best way ever.

Solar Thermal Brayton Cycle (STBC) is a Parabolic Dish CSP technology chosen for the research. promising among the CSP, thanks to the major peak efficiency, due to the higher operating temperature reachable and concentration ratio designed. Particularly, the small-scale plant (1-20kW) has been analysing, thought to provide electricity for the small villages and isolated communities, which aren’t often linked to the main grid as the transmission line can’t cross vast stretches of land. Parabolic Dish is still at the preliminary experimentation stage. According to [V] there are just two demonstration projects in the world: the Maricopa Solar Project and the Tooley Army Depot. Placed both in the USA, they are large scale plants with a power production of 1.5 MW and they work with a Stirling engine as power block generation. Currently, they are not operational anymore. Still being at preliminary demonstration stage, STBC technology has been investigated by many authors in the literature, so far. As Dr. W. G. LeRoux from University of Pretoria (South Africa), who has been working for many years on this subject, they are mainly focused on the geometrical design and the optimization of each component or of multiple component system, which works in design operating conditions. On the contrary, the evolution on time about the functioning of the plant has not been studied, yet.

So, in the first part of this research, a model of the STBC plant has been built, considering the main governing equations valid for all components: recuperator, receiver, dish and turbocharger group. After the validation, it has been involved for quasi-steady state analysis, simulating the plant function over the time, following an actual irradiance profile. To do that, some control strategies have been proposed, in order to keep the operating temperature near the design value and to avoid the turbine overheating when the overload phase occurs. Among them, the TES introduction has shown great results as control strategy: it allows to keep constant the power generation as well as the turbine inlet temperature and leads to the best exploiting of surplus solar energy without any waste. This means increasing the STBC plant efficiency during the peak hours.

In the second part, the integration of the TES in the STBC system has been studied more deeply, underling the advantages in term of working hours, plant efficiency and economical convenience. Since the literature was quite lacking about this investigation, a preliminary study has been conducted, to find the best TES typology among all available possibilities. In this view, a passive TES with sensible material since it is the cheapest technology. On the other hand, it should be placed on the ground, distant from the other plant component which are supported by the tracking system. This displacement leads a greater heat loss but is necessary owing to the enormous weight predicted. Anyway, a plant layout has been conceptually designed in order to allow the air flow in two different direction, during the charging or discharging phase. Particularly a packed-bed configuration has been selected and its more detailed model has been built. At the end the functioning of a STBC plant with the TES integration has been simulated, showing and discussing the results.

## 1.1 Pollution emissions and the greenhouse effect

One of the most alarming issues that the world is facing today is environmental pollution, which is causing serious and permanent damages to nature and human society.

The air pollution is particularly dangerous since it is a very important risk factor for health worldwide people like smoking, high blood pressure and eating risks: in according to recent studies, it causes at least 6.5 million premature deaths. Among the contaminant agent, the fine particulate matter is the worst, damaging the man's respiratory system which is not able to filter so small particles (diameter less than  $2.5\ \mu\text{m}$ ). The other toxic substances are nitrogen oxides ( $\text{NO}_x$ ) and sulphur oxides ( $\text{SO}_2$ ) which are responsible for a wide range of grave illness. Basically, the development of these pollutions is due to the high temperatures reached during the combustion process. It promotes the oxidation of the pure nitrogen in the combustion air and of sulphur present in the fossil fuel, even if in a very small amount.

Fig. 1.1, Fig. 1.2, Fig. 1.3 give an idea of the amount of pollution emission for each world region, specifying the main sectors involved. On the whole power generation, industrial process and transports have the greatest responsibility for air contamination.

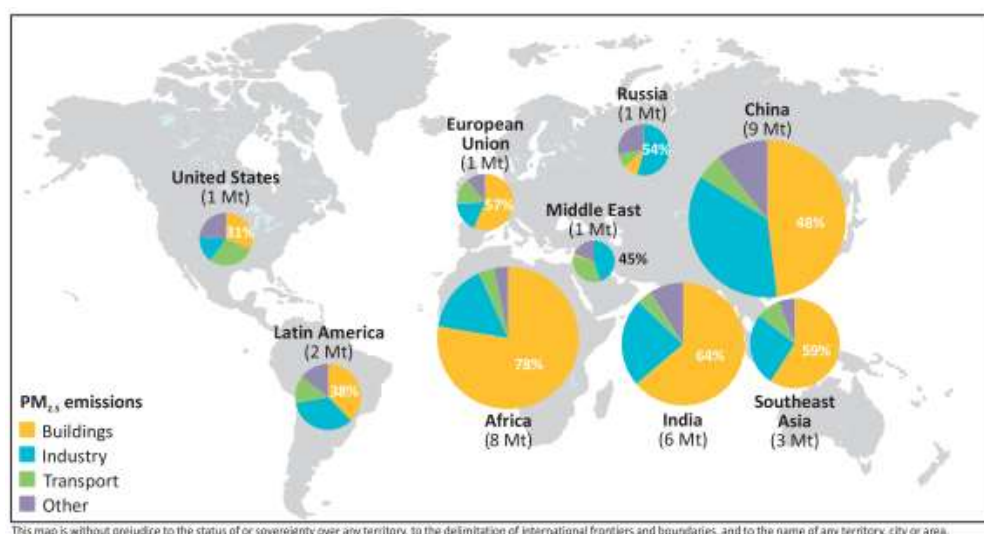


Figure 1.1: Amount of PM2.5 emission by region and sector from [1]

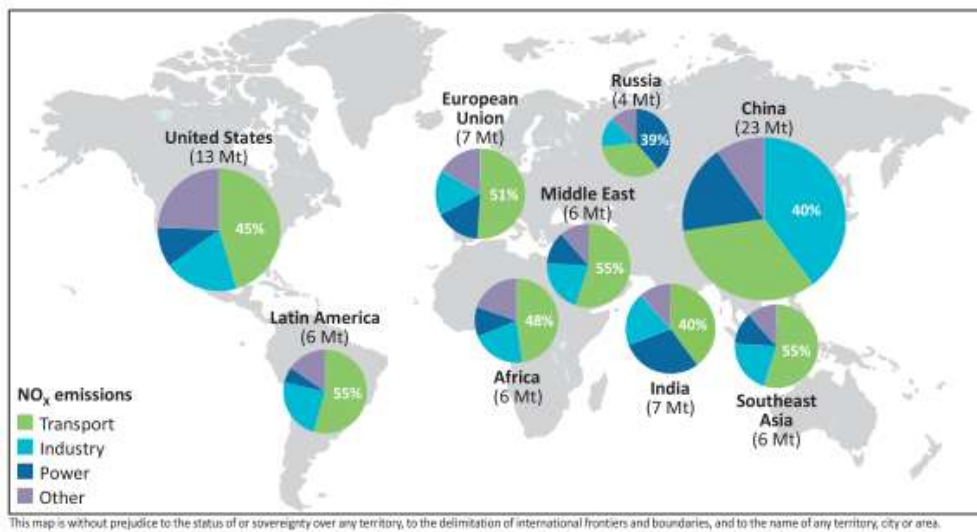


Figure 1.2: Amount of NO<sub>x</sub> emission by region and sector from [1]

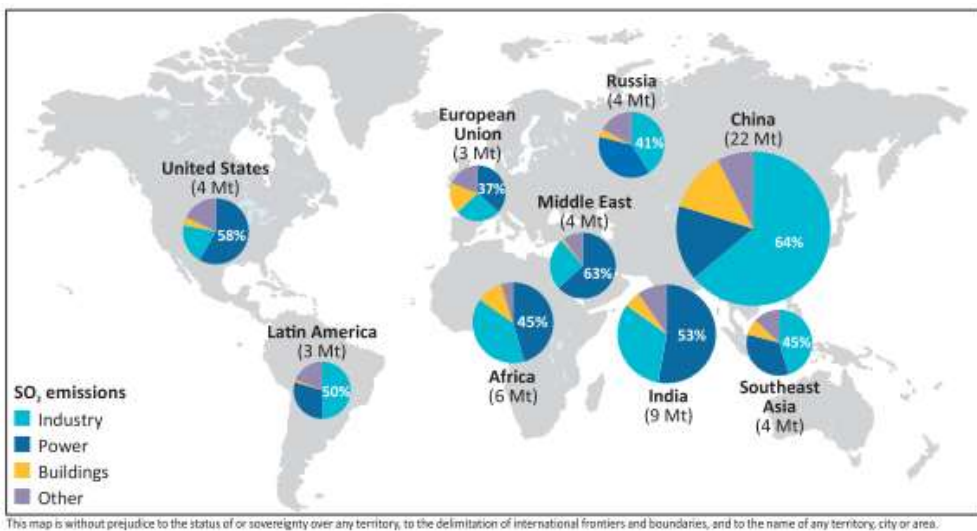


Figure 1.3: Amount of NO<sub>x</sub> emission by region and sector from [1]

Another crucial issue which is worrying a lot the worldwide society is carbon dioxide (CO<sub>2</sub>) emission. It can't be considered proper pollution since it is a product of the ideal combustion. On the other hand, its extreme presence in the atmosphere causes the greenhouse effect, the main responsible for worldwide warming. The carbon dioxide works as a blanket during a cold winter night which keeps the body warm not because it releases any energy, but because it is able to trap the body heat, avoiding the escaping to the colder surroundings. In the same way, CO<sub>2</sub> blanket traps the longwave radiation given off by the Earth, following the quantum mechanics laws. When the frequency of the radiation from the planet and the atmosphere is the same as the carbon dioxide vibration frequency, the radiation is absorbed by CO<sub>2</sub>. This energy is converted to heat by collision with other air molecules and then released again towards the Earth surface, promoting the rising of the temperature and so the climate changing [2]. The global temperature increase generates terrible consequences, endangering the survival of the Earth's flora and fauna, including human beings. The



biggest impacts include the melting of the ice mass at the poles, which causes rising sea level, producing flooding and jeopardizing coastal environments through which small island states risk disappearing entirely. Climate change also increases the development of more violent weather phenomena, drought, fires, the destruction of the food chain and the extinction of some animal and plant species.

Figure 1.4 shows the main economic sector linked to global greenhouse gas emissions.

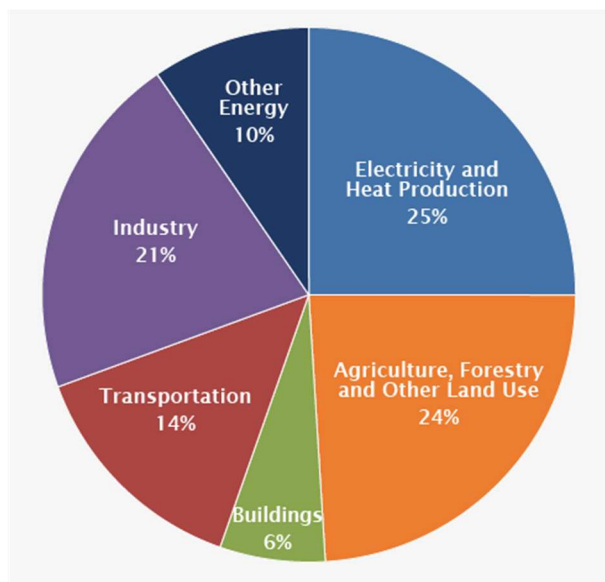


Figure 1.4: Global Greenhouse Gas Emissions by Economic Sector from [1]

As the contaminant agent view before, the CO<sub>2</sub> production is mainly due to the electricity and heat production (25%), with the industry process (21%) and the transports (14%). Differently, more relevant is the effect of the primary sector, linked to agriculture and all other land use.

All this data is very terrifying and allow us to understand that the humanity is facing the biggest environmental challenge our species has ever seen: it is necessary acting soon as possible to can save the world in time, avoiding the whole life's destruction. For this reason, the modern scientific community is working very hard to develop some innovative technologies to make our world more sustainable.

## 1.2 Renewable resources for power production

---

As is shown before, the power and heat production are an economic sector characterized by a greater impact on the environmental emergency, considering both contaminant agents and greenhouse gas emissions. Besides, the traditional ways to generate electricity involve the combustion of fossil fuels like coal, oil, gas which are a "finite sources": they will be completely used in the next future (Figure 1.5), in according to ever-increasing energy demand and to constant population growth (Figure 1.6).

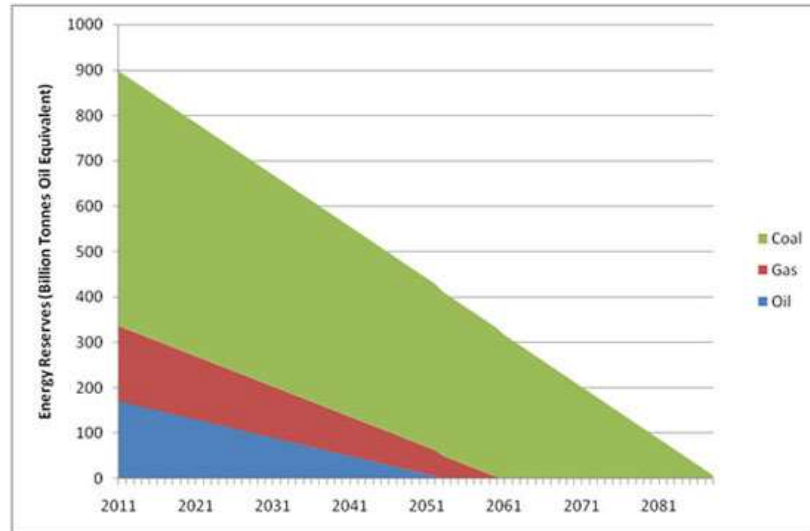


Figure 1.5: Prediction about the fossil fuel reserve in the future, from [11]

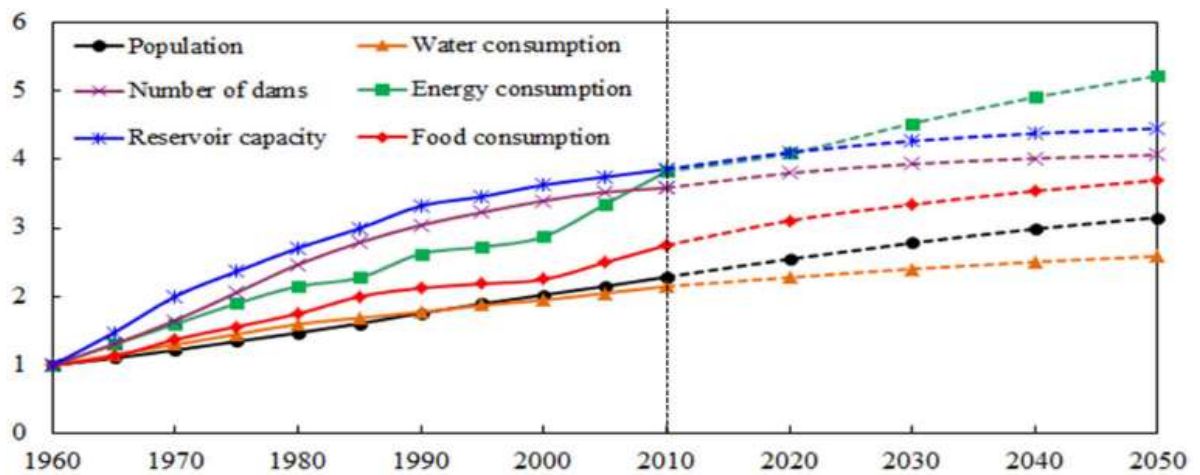


Figure 1.6: Projection of population increase, with energy consumption from [3]

Variable	2010	2020	2030	2040	2050	2050/2010
Population (billion)	6.92	7.71	8.42	9.04	9.5	1.37
Energy consumption (1000 TWh)	134	143	159	172	183	1.37
Food consumption (billion ton)	2.2	2.49	2.67	2.83	2.96	1.34
Water consumption (km <sup>3</sup> )	4,300	4,557	4,809	5,014	5,175	1.20
Number of dams	32,473	34,423	35,623	36,363	36,813	1.13
Reservoir capacity (km <sup>3</sup> )	7,975	8,483	8,823	9,051	9,204	1.15

Table 1.1: Data related to Figure 1.6, from [3]

Given all of that, in the last decades, the society has studied a lot of ways to make “green” the power production, exploiting the renewable sources offered by the planet. There are:

- **Solar energy:** for the planet, the Sun is the most plentiful energy source. There are a lot of ways to collect and convert this power. The range is from solar water heating using solar

collectors for domestic use to the complex plant technologies of direct conversion of sunlight to electrical energy with mirrors or photovoltaic cells.

- **Hydroelectric energy:** it is the most common since it supplies 4% of the worldwide energy request. Basically, the natural motion of rivers and stream are exploited to continuously move a turbine for electricity production. Otherwise, it is possible to gather water in a wide pond through dams to draw whenever it is required.
- **Wind energy:** thinking about the mills, this resource can be considered the first one to be used by man. Today the plants use some wind turbine is moved by the movement of the atmosphere, driven by differences of temperature at the Earth's surface. To have a significant amount of energy, a very extensive area is required, better if it is near seas and oceans.
- **Geothermal energy:** it is able to use the heat of Earth to raise the temperature of the water in the underground which comes out as steam. Then it is exploited in some thermal plants to produce electricity. However, this possibility is limited to a few locations on Earth and many technical problems exist that limit its utility.
- **Biomass:** it is the term for energy from the combustion process of plants and all organic matter. Unfortunately, the most popular is the burning of trees for cooking and warmth. This process releases great amounts of carbon dioxide gases into the atmosphere, contributing to making unhealthy the air in many areas.

Figure 1.7 shows the power generation by renewable energy for some countries, specifying the typology of the used resource.

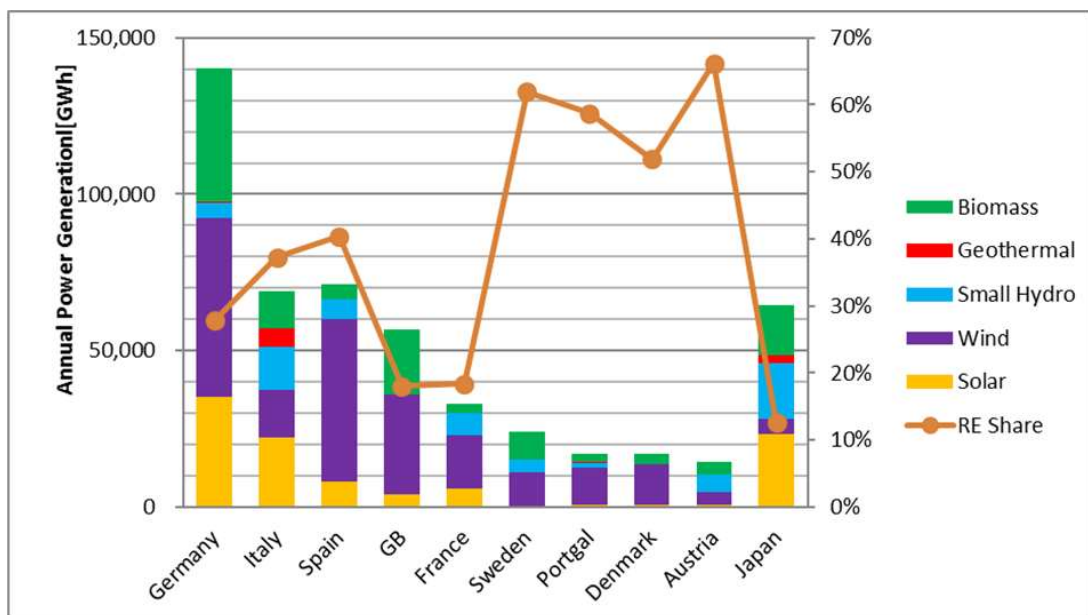


Figure 1.7: Power generation by renewable energy for some countries, [III]

Like it is evident, Germany is absolute leader of “clean energy” generation with an annual amount of 140 GWh, followed by Japan, Spain, and Italy which can annually produce power less than 70 GWh. Overall, the wind, sun, and biomass are the most used resource.

### 1.2.1 Solar power generation: PV vs CSP

In the last years, solar energy has captured a great interest as an important source of renewable energy, owing to its abundance. The Sun can release an enormous amount of radiation energy to its surroundings: 174 PW (1 PW =  $10^{15}$  W) at the upper atmosphere of the Earth. [4] Before the energy reaches the Earth's, it has been attenuated twice by both the atmosphere (16% by absorption and 6% by reflection) and the clouds (20% by reflection and 3% by absorption), as shown in Figure 1.8. In the end, just 51% (89 PW) of the total incoming solar radiation is available, arriving on the land and the oceans.

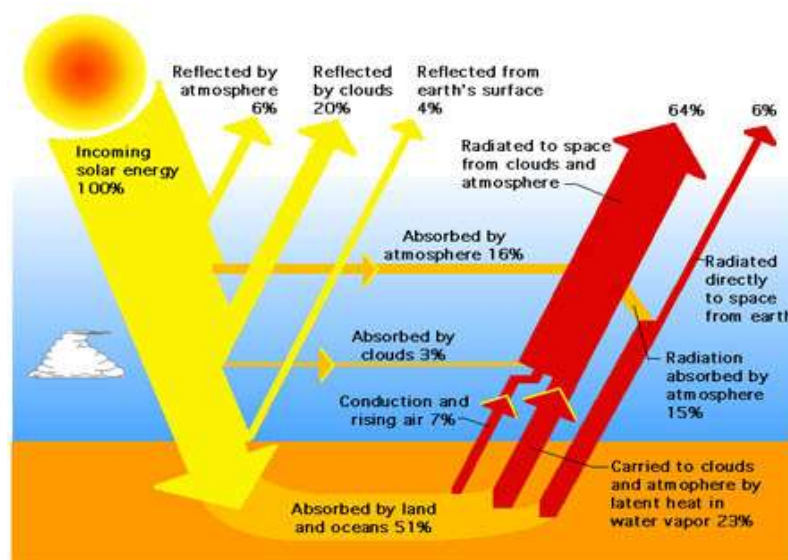


Figure 1.8: Earth's energy budget

Despite the attenuation, the total amount of solar energy accessible on the Earth is still of an enormous amount but because it is of low-density and intermittency, it needs to be collected and used through a proper strategy.

Today, most of the solar power systems in the market can be categorized into two major groups: the direct solar power and the indirect one. The former refers to a system that converts solar radiation directly to electricity using a photovoltaic (PV) cell. The latter refers to a system that converts the solar energy first to heat and after that to electrical energy, as in the case of concentrated solar power (CSP). In a CSP plant, radiation is focused on a heat exchanger and the heat is used to increase the temperature of a heat-transfer fluid (HTF) which drives the turbine.

Thinking about the historical development of these two technologies, CSP seemed set to beat solar PV. When both arrived in the market (the 1980s) the PV relied on expensive solar modules more often used in small consumer electronics than in power plants, while the CSP concept was appeared based on tried and true technologies from the old coal plants.

Several years later, the situation is totally changed, like is depicted in Figure 1.9. In 2010 PV had a global installed capacity of about 35 GW, while the CSP's one is only 1.5 GW.

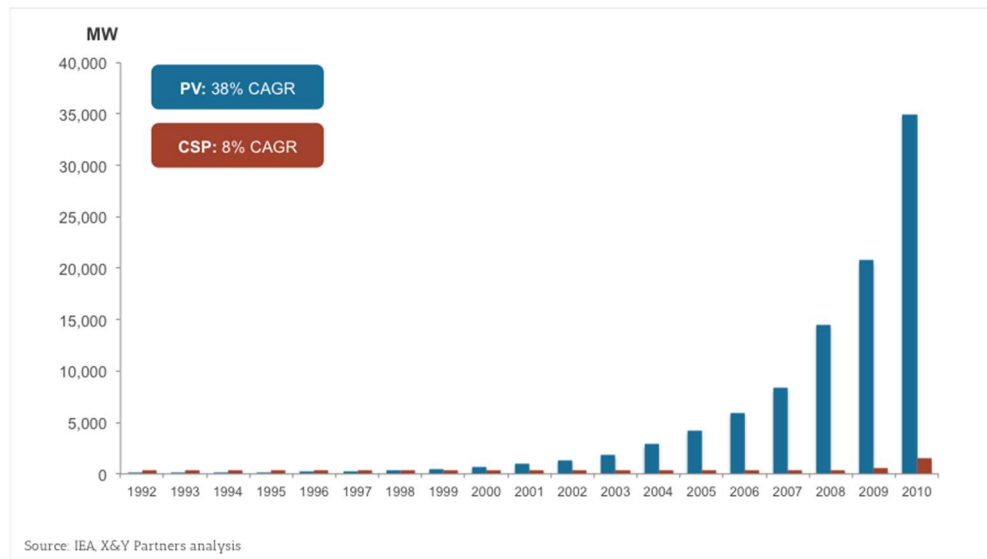


Figure 1.9: Evolution of PV and CSP global installed capacity (MW), [IV]

This clear overturning of the trend can basically find its reasons in two main aspects:

- **Market size:** PV can be installed almost everywhere unlike the CSP plant. This is because the CSP technologies need higher levels of irradiance, access to water (just like a coal plant) and large-scale deployments (typically more than 20 MW, compared with the few kW of a residential PV system).
- **Technological simplicity:** the PV revolves around the solar cell, while the latter is a combination of equally critical components (turbine, heat exchanger, working fluid, collector, receiver). For this reason, the PV makers have focused on the decreasing of cost per Watt, while the CSP industry has faced a various challenge e.g. improving the optical efficiency of collectors, researching new heat transfer fluids or procuring higher efficiency turbines.

Anyway, CSP technologies are regaining a certain interest in the research community, thanks to the major advantage over PV: dispatchability. Current CSP plants can store thermal energy for up to 16 hours, which means that their power production can be shifted according to demand, becoming less dependent on the time and daily weather conditions. PV is not dispatchable since a feasible commercial energy storage system does not yet exist.


In the last years, a hybrid photovoltaic/thermal (PVT) solution is being developed. It can simultaneously convert solar energy into electricity and heat. A typical PVT collector consists of a PV module and an absorber plate (acting as a heat removal device) attached on the back. The heat removal plate cools the PV module down to a suitable temperature for better electrical performance, collecting the waste heat, which can then be utilized for low-temperature applications, such as domestic hot water production.

### 1.3 Concentrated Solar Power (CSP) plant

Concentrated solar power systems use lenses or mirrors to concentrate a large area of sunlight, onto a small area where a heat exchanger (receiver) is placed. Here the solar thermal energy is used to heat up the heat transfer fluid (HTF). Then the HTF is used to operate a conventional power cycle, such as Rankine (steam engine), Brayton (gas turbine engine) or Stirling engine.

Solar thermal radiation can be collected by different kind of CSP technologies to provide a high-temperature heat source. Basically, these technologies differ depending on the distribution of an optical concentrator:

- **Parabolic Trough systems:** they represent 90% of the CSP in commercial operation in the world. Trough-shaped reflectors, parabolically curved concentrate the sun rays onto a receiver pipe running along about a meter above the curved surface of the mirrors, along the focal direction. A collector field is composed by multiple parabolic trough-shaped mirrors in parallel rows aligned to allow single-axis trough-shaped mirrors to track the sun from east to west during the day to ensure that the sun is continuously focused on the receiver pipes.
- **Power Tower systems:** utilizing sun-tracking mirrors called heliostats, sunlight is focused onto a receiver at the top of a tower. The HTF heated in the receiver up to generates steam, which, in turn, is used in a conventional turbine-generator to produce electricity.
- **Linear Fresnel Systems:** like the long arrays of a parabolic trough CSP system, this technology exploits many collectors flat on the ground in parallel rows which reflect the sunlight to the pipe above. These are typically aligned in a north-south orientation to maximize annual and summer energy collection.
- **Parabolic Dish systems:** they consist of a parabolic-shaped point focus concentrator in the form of a dish that reflects solar radiation onto a receiver mounted at the focal point. The collectors are mounted on a structure with a two-axis tracking system to follow the sun. The collected heat is typically utilized directly by a heat engine mounted on the receiver moving with the dish structure. The most power engines used are Stirling and Brayton cycle.



	Parabolic Trough	Central Receiver	Compact Linear Fresnel	Parabolic Dish
Operating Temperature [°C]	350-550	250-565	390	550-750
Plant Peak Efficiency [%]	14-20	23-35 <small>Note – 35% achieved with combined cycle</small>	18	30
Annual Capacity Factor [%]	25-28 (no TES) 29-43 (with TES)	55 (with 10h TES)	22-24	25-28
Collection Concentration [suns]	70-80	>1,000	>60 suns (with secondary reflector)	>1,300
Steam Conditions [°C/bar]	380-540 / 100	540 / 100-160	260/50	N/A
Water Requirement [m³/MWh]	3 (wet cooling) 0.3 (dry cooling)	2-3 (wet cooling) 0.25 (dry cooling)	3 (wet cooling) 0.2 (dry cooling)	0.05-01 (mirror washing)

Table 1.2: Principal CSP technologies used within industrial practice [5]



Table 1.2 presents a sketch about the main CSP technologies with their main featuring about working conditions. From an efficiency point of view, the Parabolic Dish is the best solution, since it can reach 30% during the peak. It is followed by the Power tower system (an average of 27%) and the other “line focusing” solution. As it will be explained right now, this is strictly linked to the higher values for two main plant-cycle features: the operating temperature and the concentration ratio.

The theoretical conversion maximum efficiency that can be achieved by a CSP is determined by two factors. The efficiency of the heat engine, influenced by the difference between the lowest and highest temperatures reached in one cycle and the collector system efficiency, determined by the thermal losses of the solar receiver. As it is clear, the former increases with temperature (Carnot’s efficiency relation) while the latter shows the opposite behaviour considering that the heat losses are proportional to the fourth power of its surface temperature. Therefore, the efficiency gains of the power block from a higher temperature can be potentially negated by the increasing thermal losses from the receiver due to higher temperatures.

Figure 1.10. depicts the trend described just now: it shows the whole CSP efficiency with the two subsystems one, as a function of energy amount produced and the operating temperature.

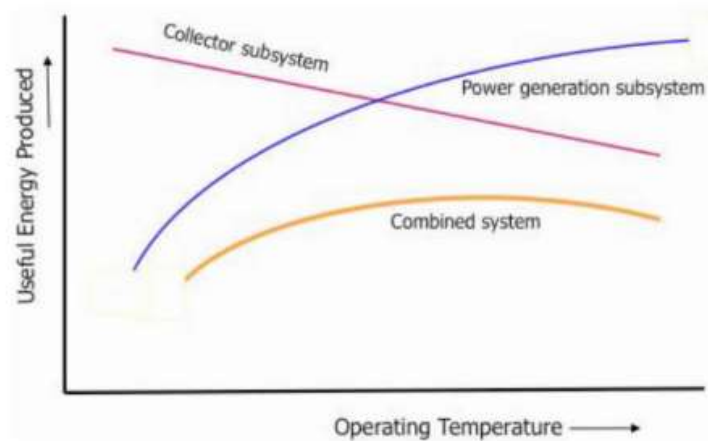


Figure 1.10: CSP system efficiency with operating temperature

However, there is a way to maximize the plant efficiency with the increasing of temperature: a high concentration ratio, which is the ratio between the collector surface and the smaller area where they are concentrated. So, it is possible to keep thermal losses constant for the same receiver surface area, despite yielded solar power increasing. This is what illustrated by Figure 1.11 which presents

CSP systems with varying concentration ratios and their respective maximum system efficiencies compared to the Carnot's one.

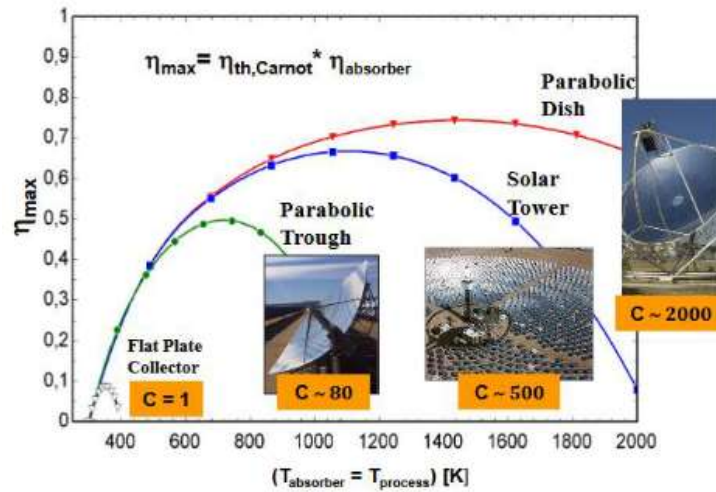


Figure 1.11: CSP technology theoretical efficiencies with respect to concentration ratio and absorber temperature

To have an idea about the distribution level of these technologies, can be useful to know that during the 2016 CSP market had a total capacity of 5840 MW<sub>e</sub> worldwide, among which 4800 MW<sub>e</sub> is operational and 1040 MW<sub>e</sub> is under construction. Spain had a total operational capacity of 2405 MW and 100 MW is under construction, making it the world's leading country in CSP. It is followed by the USA with an amount of 1795 MW and a growing interest can be found in India, South Africa, Chile, China, Australia, and some Middle East countries [6].

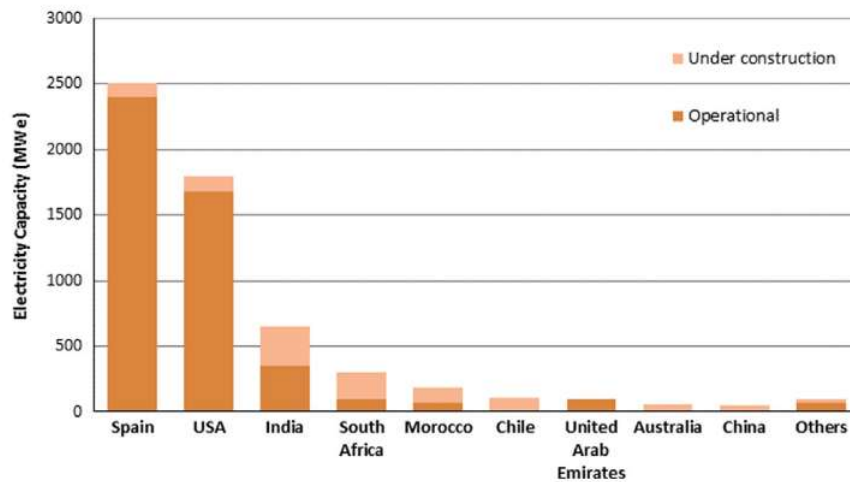


Figure 1.12: Worldwide CSP capacity [6]

Today, the most spread CSP technology is the Parabolic trough one which dominates the global market, being installed in more than 80% of the CSP plants in operation and under construction. Tower systems have just started to be introduced into commercial applications and linear Fresnel plants are currently making the transition to commercial applications. Currently, parabolic dish systems are at the early demonstration stage. However, in the last years, it has gained a great



interest by all the scientific community for power production, considering its advantage in terms of efficiency. So, in the next future, it could be a very promising CSP technology.

## 1.4 Thermal Energy Storage (TES)

---

Although solar energy is clean and plentiful, converting it into electric power entails two major challenges: the low-intensity radiation level, and the intermittency of solar radiation. The former is addressed through concentration of solar beam, employing focusing mirrors and collectors, like it is done for the CSP plant. The latter is managed by embedding an energy storage system for time when solar radiation is unavailable. Talking about techniques for energy storage, various solutions exist and each one is suitable for a specific application. In the field of electrical power generation from solar energy, the collection methods change between PV and CSP options. PV technology usually stores electrical energy as chemical energy in batteries, while CSP uses Thermal Energy Storage (TES) to store solar energy in thermal energy form. Many comparisons have been done between different energy storage technologies. TES has several advantages when compared to chemical storage strategy as well as mechanical one. At a large scale, TES is found to be more suitable than battery technology with its higher load capacity, lower capital costs, longer storage duration with very high operating efficiencies.

A thermal energy storage system mainly consists of three parts: the storage medium, heat transfer mechanism and containment system. The storage medium is the operating part of TES, which is able to collect energy in such a way, exploiting some its particular thermo-physical proprieties. The purpose of the energy transfer mechanism is to supply and then extract heat from the storage medium. The containment system holds the storage medium as well as the energy transfer equipment and insulates the system from the surroundings, trying to limit losses and irreversible phenomena.

Nowadays, the methods to thermally store energy are:

- Sensible heat storage: it stores heat energy in their specific heat capacity  $c_p$ . During the heat energy absorption process, there is no phase change happening and materials experience a raise in temperature. The amount of heat stored is proportional to the density, volume, specific heat and variation of temperature of the storage material, following the simple expression:

$$Q = m C_p \Delta T \quad [J] \quad 1.1$$

with  $C_p \left[ \frac{J}{kg K} \right]$  equals to the specific heat capacity. The most common sensible heat storage materials are liquid as molten salt, mineral oil and water, and solid like rocks, concrete and sand.

- Latent heat storage: also called as phase change materials (PCM), these substances absorb heat energy as their “latent heat of fusion” during the melting process. Hence the heat energy absorption process involves a phase change and a very small temperature swing. The thermal energy stored in phase change material can be expressed:

$$Q = m L \quad [J] \quad 1.2$$

where  $L \left[ \frac{J}{kg} \right]$  is the latent heat of fusion. Solid–liquid phase change process is usually used, even if liquid-gas transformation has the highest latent heat of phase change. The reason is the enormous variation in terms of volume materials associated with the evaporation/condensation phenomena, which make the storage complex and highly impractical. Concerning the material functioning like PCM, it is possible to find organic and inorganic medium (paraffins, alcohols or salts, metal alloys) as well as graphite composites;

- Chemical reaction heat storage: this energy collection uses a reversible chemical reaction. The heat energy stored is equal to the reaction enthalpy. Charging process consists of a forward endothermic reaction absorbing heat and the absorbed thermal energy is used to dissociate a chemical reactant (A) into products (B) and (C). During the discharging process reactants (B) and (C) undergo backward exothermic reaction producing (A) and releasing heat. The products of both reactions can be stored either at ambient temperature or at working temperature. The amount the thermal energy stored in thermochemical material is:

$$Q = n \Delta H \quad [J] \quad 1.3$$

$n [mol]$  is the mol number of the reactant A and  $\Delta H$  is the reaction enthalpy.

While thermochemical storage technology is still at laboratory stage, sensible and latent heat technologies are matured and are at industrial stage. Particularly, sensible storage is the dominant TES technology used in CSP plants; it is the most developed technology that has been studied, tested and installed most notably in Spain.

Kuravi et al. [7] present a very detailed review about the TES design and its integration in the CSP plants. In this work, the key requirement for a TES system developing are:

- High energy density of storage material;
- Efficient heat transfer between the storage material and the HTF provided by a proper design of the heat exchange equipment;
- Fast response to load changes in the discharge mode;
- Low chemical activity of storage material and HTF towards the materials of construction;
- Good chemical stability of storage material/HTF and of temperature reversibility;
- High thermal efficiency and low parasitic electric power for the system;
- Low potential contamination of the environment caused by an accidental spill of large amounts of chemicals used in the TES system;
- Low cost of storage material, considering the embodied energy (carbon);
- Ease of operation and low operational and maintenance cost.

These features are very important for the development of an efficient and cost-effective TES system, which is crucial for the future of CSP technologies. Figure 1.13 indicates the percentage of plants which have a TES system implementation. About half of the plants (47%) currently in operation work with a TES system and there is a notable increase in the use of TES for plants under construction (72%) and planned (77%).

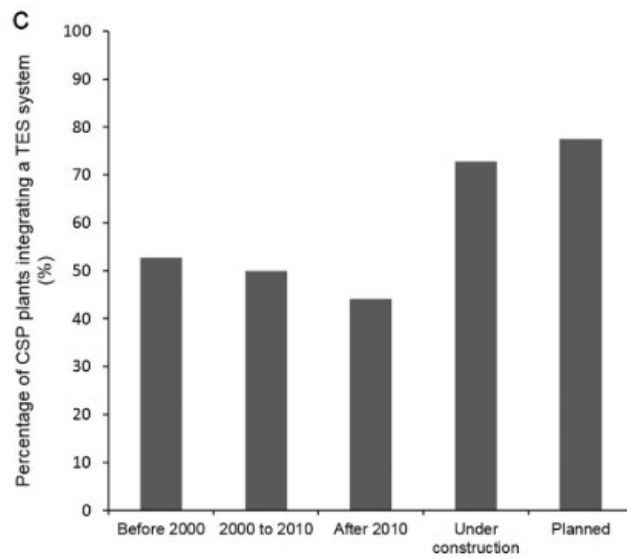


Figure 1.13: Presence of TES system in CSP plants, from [8]

This increase can be partially explained by the technological progress and advancements achieved in TES systems, thanks to the research work done by the scientific community about this subject. The literature offers a lot of paper where the integration of TES in a solar power plant is discussed. Chacartegui et al. [9] investigates a parabolic trough plant integrated with an Organic Rankine cycle power block and thermal storage, considering two different heat storage layouts: direct and indirect one. Turrini et al. [10] has been designed an innovative plant configuration joining a thermal energy storage device with parabolic solar dish collector. This is a small-scale solar plant prototype where the molten salts are used both as fluid carrier and thermal energy storage medium.

## 2. The Solar Thermal Brayton Cycle (STBC): system, model and validation

### 2.1 Overview: the regenerative Brayton cycle

Before to detailly analyse the STBC, a brief overview of the reference cycle from which it comes. The Brayton Cycle (BC) is the theoretical cycle used to represent the internal working cycle of a basic gas turbine engine. Its birth is due to the American engineer George Brayton, who first developed it in 1872 as the basis for his "Ready Motor": a piston engine consisting of a compressor and expander. From that moment this fundamental idea has been experienced several changes as well as innovative extension, arriving to have the modern turbine engines, which makes the aircraft flight possible. Basically, the Brayton-type engine consists of three components: a compressor, a combustion chamber, and a turbine. The plant and the ideal cycle are proposed in Figure 2.1

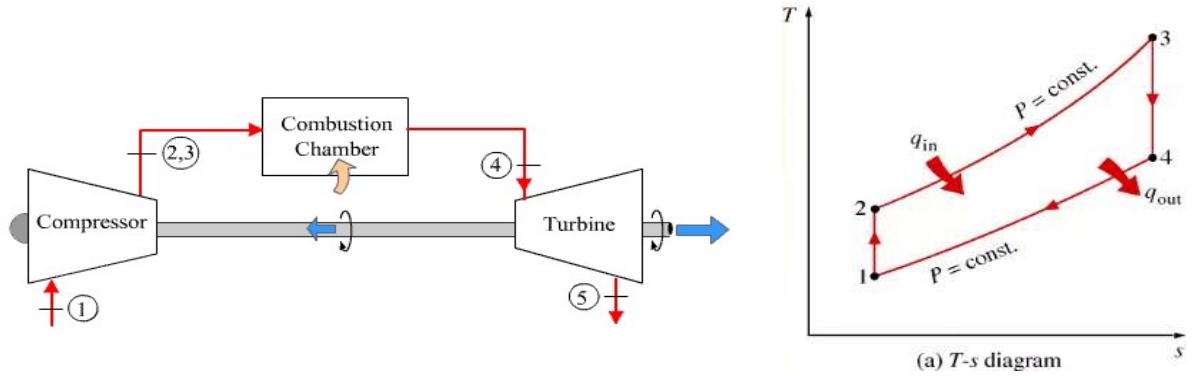


Figure 2.1: The Brayton Cycle plant and cycle

Ideally, the BC thermal efficiency can be written using the Carnot efficiency:

$$\eta_{BC} = 1 - \frac{T_C}{T_H} = 1 - r_p^{\frac{1-k}{k}} \quad 2.1$$

where  $T_C$  and  $T_H$  are the minimum and the maximum temperature reached in the cycle respectively and  $r_p$  is the pressure ratio.

A strategy adopted to increase efficiency is the regeneration. It allows exploiting the heat of the exhaust gas at the turbine end to pre-heat the air after compression, through the adding of a simple heat exchanger (Figure 2.2). In this way, for the same power production, the fossil fuel amount requested by cycle is lower.

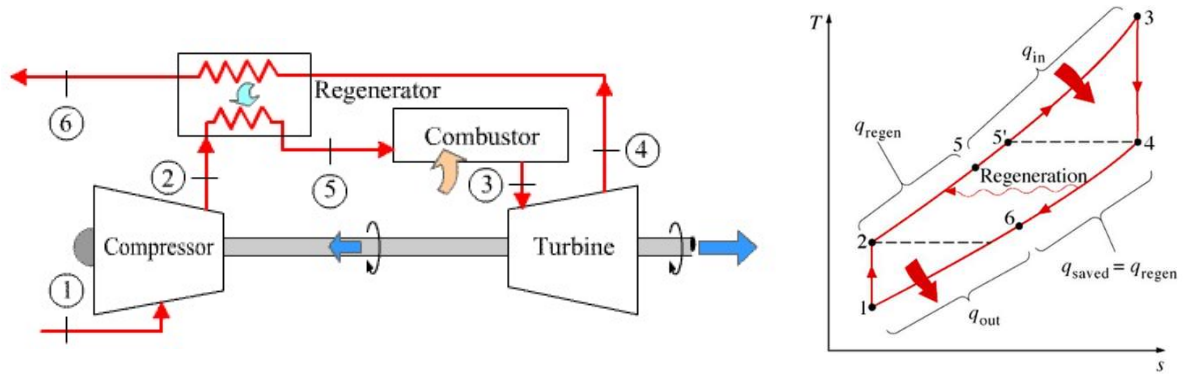


Figure 2.2: The Brayton Cycle plant and cycle, with the regeneration

In this way, the BC thermal efficiency expression is:

$$\eta_{BC} = 1 - \frac{T_C}{T_H} = 1 - \left( \frac{T_C}{T_H} \right) r_p^{\frac{1-k}{k}} \quad 2.2$$

The efficiency of BC is shown in Figure 2.3 both with and without regeneration.

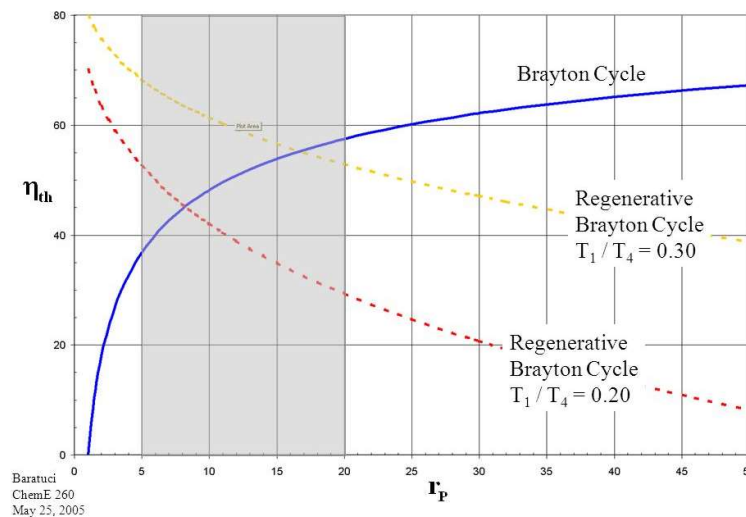


Figure 2.3: The BC efficiency with and without regeneration

According to Figure 2.3, the regeneration process is useful to increase the  $\eta_{BC}$  value, just in a certain range of operating conditions. At low-pressure level ( $0 < r_p < 20$ ) the benefits are very relevant: it's possible to raise the thermal efficiency by up to 50%. Furthermore, this positive effect is directly proportional to the cycle operating temperature. On the other hand, if the pressure ratio is high ( $r_p > 20$ ), the regeneration is not convenient since it results in a  $\eta_{BC}$  reduction.

This aspect has been widely used in the CSP applications, particularly in the Parabolic Dish ones which allow the reaching of very high temperatures, thanks to its radiation concentration strategy. The STBC consists in regenerative Brayton Cycle with a solar receiver instead of the combustion chamber. Thanks to a heat exchanger called recuperator, the hot exhaust gas can release their heat to the compressed air, before going into receiver. The result is not only an increase of the cycle thermal

efficiency but also a decreasing of the pressure-level which lead to several advantages, as it will be explained.

Many studies have been published about the performance and optimization of the BC and STBC showing the potential, merits, and challenges of this technology.

The method of total entropy generation minimization is applied to optimize the geometries of the receiver and recuperator at various steady-state weather conditions; for each steady-state weather condition, the optimum turbine operating point is also found. [11] Another optimization work is done by considering the implementation of the second law of thermodynamics and how it relates to the design of the heat exchanging components within it, including one or more regenerators and the receiver [12]. The thermodynamic model for the prediction of the performance records of an STBC hybrid solution, considering variable irradiance and ambient temperature conditions [13].

## 2.2 System description

The components of an STBC plant are:

- **Parabolic Dish:** the device useful to the solar beam collection,
- **Receiver:** a heat exchanger where the solar radiation is focused, promoting the air heating up,
- **Recuperator:** a heat exchanger which lead to the regeneration process,
- **Turbocharger group:** composed by the gas turbine and the compressor, placed on the same shaft.

Figure 2.4 shows a scheme of the STBC plant, giving an idea about the true size of the component.

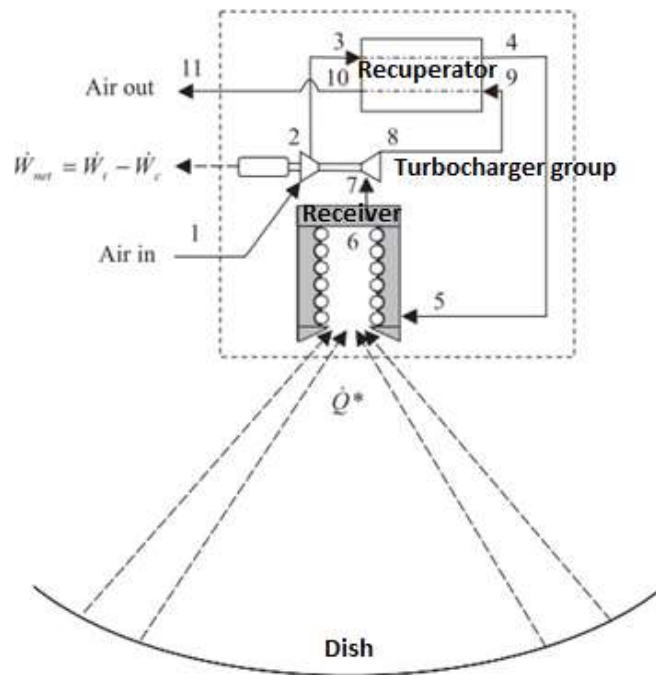


Figure 2.4: Scheme of STBC plant

With reference to the sketch, the compressor (1 - 2) increases the air pressure from the environment and lead it to the recuperator (3 - 4), where it is pre-heated through the air exhausts, exiting from the turbine. Then there is the solar receiver (5 - 6), where a parabolic dish reflects and concentrates the sun's rays, converting the irradiance beam into thermal energy for the cycle. The dish is able to follow the sun movement during the day since a two-axis solar tracking system is required; in this way, the irradiation will be focused onto the aperture of receiver, which is fixed on the dish focal point. Anyway, the compressed and heated air expands in the turbine (7 - 8) and it produces rotational shaft power for the compressor and the electric load. Due to the regeneration process, hot turbine exhaust air provides their heat to the input working fluid (9 - 10), before to be emptied in the environment.

### 2.2.1 Advantages of the STBC plant

The STBC plant would be very promising among the CSP technologies, as it offers a lot of advantages:

- High energy conversion efficiency: it can reach 30% with a high turbine inlet temperature;
- Small-scale range power generation: designed to provide energy for small communities located in isolated areas, so far from the main grid, avoiding that the transmission lines must cross vast stretches of land;
- Working fluid: it is air, very attractive for the use in the water-scarce countries;
- Power block: it is a simple microturbine which can be recovered from turbocharger from the vehicle market off the shelf, making it cheap and easily available;
- Low-pressure cycle: thanks to the regeneration strategy, the high thermal efficiency can be reached through low-pressure ratio. All plant components have not to be so much sophisticated, leading to a decreasing of costs;
- Low costs: linked to simplicity of components;
- Mobility: it requires less area for its installation, compared to the other CSP technology;
- Bulk Manufacturability: it is robust and easy to maintain.

## 2.3 Modelling methodology

---

The modelling of the small-scale dish-mounted STBC plant has been conducted using the software EES, which is a general equation-solving program that is able to numerically solve non-linear algebraic and differential equations. Beside it provides high accuracy thermodynamic and transport property database used to easily define the features of the substances involved in the analysis.

The STBC model can evaluate all the thermodynamic properties on the various points of the cycle. The inputs for the model are:

- Geometries of the involved components. These values were often chosen among the optimized ones, known from the literature review or they are simply hypothesized.
- Supposed irradiance daily variation, inspired by the actual one in Pretoria, South-Africa;

- Some hypothesis about the operating condition, which will be explained in detail each time they will be introduced in the next paragraphs.

As already explained, the reader has to consider that this first part of work has not the purpose to predict with exceptional accuracy the working condition of this plant. Otherwise, it would be an optimization or design study. It wants to be a good tool to allow a reliable and reasonable investigation about the coupled between this plant and a proper TES, which is the main aim of this work.

In the next paragraphs, there is a detailed explanation of the modelling methodology used for each component, with the hypothesis done and all equation involved.

### 2.3.1 Receiver

The receiver is one of the most critical components of the STBC plant since its design is very challenging for all interested researchers. To allow a high efficiency of the cycle, the receiver needs to work at a very high temperature with a huge amount of heat losses through the surrounding. Considering that, the shape of this components must be designed in a proper way: it should catch the greatest quantity of concentrated rays from the parabolic dish, gaining a huge amount of heat to transfer to the air but keeping down the heat losses. Besides the pressure drops have to be very low, as the cycle works with a low-pressure level. Furthermore, the challenge of the receiver design become very hard if the combined effects of some specified phenomena are considered (thermal oxidation, pressure- induced stress, daily thermal cycling, material creep, and thermal shocks).

Considering all of that, the literature has a lot of works about receiver analysis, optimization, and investigation. Le Roux [14] applies a thermodynamic optimization to maximize the net power output of the system; Daabo [15] investigates various configurations of open cavity solar receivers including cylindrical, conical and spherical to discover the effects of coil pitch and tube diameter on the working fluid's exit temperature; Abbasi-Shavazi's study [16] examines experimentally the heat loss from a model solar cavity receiver.

Solar receivers can be categorized into tubular, volumetric and particle receivers, which present different features, considering the various application scenarios. In this work, the receiver chosen is tubular one, since it is more suitable for a small-scale range of 1–100 kW. Particularly, it is a rectangular open-cavity receiver, constructed with a stainless-steel tube, shown in Figure 2.5.

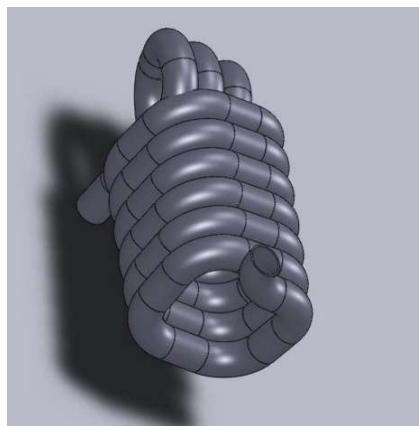


Figure 2.5: A rectangular open-cavity solar receiver, from [17]



The heat absorbed by the inner wall of the receiver is used to heat the air, following the energy balance:

$$\dot{Q}_{net,receiver} = \dot{m}_a c_{p,a} (T_6 - T_5) \quad 2.3$$

Where:

$$\dot{Q}_{net,receiver} = \dot{Q}_{cavity} - \dot{Q}_{losses} \quad 2.4$$

$\dot{Q}_{cavity}$  is the power available at cavity aperture, thanks to the concentrated sun rays. The model considers that this amount of heat is homogeneously absorbed by the inner wall of the receiver without any specification about the heat distribution in terms of receiver height.

The heat is lost from the receiver through the convection, radiation and conduction phenomena.

$$\dot{Q}_{losses} = \dot{Q}_{loss,conduction} + \dot{Q}_{loss,radiation} + \dot{Q}_{loss,convection} \quad 2.5$$

They have been singularly modelled, according to the approach used by Le Roux in [17].

Concerning the conduction heat losses:

$$\dot{Q}_{loss,conduction} = \frac{S_{loss} (T_{rec} - T_{env})}{R_{cond}} \quad 2.6$$

$$S_{loss} = 4 a_{ap} h_{receiver} + A_{ap} \quad 2.7$$

Where:

- $T_{rec} = \frac{T_5 + T_6}{2}$ , it is the average air temperature in the receiver,
- $a_{ap}$  is the length of the receiver aperture side, and so  $A_{ap} = a_{ap}^2$  since a square shape is supposed,
- $R_{cond} = \frac{1}{h_{out} A} + \frac{t_{ins}}{k_{ins} A}$  is the thermal resistance due to the conduction which is, for simplicity, kept constant. Through all the consideration made in [17] about natural and forced convection and the standard value of thickness and conductivity insulation, this value is supposed to be equal to  $1.86 \left[ \frac{m^2 K}{W} \right]$ .

For the radiative loss mechanism, the Stefan-Boltzmann expression has been considered:

$$\dot{Q}_{loss,radiation} = \varepsilon \sigma A_{ap} (T_{rec}^4 - T_{env}^4) \quad 2.8$$

And for the convection one:

$$\dot{Q}_{loss,convection} = 9 h A_{ap} (T_{rec} - T_{env}) \quad 2.9$$

To evaluate  $h$ , the Nusselt formulation used in [17], for the open-cavity receiver surface is:

$$Nu_{cav} = \frac{h L_{rec}}{2 k} = 0.52 B(\theta) (Gr_L Pr)^{(1/4)} \quad 2.10$$

$$Gr_L = L_{rec} g \beta(T_{rec} - T_{env})/\nu^2 \quad 2.11$$

$$L_{rec} = \sqrt{\frac{2 a_{ap}^2}{\pi}} \quad 2.12$$

$$\beta = \frac{1}{T_{prop}} = \frac{1}{\frac{11}{16} T_{rec} + \frac{3}{16} T_{env}} \quad 2.13$$

$$B(\theta) = \cos^{3.2}(\theta) \quad 2.14$$

The symbol  $\theta$  represents the elevation of tracking system (sun's elevation from horizontal), which is supposedly equal to  $34^\circ$ , an average value, in according to some data contained in [18].

### 2.3.2 Parabolic Dish

The CSP systems use mirrors or lenses with concave reflecting surfaces to intercept and focus the solar irradiation to a much smaller receiving area, resulting in an increased heat flux so that the thermodynamic cycle achieves higher Carnot efficiency at higher temperatures. In order to ensure that the sun's rays stay focused on the receiver aperture throughout a typical day, a two-axis solar tracking is required, and its accuracy intensely influences the cost and the performance of the receiver-collector sub-model. Furthermore, the dish optics is a very important factor, since the reflected rays form an image of finite size centred on its focal point. The accuracy of a parabolic dish mainly depends on the parabolic function, slope and specular error, shadowing and reflectivity and these factors affect the heat flux distribution at the receiver surface. A lot of works has been conducted about this argument. Among these, Li [19] presents an analytical function to predict the performance of a paraboloidal dish solar concentrator with a cavity or flat receiver and Wolff [20] analyse the spillage and flux map of a parabolic dish in its construction phase through a lunar test using the full moon.

The common parabolic dish used in the STBC is shown in Figure 2.6.

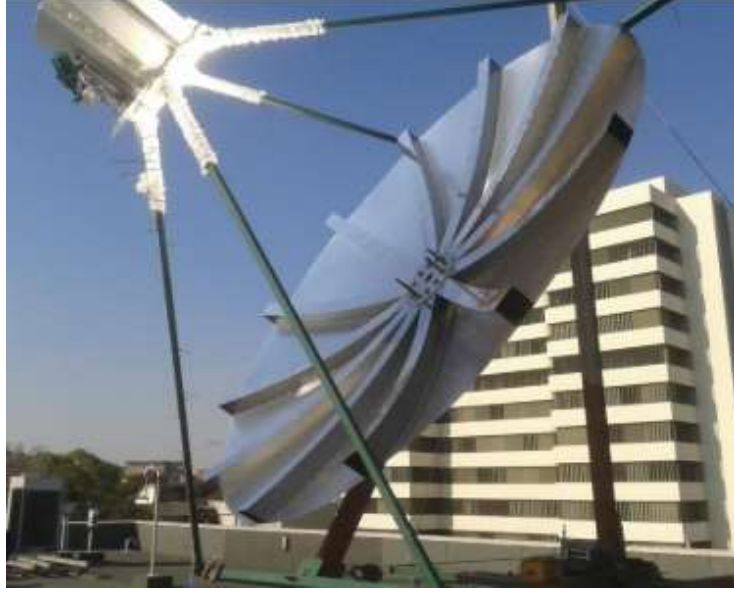


Figure 2.6: Parabolic dish for STBC plant

In order to obtain the amount of heat transferred to the receiver, the definition of optical efficiency has been considered:

$$\eta_{optical} = \frac{\dot{Q}_{cavity}}{\dot{Q}_{focus}} \quad 2.15$$

Where:

$$\dot{Q}_{focus} = Irr A_{dish} \eta_{reflect} \quad 2.16$$

According to the results of [17], the value of  $\eta_{optical}$  is supposed constant and equal to 95%.

$$\eta_{optical} = cost = 0.95 \quad 2.17$$

Concerning  $\eta_{reflect}$ , a value of 85% has been chosen, since the dish surface is modelled as aluminium.

### 2.3.3 Recuperator

A component which is instrumental to the small-scale STBC's success is the recuperator, which is essentially a heat exchanger that utilizes the left-over heat emitted from the outlet of the turbine and transfers it to the cool air coming out the compressor, going into the open cavity solar receiver. This regeneration process allows for less external heat input (fuel or solar irradiance) as well as lowers pressure ratios, reaching higher thermal efficiency. As a heat exchanger, the recuperator must be efficient, safe, economical, simple and convenient and it is often designed as integral to the micro-turbine. In his research, Dellar [21] presents a test design for a low-pressure and high-temperature recuperator, focusing on its low-cost manufacturing. Le Roux [22] investigates about optimization of recuperator geometries so that the net power output of the system is a maximum.

For the STBC plant, the most suitable recuperator type is the counterflow plate arrangement, thanks to the high effectiveness and compact size required. Its scheme is proposed in Figure 2.7.

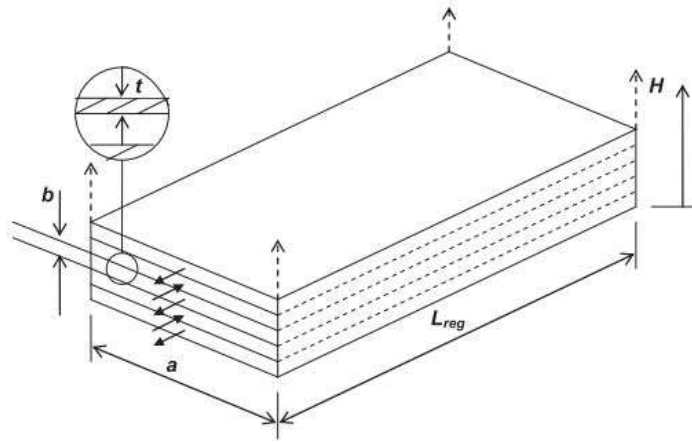


Figure 2.7: A counter flow plate type recuperator

In the model, the recuperator performance is evaluated using the  $\varepsilon - NTU$  method. According to [23] the effectiveness of a counter flow heat exchanger is:

$$\varepsilon = \frac{1 - \exp[-NTU(1 - c)]}{1 - c \exp[-NTU(1 - c)]} \quad 2.18$$

$$\dot{Q}_{recuperator} = \varepsilon \dot{Q}_{recuperator,MAX} \quad 2.19$$

$$\dot{Q}_{recuperator} = C_c (T_4 - T_3) = C_h (T_9 - T_{10}) \quad 2.20$$

$$\dot{Q}_{recuperator,MAX} = \min(C_c, C_h) (T_9 - T_3) \quad 2.21$$

The NTU is calculated like is done in [21], considering a heat exchanger which operates within a laminar fully developed flow regime:

$$NTU = \frac{A_s}{C_{P,c} \dot{m}_{channel} \left[ \frac{2ab}{Nu_{reg}(a+b)} \left( \frac{1}{k_c} + \frac{1}{k_h} \right) + 2R_f + \frac{t}{k_{steel}} \right]} \quad 2.22$$

In the expression:

- $Nu_{reg} = 8.24$  and it is constant for the specific channel geometry where  $\frac{a}{b} \gg 8$ ,
- $R_f = 0.0018$  is the air fouling factor,
- $k_{steel} = 60 \left[ \frac{W}{mK} \right]$  is the steel conductivity hypothesized.

For simplicity, the heat losses of this component have been neglected.

### 2.3.4 Turbocharger group

A turbocharger from the off-the-shelf vehicle market can be used as micro-turbine in the STBC, like the one reported in Figure 2.8. This fact allows for lower costs and immediate availability due to high production quantities. On the other hand, it is true that in these turbochargers the turbine and compressor combination is already set and optimized for a specific task in a vehicle, not for the power generation. Consequently, efficiency is not the best possible ever.



Figure 2.8: Turbocharger Group from Garrett

For this reason, Le Roux's [22], [24] models the turbocharger group using Garrett particular maps for the turbine and the compressor, since isentropic efficiencies, corrected mass flow rates and pressure ratios are intrinsically coupled to each other.

The STBC model of this analysis requests as input:

- $G$ ,
- $\eta_{is,compressor}$ ,  $\eta_{is,turbine}$ ,
- $\beta_{compressor}$ ,  $\beta_{turbine}$ .

In order to choose these values in a realistic and reliable way, avoiding the maps use, some literature results, as well as a commercially available micro-turbine data, have been considered. These are listed in Table 2.1, where they are divided into three cases, referring to the three different power amount generation. The data of Case 1 have been used in this research, keeping them constant since the turbocharger group shows the best performance working at the constant operating condition.

Table 2.1: Different cases about turbocharger operating condition

	Case 1	Case 2	Case 3
$G$ [kg/s]	0.06	0.1	0.13
Rotor speed [rpm]	180000	210000	240000
Heat input [kW]	9	14.5	20
$\beta_{compressor}$ [-]	1.5	1.75	2
$\beta_{turbine}$ [-]	1.5	1.65	1.8
$\eta_{is,compressor}$ [%]	62	66	70
$\eta_{is,turbine}$ [%]	62	65.5	69
Net electric power [kW]	1	2	3

In off-design condition, the inlet temperature can significantly vary, promoting a changing of the turbine efficiency even if pressure ratio, air-flow rate, and rotor speed are constant. According to [22], this variation can be evaluated using the Blade Speed Ratio:

$$BSR = \frac{\frac{2 \pi N}{60} \frac{D_t}{2}}{\left[ 2 h_{in} \left( 1 - r_t^{\frac{1-k}{k}} \right) \right]^{0.5}} \quad 2.23$$

$$\eta_{is,turbine} = \eta_{turbine,MAX} \left( 1 - \left( \frac{BSR - 0.6}{0.6} \right)^{0.2} \right) \quad 2.24$$

The turbine diameter  $D_t$  has been supposed equal to 30 mm, considering an average value.

Thanks to the definition of isentropic turbomachine efficiencies, the exit condition of the working fluid has been evaluated by the model:

$$\frac{T_{out,ideal}}{T_{in}} = \left( \frac{p_{out}}{p_{in}} \right)^{\frac{k-1}{k}} \quad 2.25$$

$$\eta_{is,compressor} = \frac{T_{2,ideal} - T_1}{T_2 - T_1} \quad 2.26$$

$$\eta_{is,turbine} = \frac{T_7 - T_8}{T_7 - T_{8,ideal}} \quad 2.27$$

## 2.4 Model validation

---

After the building of the model, the validation is requested to understand how closely it reflects the system definition. Some data from the literature have been used for this purpose. In order to achieve a great level of confidence about the model reliability, it has been conducted on two levels:

- Plant-level: all component sub-models have been put together, forming a single system. All the equations in the model are coupled with each other and the validation has been made considering the whole process results and features;
- Component-level: for the most complex device of the plant, the receiver, just its sub-model has been run. It allows the comparison between trend describing some parameter variation rather than single output values.

### 2.4.1 Plant-level validation

For the plant-level validation, the results from Le Roux's research [24] have been examined. Here an analytical model of the small-scale STBC in MATLAB has been developed, using the method of total entropy generation minimization. Besides, it contains a great investigation about dish optic, with SolTrace which allows taking into account tracking error, optical error, reflectance, spillage, and

shadowing. The work is more detailed also about recuperator model since it can consider the effect of heat losses.

The results of the comparison are visible in Table 2.2 and

Table 2.3, in terms of main plant parameters and cycle operating temperature of the air, respectively.

**Table 2.2: Comparison between the model and the literature results with the percentage errors**

Parameters	Model	Le Roux [24]	Error %
Receiver heat input [kW]	7.36	7.24	1.6575
Compressor Power [kW]	3.5	3.663	4.4499
Turbine Power [kW]	4.64	4.69	1.0661
Recuperator Efficiency [-]	0.95	0.955	0.5236

**Table 2.3: Temperature of cycle points; comparison between the model and literature results, with the percentage error**

Temperature [K]	Model	Le Roux [24]	Error %
$T_1$	300.2	300.20	0.00
$T_2$	358.8505	359.00	0.04
$T_3$	358.8505	359.00	0.04
$T_4$	1119.353	991.90	12.85
$T_5$	1119.353	991.90	12.85
$T_6$	1225.397	1094.00	12.01
$T_7$	1225.397	1094.00	12.01
$T_8$	1158.746	1026.00	12.94
$T_9$	1158.746	1026.00	12.94
$T_{10}$	405.3178	389.10	4.17

The evaluation error of temperature as well as the other plant parameters is mainly due to the neglecting of some “local effects” of component: heat distribution along the receiver tube, heat losses of the recuperator and the optical dish performance. Anyway, with a maximum error of 12%, the results of the model are satisfying, allowing to have information about the plant working conditions with an acceptable grade of approximation.

#### 2.4.2 Receiver sub-model

The receiver sub-model is validated considering the data from the work carried out by Le Roux in [17], where different variables have been detailly modelled as air temperature increasing factors through the receiver. These variables include concentrator shape, concentrator optical error, concentrator diameter, concentrator reflectivity, concentrator rim angle, solar tracking error, receiver aperture area, receiver material, wind effect, receiver tube diameter, inlet temperature, and mass flow rate through the receiver.

From that, values about the average receiver temperature  $T_{ave}$  and the receiver efficiency  $\eta_{receiver}$  are obtained, becoming a useful term for the comparison. Equation 2.28 expresses the definition receiver efficiency:

$$\eta_{receiver} = \frac{\dot{Q}_{net,receiver}}{\dot{Q}_{cavity}} \quad 2.28$$

The numerical values for this validation with the percentage error calculation can be read in Table 2.4

Table 2.4: Comparison between model and literature results about receiver average temperature and efficiency

<b>G</b> [kg/s]	<b><math>T_{in}</math>[K]</b>	<b>Model</b>	<b>Le Roux</b>	<b>Error</b> [%]	<b>Model</b>	<b>Le Roux</b>	<b>Error</b> [%]
		<b><math>T_{ave}</math>[K]</b>			<b><math>\eta_{receiver}</math></b>		
0.06	900	973.909	1080	10.893	0.689	0.61	11.499
0.06	1000	1063.720	1153	8.393	0.603	0.52	13.763
0.06	1070	1125.802	1205	7.035	0.533	0.45	15.552
0.07	900	964.222	1062	10.141	0.698	0.63	9.690
0.07	1000	1055.468	1138	7.819	0.612	0.53	13.346
0.07	1070	1118.646	1191	6.468	0.541	0.48	11.346
0.08	900	956.774	1047	9.430	0.704	0.64	9.077
0.08	1000	1049.103	1126	7.330	0.618	0.55	11.031
0.08	1070	1113.112	1181	6.099	0.548	0.48	12.403

First, it is possible to do some consideration on the effects of mass flow rate and the receiver tube air inlet temperature changing on the receiver performance, in terms of  $T_{ave}$  and  $\eta_{receiver}$ . Clearly, the higher the inlet temperature, the higher the average receiver temperature is and the less efficient the receiver becomes (due to the heat losses increasing). On the other hand, increasing the air flow rate, the surface temperature decreases, promoting a greater receiver efficiency (due to the reduction of heat losses).

As it is shown, the receiver model built is able shows good result since there is a quite accurate evaluation of both  $T_{ave}$  and  $\eta_{receiver}$ , with an error lower than 11% and 16%, respectively.



### 3. Analysis of STBC plant

---

As it has been already explained, the building of model has the purpose to provide a good tool for a more detailed investigation about the plant, with its features during the functioning. In this view, the validation process allows attributing a certain level of reliability to the results obtained. Concerning the analysis, two different approaches have been followed: the steady-state and the quasi-steady-state. The former has been useful to study the main features of the plant, considering the design operating conditions. The latter has been used to conduct the time-dependent analysis, simulating the actual variable operating condition. It has been particularly interesting, since the STBC system is not operational on the power generation market now, and so the best working strategy has to be designed.

#### 3.1 Feature of the STBC plant

---

The STBC plant is composed of various components which have been widely studied and optimized in the literature, as single objects, in order to obtain the maximum efficiency, minimizing all the irreversibility.

Hence, in this research, the geometrical features of the plant elements have been selected from some previous works which are all mentioned in [24]. They are listed in Table 3.1.

Table 3.1: Geometries of receiver, collector, and recuperator of the STBC plant analysed, from [24]

Receiver:	Data
Cavity geometry [ $m^2$ ]	0.25 x 0.25
Depth Receiver $h_{rec}$ [m]	0.5
Steel Tube Emissivity [-]	0.7
Collector:	Data
Diameter [m]	4.8
$\eta_{optical}$ [-]	0.95
$\eta_{reflec}$ [-]	0.85
Recuperator:	Data
Width [m]	0.5
Length [m]	0.6
Height channel [m]	0.002
Number of channel pairs [-]	40
Thickness plate [m]	0.001

Concerning the operating conditions, they have been chosen from Case 1 of Table 2.1. As already said, this data considers commercial turbochargers with an already-combined compressor and turbine, since a standard off-the-shelf turbocharger from the vehicle market is involved. It allows to considerably decrease the plant costs.

Table 3.2: Operating conditions of turbocharger group

Operating Condition:	Data
Air flow rate $G$ [kg/s]	0.06
$\beta_{compressor}$ [-]	1.5
$\beta_{turbine}$ [-]	1.5
Useful Power [W]	1000
Turbocharger Group	Data
$\eta_{is,compressor}$ [-]	0.62
$\eta_{is,turbine,MAX}$ [-]	0.62
$\eta_{mech,compr}, \eta_{mech,turb}$ [-]	0.97
Rotor speed [rpm]	180000

For the surrounding, the Pretoria conditions have been considered, thinking of the great advantages that South Africa has in terms of the solar resource.

Table 3.3: Environmental conditions considered in the analysis

Environment	Data
$p_1$ [Pa]	86000
$T_1$ [K]	300.2

### 3.2 Steady-state approach: design conditions

The steady-state analysis allows defining the behaviour of the STBC plant, considering the input variable unchanging in the time. So, this approach has been used to choose the proper design condition for the plant, in terms of irradiance.

This has been set:

$$Irr_{DESIGN} = 900 \left[ \frac{W}{m^2} \right] \quad 3.1$$

thinking about two important factors:

- Power generation: the production of electricity reaches the design value of about 1 kW,
- Turbine Inlet Temperature: this represents the limit for temperature reachable in the cycle. Since the turbocharger group is provided by the vehicle market off-the-shelf, leading to a great cost reduction, a not so sophisticated turbine involved has to be accepted. The maximum acceptable temperature is:

$$T_{7,MAX} = 870 \text{ } ^\circ\text{C} = 1143 \text{ K} \quad 3.2$$

Keeping the temperature lower than the maximum limit, the damages for the turbomachine due to collapse phenomena of the material, are avoided as well as a decreasing of its working life duration.

The results produced by the model in the design conditions are listed in Table 3.4, in terms of thermodynamic proprieties of the working fluid. Table 3.5 shows the main features of the plant which operates in design conditions.

**Table 3.4: Thermodynamic proprieties of working fluid during the design operating conditions**

Points of Cycle	Temperature [K]	Enthalpy [kJ/kg]	Entropy [J/kg-K]
1	300.2	300.63	5749
2	359.5	360.355	5815
3	359.5	360.355	5815
4	1038	1090	6941
5	1038	1090	6941
6	1143	1212	7052
7	1143	1212	7052
8	1076	1133	7098
9	1076	1133	7098
10	403.2	404.50	6047

**Table 3.5: Main features of STBC plant during design operating conditions**

Parameters	Results
Irradiance [W/m <sup>2</sup> ]	900
Solar power collected [kW]	16.286
Receiver net power [kW]	7.3
Compressor Power [kW]	3.583
Turbine Power [kW]	4.710
Useful power [kW]	1.09
Receiver Efficiency [-]	0.55
Recuperator Efficiency [-]	0.95

To evaluate the system performance, two efficiency definitions have been introduced:

- Brayton Cycle Efficiency: it indicates the capability of the Brayton Cycle to convert heat input to mechanical power as output.

$$\eta_{BC} = \frac{P_u}{\dot{Q}_{net,receiver}} = 14,9\% \quad 3.3$$

- Solar Thermal Brayton Cycle Efficiency: it shows the overall sola-to-mechanical efficiency.

$$\eta_{STBC} = \frac{P_u}{\dot{Q}_{solar}} = \frac{P_u}{Irr A_{conc}} = 6,7 \% \quad 3.4$$

The low  $\eta_{BC}$  that the plant reaches in this condition is mainly due to the already-combined compressor and turbine coupling offered by the commercial turbochargers with in order to optimize the vehicle performance rather than the power generation. Furthermore, the overall efficiency is decreased by the receiver, which is characterized by greater heat losses since it works at a very high

temperature. Obviously, a lot of aspects can be improved in further researches to increase this value, like:

- The exploiting of the heat from the exhaust gas, before their releasing in the surrounding. It could be employed in some low-temperature application, like the water heating;
- The study about compressor and turbine matching, in order to identify better combinations for the power generation;
- Improvements of the receiver design and optimization, considering high absorptivity and low emissivity coating.

### 3.3 Quasi-steady-state analysis approach: off-design conditions

Like it is well known, the actual conditions are so far from the steady-state one. The solar power isn't a constant resource: it shows periodicity in availability and some fluctuations in magnitude. In this view time-dependent analysis is essential to investigate the effect of the irradiance variation on the plant working condition. This study is performed like a quasi-steady-state analysis that means that the time-variation is considered as a series of consecutive steady-states and so the transitory effects are neglected. Hence the inputs are fixed, the STBC plant model has been run for different values of the irradiance, following the trend depicted in Figure 3.1. It represents the actual values measured in the CSIR Energy Centre located in Pretoria, on the 22nd January 2019 (data available on [VI]).

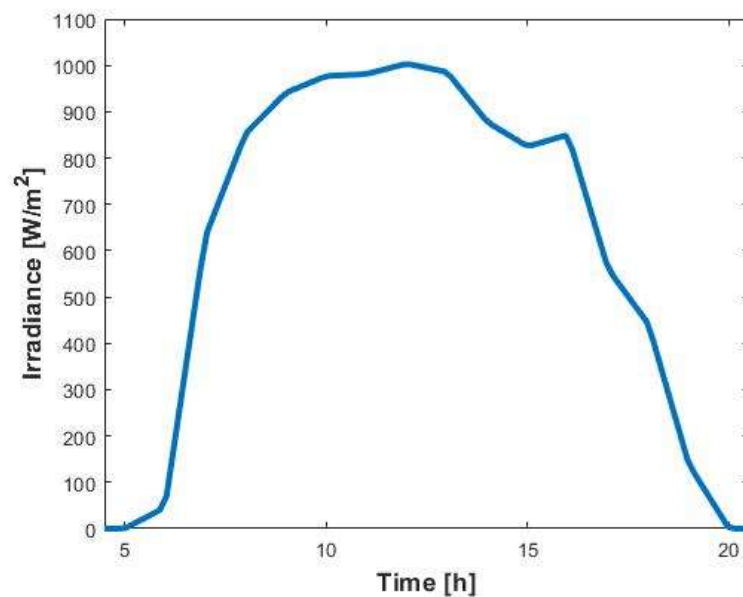


Figure 3.1: Actual daily irradiance measured in Pretoria on 22nd January 2019

Actually, the STBC plant isn't able to generate a constant amount of power during the day, since solar energy isn't available with the same intensity on time. So, this time-dependent analysis needs to define a range of design irradiance, further a single value like it was previously considered. The range is limited by the values of:

$$Irr_{design,MAX} = 900 \left[ \frac{W}{m^2} \right] \quad 3.5$$

This value leads to the maximum turbine inlet temperature, which was previously introduced in Equation 3.2. All the time range characterized by an excess irradiance will be defined as an **overload phase**, which needs to be specifically managed to avoid the overheating of the components and so that a damaging of the plant.

The other limit is:

$$Irr_{design,MIN} = 640 \left[ \frac{W}{m^2} \right] \quad 3.6$$

It represents the minimum value of irradiance which allows having a turbine generated power higher than the compressor one, and so a positive useful power available for the user. Hence, power production occurs during the **design phase**, when the irradiance is included between the two extreme values. Everything is graphically visible in Figure 3.2.

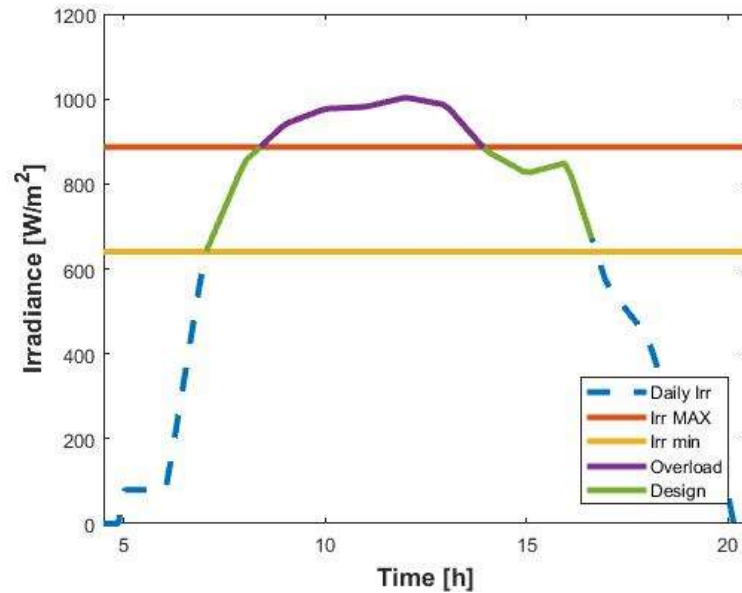


Figure 3.2: Overload and design phases, divided by the irradiance values

Before to judge the performance of the STBC plant during a daily variation of the irradiance, it is necessary to design a proper control strategy for the overload phase. Through that, the correct functioning of the plant is safeguarded, keeping the cycle temperature in the design operating range. In the literature Wang [25] has proposed some control strategies for the dish-Brayton system: these have been great inspiration for the methods describes in the following paragraphs.

### 3.3.1 Shaving device method

A first control strategy employed during the overload phase I based on a shading device placed on the centre of the dish. When the local irradiance value exceeds the design range, the device opens, and part of the dish is shaded to reduce the effective dish aperture area, keeping  $\dot{Q}_{solar}$  constant. A scheme of the plant layout is available in Figure 3.3.

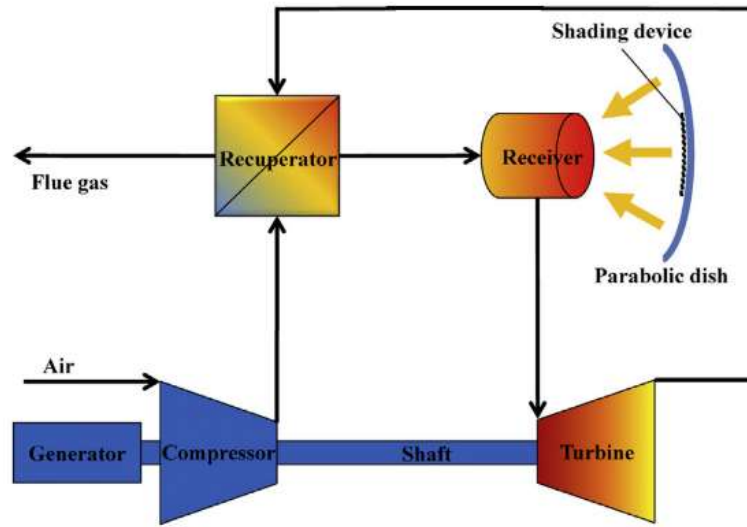


Figure 3.3: Control strategy based on a shaving device on a dish

Assuming that there is no optical efficiency change after using this device, its size has been estimated based on the following equation:

$$\frac{D_{conc}^2 - D_{shave}^2}{D_{conc}^2} = \frac{Irr_{design,MAX}}{Irr_{MAX}} \quad 3.7$$

The dimension of the device is clearly designed considering the worst case which corresponds to the hypothesis:

$$Irr_{MAX} = 1000 \left[ \frac{W}{m^2} \right] \quad 3.8$$

Hence:

$$D_{shave} = 1.61 [m] \quad 3.9$$

The results of the simulation are plotted in the following figures, in terms of inlet turbine temperature, power production (Figure 3.4) and the plant efficiencies (Figure 3.5), referring just to the design and the overload phases.

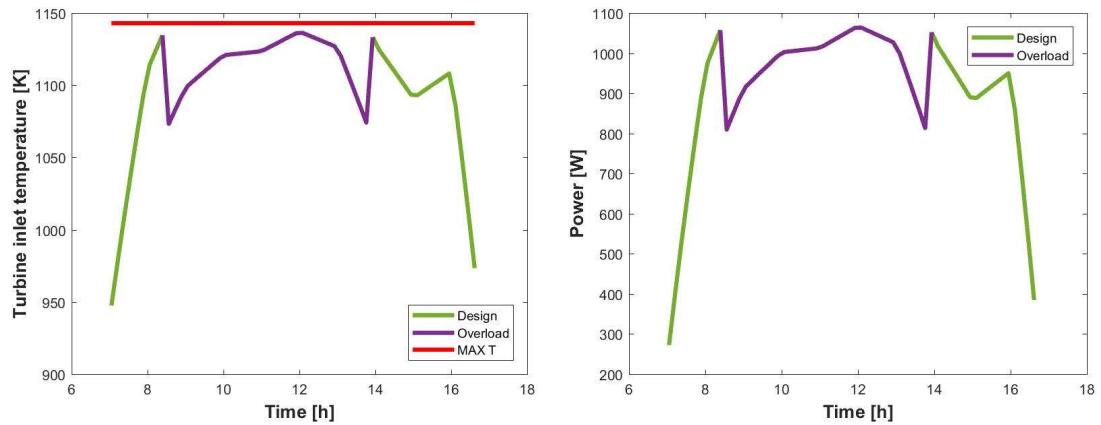


Figure 3.4: Turbine inlet temperature and power production during the design and overload phase, (shaving device strategy)

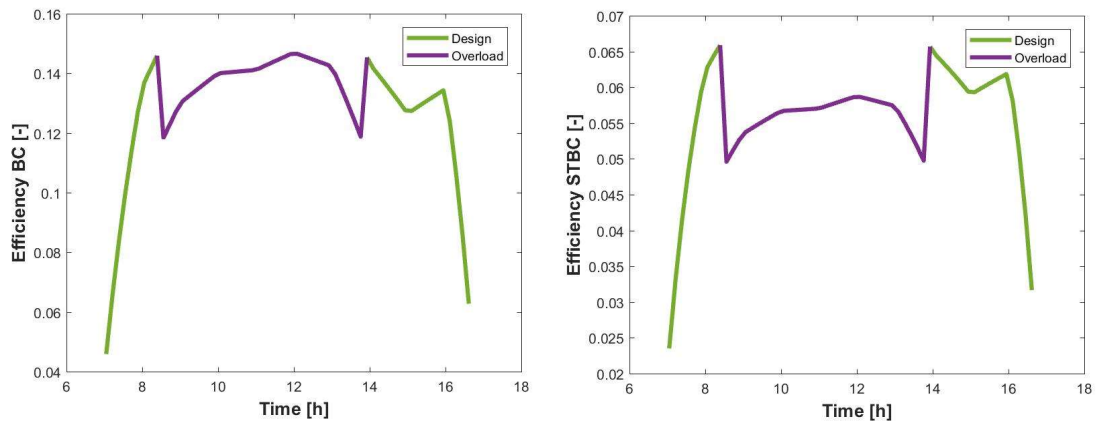


Figure 3.5: Plant efficiencies during the design and overload phases, (shaving device strategy)

This control strategy is an ON/OFF typology: it means that the shaving device dimensions are designed to limit the turbine inlet temperature in correspondence of the  $Irr_{MAX}$ , in order to ever avoid the exceeding of the critical condition. Obviously, this amount of solar power is not always present during the overload phase, further, it occurs just for a less time range. This is the reason why the power generation as well the plant efficiencies have a parabolic trend during the overload phase. Overall, this kind of adjustment is able to avoid the overheating of the turbine and so that damaging, assuming that the user is willing to accept the decreasing of the power during the central hours of the day. On the other hand, the strategy is highly dissipative, since it isn't able to exploit the whole radiation coming on the Earth surface like it is underlined in Figure 3.6.

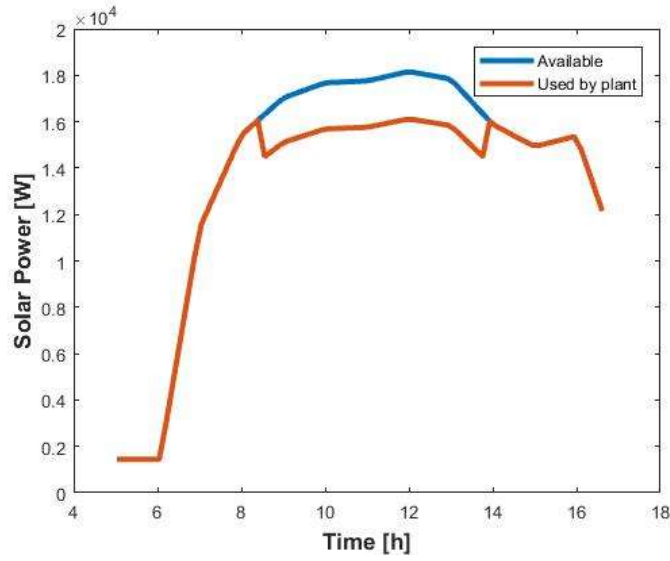


Figure 3.6: Difference between the available and the used solar power

In this way, the amount of energy wasted can be on average:

$$Energy_{wasted} = 10 [kWh] \quad 3.10$$

To overcome this issue the future research could focus on the innovative development of the shaving device, based on a gradual aperture of the dish: it allows to have the optimized dish diameter covering the required area at a certain value of irradiance exceeding the design value. The control system of the shading device can be designed by coupling an electric motor driven by a pyrliometer which measures the DNI. The electrical signal from the pyrliometer can be used to control the electric motor, obtaining the required diameter. Before to reach this technological level, this control strategy idea is not very convenient and can be easily substituted for the other one proposed.

### 3.3.2 Air-flow rate adjustment

This control strategy is based on an adjustment of the air-flow rate, occurring through a by-pass three-way valve placed between the compressor and recuperator. The plant scheme is showed in Figure 3.7.



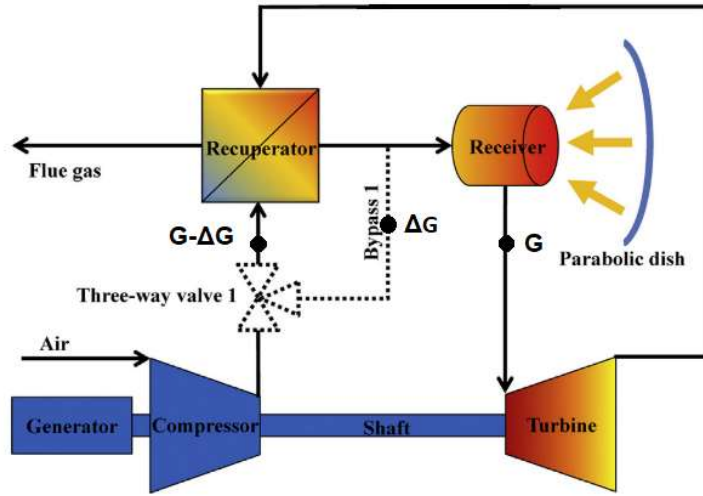


Figure 3.7: Control strategy based on the adjustment of the air flow rate through a three-way valve

When the irradiance is higher than the admissible value, the valve opens, and the spillage  $\Delta G$  bypasses the recuperator, avoiding the temperature increasing. This flow rate amount remains cold and it makes the temperature lower for the whole  $G$ , after the mixing. The aperture level of the valve can be chosen in such a way that after the passing through the receiver, the inlet turbine temperature can be very near to the maximum reachable, ever less for safety reason. Hence the spillage quantity increases proportionally to the irradiance increasing, making the adjustment continuous and so more efficient. The  $\Delta G$  variation in time is shown in Figure 3.8

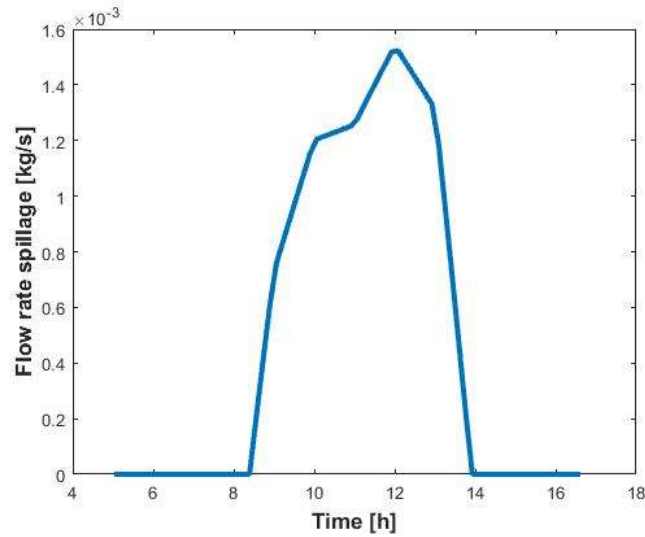


Figure 3.8: Variation of spillage on time

It reaches its maximum at the daily highest irradiance of the day:

$$\Delta G_{max} = 0.015 \left[ \frac{kg}{s} \right] \quad 3.11$$

Furthermore, the three-way valve can be automatically controlled through the integration of an electric motor, a proportional–integral–derivative (PID) controller and a pyrheliometer. The

pyrheliometer aim is measuring the DNI value and sending electrical signals to the PID controller, which controls the motor to drive the three-way valve to the right position. Concerning the other working parameter, let's see Figure 3.9 and Figure 3.10.

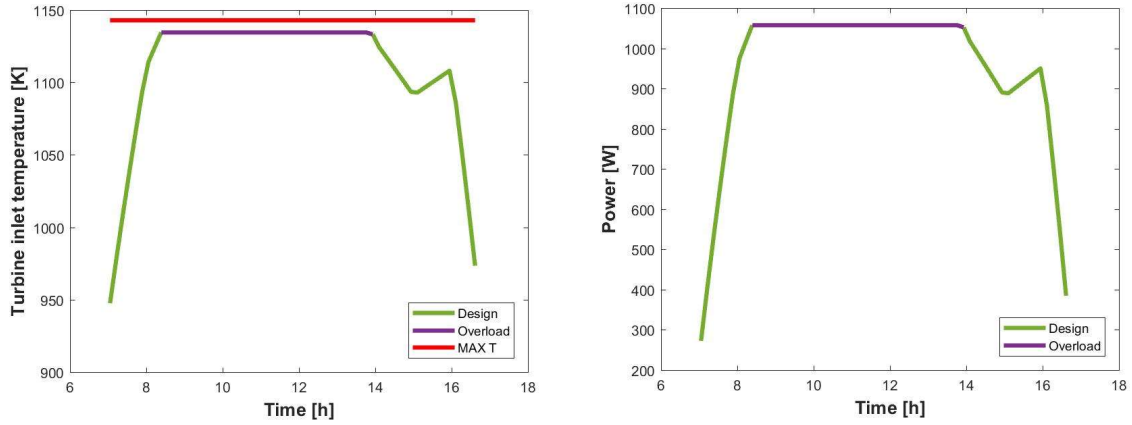


Figure 3.9: Turbine inlet temperature and power production during the design and overload phase (air flow rate adjustment)

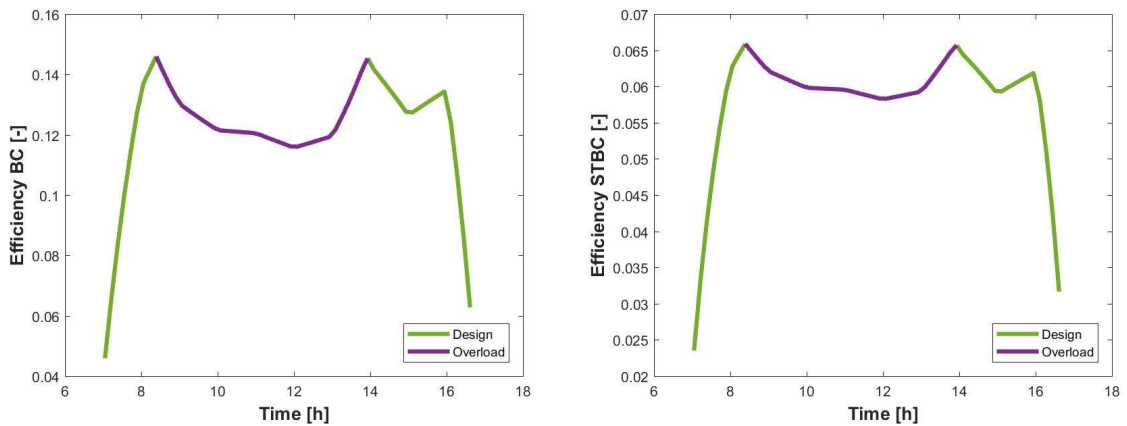


Figure 3.10: Plant efficiencies during the design and overload phases (air flow rate adjustment)

Unlike in the previous case, this control strategy is able to generate the same power amount during the whole overload phase:

$$P_u = 1.05 \text{ [kW]} \quad 3.12$$

keeping constant the turbine inlet temperature, slightly lower than the maximum permissible for safety reasons:

$$T_7 = 1134 \text{ [K]} \quad 3.13$$

Although this aspect represents a great advantage for this adjustment, making it interesting and more attractive, there are some limits which have to be considered. First of all, the plant efficiencies decrease during the overload phase, as it is visible in Figure 3.10. This is owing to the high value of solar power, which could lead to obtaining more generation power from the STBC plant. It means that it is not possible to exploit in the best way the energy surplus provided by the sun during those hours of the day. Besides, all components of the plant have to work in a not steady-state condition,

due to the continuous change of the air flow rate which clearly causes a worsening of the plant parts performance.

All in all, this control strategy typology is a good way to make operating the STBC plant during the overload period, allowing to provide the design value to electricity to the user.

### 3.3.3 TES integration

Another solution that could solve the issue about the STBC plant functioning when the irradiance exceeds the range design is the adding of a thermal store between the receiver and the turbine. A conceptual scheme is available in Figure 3.11.

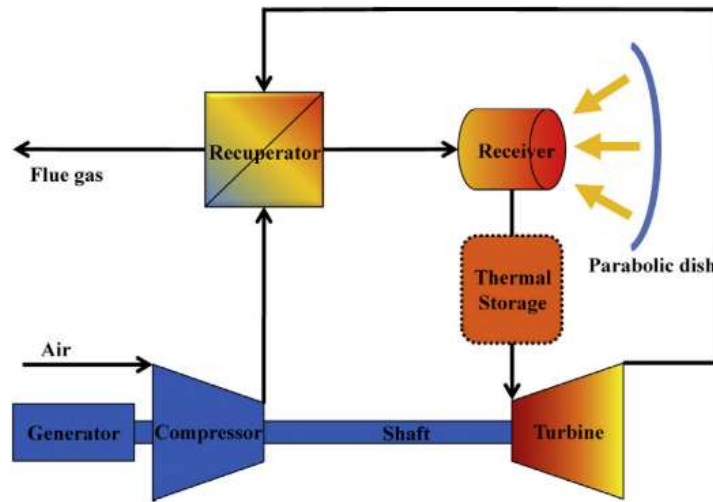


Figure 3.11: Control strategy based on the adding of thermal storage in the plant

By introducing a TES, the turbine inlet temperature  $T_6$  can be different from the receiver outlet temperature  $T_7$ , allowing to store the surplus thermal energy. In first approximation this energy amount  $Q_{TES}$  has been evaluated considering an ideal storage process, which leads to keeping constant the value of  $T_7$  (see 3.13).

So that:

$$Q_{TES} = \int G c_p (T_6 - T_7) dt \quad [kWh] \quad 3.14$$

Graphically, the temperature difference is plotted in Figure 3.12, with the amount of energy associated.

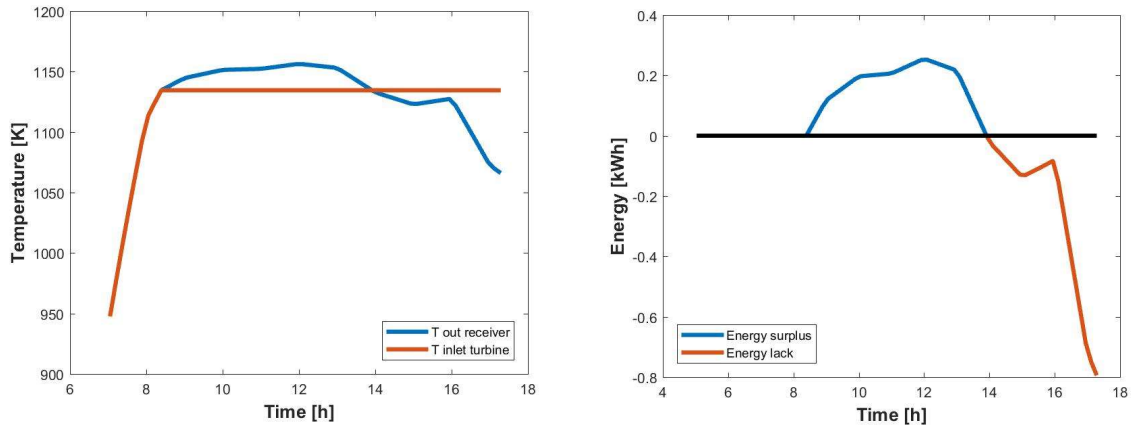


Figure 3.12: the temperature difference between the receiver outlet and inlet turbine. On the right, the energy surplus/lack associated

The energy surplus provided by the sun during the overload period is not wasted rather it is stored by the TES: this process is called charging for the TES. Later, when the DNI available decreases, the discharging operation occurs, which leads to a heating up of the working fluid and to an increase of the power generation. The  $Q_{TES}$  involved in these processes is plotted in Figure 3.13.

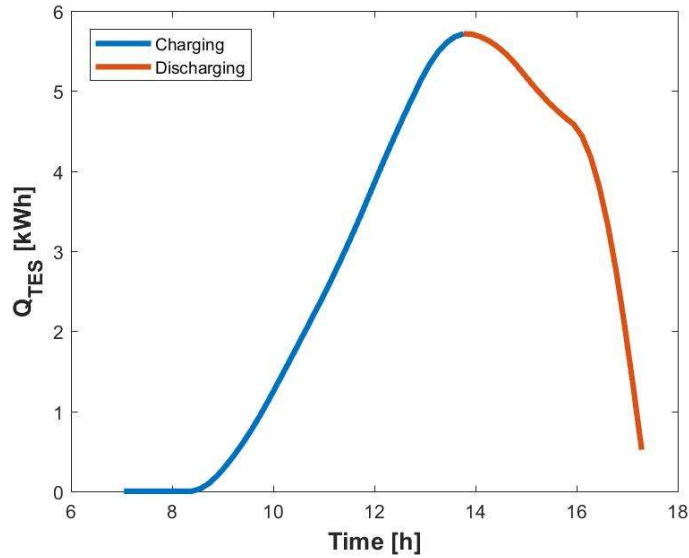


Figure 3.13: Energy involved in the charging\discharging process in the TES device

As is presented, it is possible to store thermal energy for an amount of:

$$Q_{TES} = 5.72 [kWh] \quad 3.15$$

Concerning its exploiting, various strategies can be considered, according to the user requirements. There are many options which basically consist of the beginning of the discharging process. In this research, it starts when the irradiance is lower than  $Irr_{design,MAX}$ , hence just after the overload hours. This is the case of a user who doesn't admit the power generation decreasing, even it occurs during the design time range. Otherwise, there is the possibility to accept a lower production, choosing the best DNI value from what starts the discharging. The advantage is a greater increase in

the plant working hours. In this research, the first strategy has been chosen for the investigation, as the results in Figure 3.14 shows.

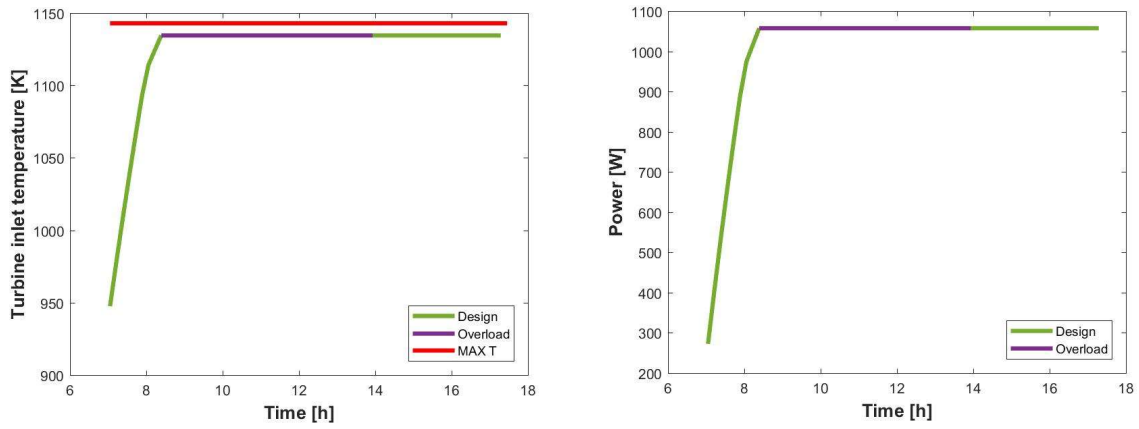


Figure 3.14: Turbine inlet temperature and power production during the design and overload phase (TES integration strategy)

From the peak hours to the plant turning off, the values of  $P_u$  and  $T_7$  is constant and it is the same evaluated respectively in 3.12 and 3.13.

From an efficiency point of view, in order to consider, the TES performance, the formulations are again defined. During the charging:

$$\eta_{BC}^* = \frac{P_u + \dot{Q}_{TES}}{\dot{Q}_{net,receiver}} \quad \eta_{STBC}^* = \frac{P_u + \dot{Q}_{TES}}{\dot{Q}_{solar}} \quad 3.16$$

and during the discharging:

$$\eta_{BC}^* = \frac{P_u}{\dot{Q}_{net,receiver} + \dot{Q}_{TES}} \quad \eta_{STBC}^* = \frac{P_u}{\dot{Q}_{solar} + \dot{Q}_{TES}} \quad 3.17$$

The results are plotted in Figure 3.15.

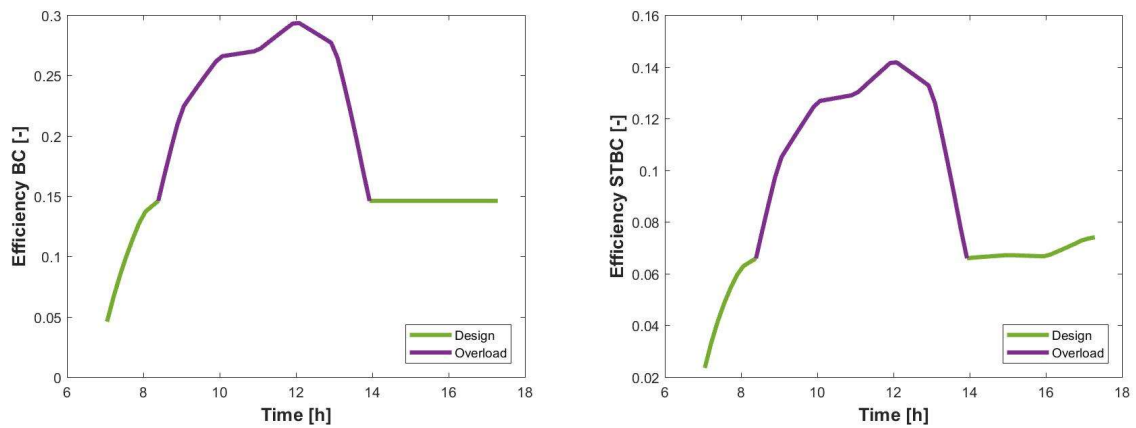


Figure 3.15: Plant efficiencies during the design and overload phases, (TES integration strategy)

Given the data on these graphs, the advantages of a TES integration are perfectly clear. First of all, it allows for obtaining a constant value of power generation for all time after the overload phase. This amount can be arbitrarily chosen, promoting a great level of adjustability for the plant as well as certain independence from the environmental conditions. Furthermore, the TES device leads to exploit the surplus of energy in the best way ever, through the storage of its thermal form. The collection of the electrical one should be more complex since it requires a more sophisticated system. Besides, in this way it is possible to keep more functioning the STBC plant, increasing its working hours. On the other hand, this energy is wasted in some way in the previous control strategy. This is the reason why efficiency assumes a greater value on average.

In order to quantify the positive impact of this control strategy, a comparison has been made considering some parameters evaluated on average on all-time range of functioning.

**Table 3.6: Comparison of the results about the different control strategies**

<b>Control Strategy</b>	$P_u$ [W]	$\eta_{STBC}$ [%]	Work. Hours [h]
Shaving Device	910	5.56	9:30
Flow rate Adjustment	952	5.81	9:30
TES integration	1010	9.29	10:10

Although the clear advantages which are shown through the parameters in Table 3.6, the TES adding into the STBC plant involve some limits. Concerning the receiver, it is not well protected and so it should be designed to be able to work at maxim irradiance amount for a relatively long time (hour level). This is not so beneficial for its efficiency since the heat losses tend to increase. The other adjustments allow decreasing the inlet turbine temperature and the receiver one as well. Furthermore, since the power block will be installed at a position where is near to the focal point of the dish and supported by a cantilever, the available space and the allowed weight for the thermal storage tank are very limited. Besides, the weight of the power block will directly affect the energy consumption of the dish itself for tracking the sun. This is true considering the need to have a TES installation very near to other components, to limit the heat losses. In this view, future researches can consider the possibility to place the TES device on the ground, developing an optimized design to reduce the losses.

By analysing the advantages and disadvantages of the different potential control strategies above, the most interest for a detailed numerical investigation is the TES integration solution, which will be faced in the following chapters; it can be a crucial point for the future development of the CSP technologies and particularly of the small scale STBC plant.

## 4. Preliminary study for the TES integration

So far, the TES introduction in the STBC plant has been explained as the optimal control strategy useful for manage the overload phase during the day. The TES presence allows to keep the cycle temperature near to the design value, avoiding the turbine overheating. Furthermore, it leads a rising of plant efficiency, since the energy surplus is not dissipated but rather it is accumulated to be used when the solar irradiation is not available anymore.

Actually, a TES system introduction is very advantageous for the plant, for a lot of other reasons. It can mitigate short fluctuations during transient weather conditions, shift the generation period from peak hours of solar insolation to peak hours of power demand and to extending the generation period when solar is not available. TES forms a key component of a solar power plant for great improvement of its dispatchability, which is very appreciated feature from an economical point of view, too. Electricity prices vary during a day depending on demand, so that the solar intensity's largest periods do not correspond to the electricity's most expensive periods. Adding a TES allows heat storage during high solar intensity periods and provides productions during high electricity cost periods, with a clear decreasing of the prices. Considering a typical winter price profile, which has highest demand and prices at the beginning and end of the day, a smart strategy about the functioning of TES and CSP is shown in Figure 4.1 [26]:

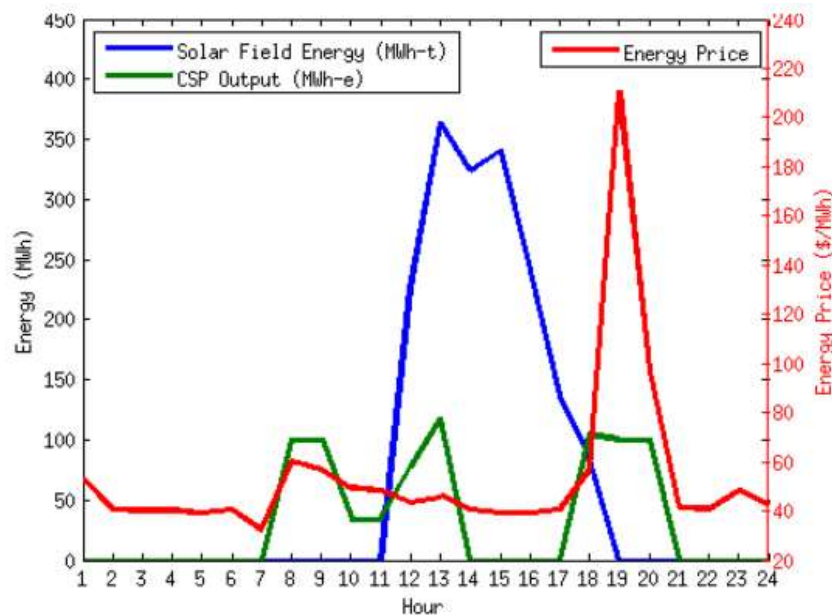


Figure 4.1: Sample strategy about the functioning of TES and CSP, during the winter, [26]

For instance, in the morning (hours 8 through 10) the power block is operated using energy from TES, which was carried over from the previous day, catching the high early-morning prices. The CSP is shutdown in hours 15 and 16, when energy prices are relatively low, and the solar energy is stored into TES. The plant then provides energy in the evening peak, using both energy from the solar field and energy from storage.

Overall, there are several benefits offered by the introduction of a TES in a CSP system. Today ongoing research is seriously focused on this subject so that great improvements have been made in the last period. Nevertheless, STBC with TES integration hasn't ever been investigated and for this reason it has been chosen as main goal of this work. During this preliminary phase of TES design, its typology has been selected among the all possible and the most suitable plant layout has been supposed.

## 4.1 Typology of TES

TES systems can be categorized as active or passive types. When the storage medium is a fluid which it is able to flow between the tanks, the systems are referred to as active type. If the storage medium is also used as the HTF the system is referred to as direct-active system. An additional heat exchanger is required when the storage fluid and HTF are different and this unit is defined indirect-active type. In cases where the storage medium is solid, the HTF passes through it just for charging and discharging. These are the passive type systems. Figure 4.2 shows the various TES system configurations classified as active and passive storage systems.

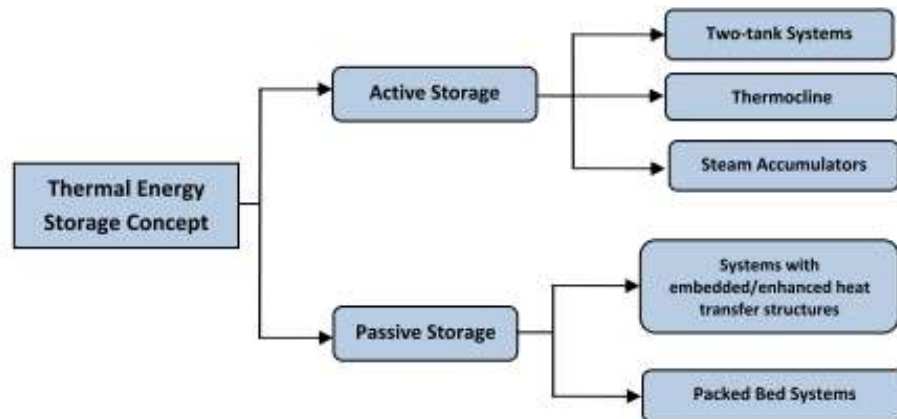


Figure 4.2: TES classification as active and passive system, in according to

Known this categorization, it is possible to think about the TES configuration most suitable for the STBC plant described in this paper. In the next sections some TES options are proposed, with a basic investigation about the material that can be involved in the application.

### 4.1.1 Active TES: indirect system

Concerning the TES active system, the direct configuration is not acceptable for the STBC plant since it involves a storage of the. In this way the accumulation operation could be very difficult from a practical point of view, because the substance in question is air at low pressure. Moreover the air flow in the turbine would be less than the one flowed through the compressor, causing the uncontrolled acceleration of the shaft in the turbocharger group and so some damages and break.



On the other hand, the active-indirect configuration is possible: there is another fluid which extract/release heat from the heated air. A hypothetical layout is proposed for the two-tank solution and in the for the thermocline one.

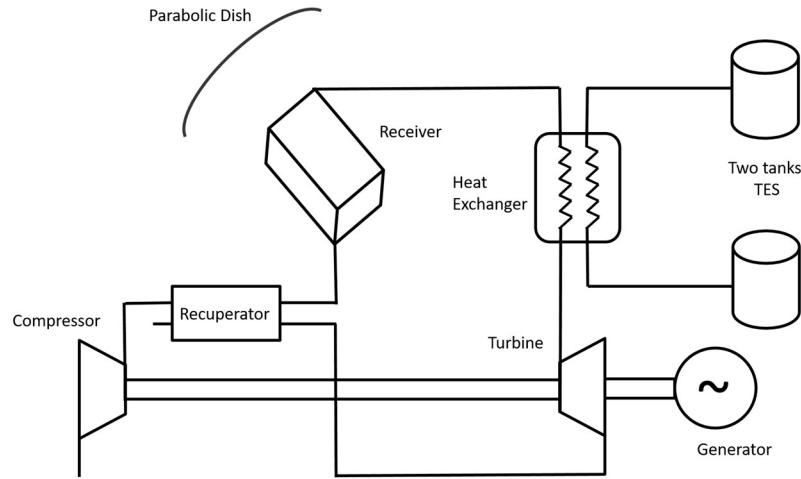


Figure 4.3: Indirect-active TES integration in the STBC plant: two tanks configuration

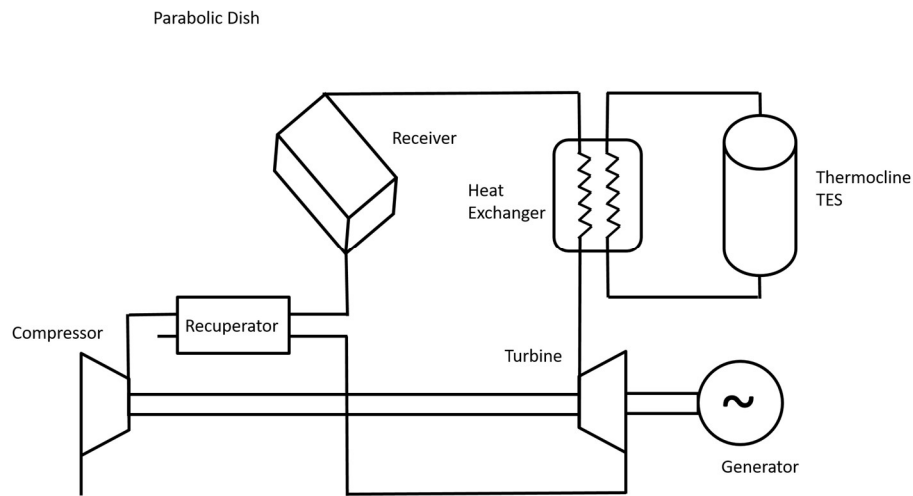


Figure 4.4: Indirect-active TES integration in the STBC plant: thermocline configuration

Since both cases are sensible storage applications, the surplus/lack of thermal energy is linked to the increasing/decreasing of storage material temperature. Considering this fact, the storage substance has to be able to work at high temperature (the maximum one should be between  $[850 \div 870]$  °C). Working at this temperature range is very difficult, since the material aren't usually stable for a chemical point of view. For this reason, in literature there are very few substances which can be candidates for this application. Some of that are listed in Table 4.1:

**Table 4.1: Liquid material for sensible heat thermal storage, [27]**

Material	$T_{min}$ [°C]	$T_{max}$ [°C]	$\rho$ [kg/m <sup>3</sup> ]	$c_p$ [J/kgK]	$\lambda$ [W/m K]
LiF-NaF-KF	454	1000	2200-1800	1890	0.6-1
Na	97.7	873	884-745	1270-1310	0.16-0.35

Like Heller reviewed in [27], the former is a molten salt called FLiNaK, which consists of LiF-NaF-KF (46.5-11.5-42 mole percentage). As molten salts, its heat transfer characteristics are not so bad: reasonably high density and mediocre specific heat capacity enable a low volume flow. On the other hand, the low thermal conductivity leads to elevated temperatures on the outside of the receiver pipes causing considerable radiation losses. Anyway FLiNaK is argument in the ongoing research thanks to its lower melting point, avoiding the salt freezing during the night or in times of low irradiation.

The use of Sodium (Na) as storage material appears attractive when the higher temperatures occur. However it is necessary to consider technical challenges of sodium, for example, reactivity with water and possibly corrosion.

#### 4.1.2 Passive TES

In passive storage systems, the storage medium is kept motionless and heated/cooled by the circulation of the HTF during the charging/discharging phases. The TES can be incorporated directly after the receiver, eliminating the need for a heat exchanger between the HTF and the thermal storage medium. In this way it promotes a quite plant simplicity, which is depicted in the scheme of Figure 4.5.

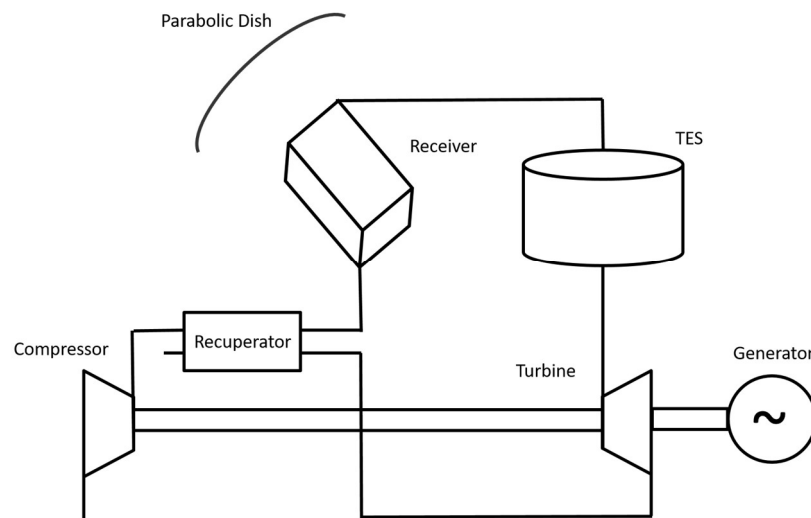


**Figure 4.5: Passive TES integration in the STBC plant**

Heat transfer can be more problematic in passive type systems since the storage medium is in solid phase rather than liquid phase. For this reason, the choice about how heat transfer mechanisms has to properly occur, is one of the major challenges for this system configuration. Several heat transfer

mechanisms exist, like packed bed type storage and embedding tubes or pipes structures. These solutions are respectively depicted in Figure 4.6.

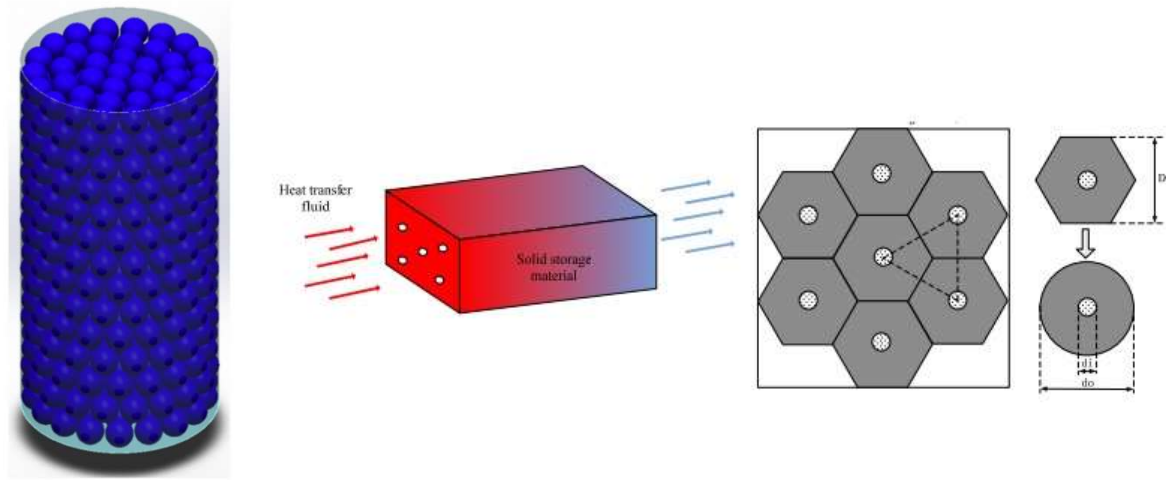


Figure 4.6: Passive thermal storage solution: Packed-bed (on the left) and Embedding tubes (on the right)

Packed bed systems consist of storage material elements in various shapes and sizes and an HTF that flows between these elements transferring heat to the storage medium. Since the fluid directly flows through the storage medium, it is not required an additional heat exchanger and heat transfer coefficients can be very large. The functioning idea for the other application is more or less the same: the HTF passes through pipes embedded in the storage concrete to heat it. To discharge thermal energy, the cold transfer fluid flows through it in the reverse direction and is heated up. A tubular heat exchanger is integrated into the storage material for efficient heat transfer.

Concerning the materials involved in the passive TES system, there are sensible options as well as PCM ones. The most suitable for the STBC application, in terms of temperature range, are listed in Table 4.2 and Table 4.3 for both cases.

Table 4.2: Materials for passive TES system: sensible option

Materials	$T_{mel}$ [°C]	$\rho$ [kg/m <sup>3</sup> ]	$c_p$ [J/kg K]
Rock	1200	2560	960
Concrete	1300	2750	916

Popular concepts are packed beds of spheres or natural rocks and high-temperature concrete blocks. Materials are proposed to enhance the thermocline in single-tank TESSs, substituting expensive/low-thermal-capacity fluid involved in the common active TES system with solids of higher density, higher specific thermal capacity, and/or lower cost.

Table 4.3: Materials for passive TES system: PCM option, from [28]

Materials	$T_{mel}$ [°C]	$\rho$ [kg/m <sup>3</sup> ]	$c_p$ [J/kg K]	$L$ [kJ/kg]
$Na_2SO_4$	884	2664	902.5	165
$SrCl_2$	875	3052	500	103

Selected from the Kenisarin's review about high-temperature phase change materials for thermal energy storage [28], these salts meet the fundamental requirements imposed upon phase change heat storage materials which are suitable melting temperature and, whenever possible, high heat of fusion.

#### 4.1.3 TES preliminary sizing

Known all the TES solutions previously described, the choice about the most suitable configuration for the STBC plant can be conducted more consciously. The decision has been based on some design criteria, which are important in terms of plant practical construction and actual feasibility.

In this case the factors used for the analysis have been volume, costs and weight of the TES evaluated thanks to a preliminary sizing calculation, valid for each specific solution.

The equation used have been:

- Active TES:

$$V_{TES} = \frac{Q_{TES}}{\rho_{TES,med} c_{p, TES med} (T_{hot} - T_{cold})} \quad 4.1$$

- Passive TES considering sensible material solution:

$$V_{TES} = \frac{Q_{TES}}{\varepsilon \rho_{air} c_{p,air} (T_{hot} - T_{cold}) + (1 - \varepsilon) \rho_{TES,med} c_{p, TES med} (T_{hot} - T_{cold})} \quad 4.2$$

- Passive TES considering PCM solution:

$$V_{TES} = \frac{Q_{TES}}{\varepsilon \rho_{air} c_{p,air} (T_{hot} - T_{cold}) + (1 - \varepsilon) \rho_{TES,med} L} \quad 4.3$$

Where:

- $\varepsilon$  is the void fraction coefficient equals to the ratio between the volume occupied by the fluid (air) and the whole one;

$$\varepsilon = \frac{V_f}{V_{TES}} = 0.4 \quad 4.4$$

- $Q_{TES}$  is the TES capacity, previously evaluated and available in 3.15;
- $T_{hot}$  and  $T_{cold}$  are the extreme temperatures involved in the process:  $T_{hot} = 1150 \text{ K}$  (which is the average temperature at outlet of receiver during the overload phase) and  $T_{cold} = 1134 \text{ K}$ , from 3.13.

The Table 4.4 resumes the material involved in the analysis, with their feature in terms of energy density  $e$  and specific cost. As it has been already explained, these materials have been selected in according to the operating temperature range suitable for the STBC application, which is:

$$\text{Operating range temperature} = [1120 \div 1140] \text{ K} \quad 4.5$$

**Table 4.4: Different material used like a storage medium for the analysis, with their features**

TES	Material	$e[kJ/kg]$	Cost [USD/kg]
Active TES	LiF-NaF-KF	30.24	64
	Na	20.64	2
Passive TES: Sensible medium	Rock	15.36	0.15
	Concrete	14.66	0.05
Passive TES:	$Na_2SO_4$	165	10.4
PCM	$SrCl_2$	103	43.36

The results of this analysis are presented in Figure 4.7, Figure 4.8, and Figure 4.9.

Volume and weight of storage have been investigated thinking to its ideal placing, which is near the power block, on the focal point of the dish. This means that TES should be supported by the tracking solar system, influencing its tracking accuracy and leading to a certain amount of energy consumption. Obviously also the specific cost of technology has been used as significant parameter for the choice, in order to estimate the amount of investment needed for the TES introduction in the STBC plant.

Concerning the active TES solution, the selected molten salts involve disadvantages considering both aspects. Particularly, Sodium (Na) needs the greatest volume for the application while LiF-NaF-KF requires an extremely high costs for the technology, major than 7000 [USD/kWh].

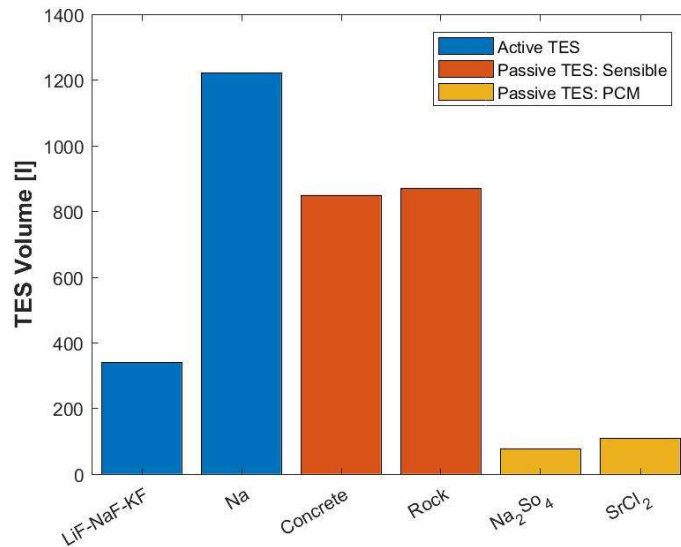


**Figure 4.7: Results about TES volume, considering different storage configuration**

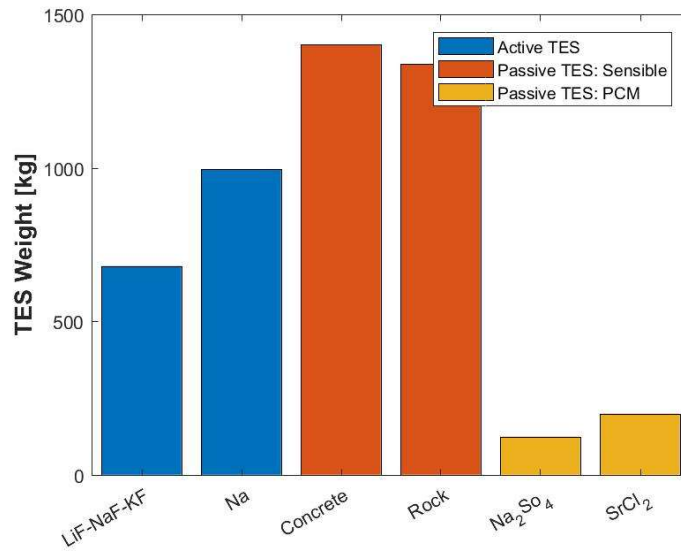


Figure 4.8: Results about TES weight, considering different storage configuration

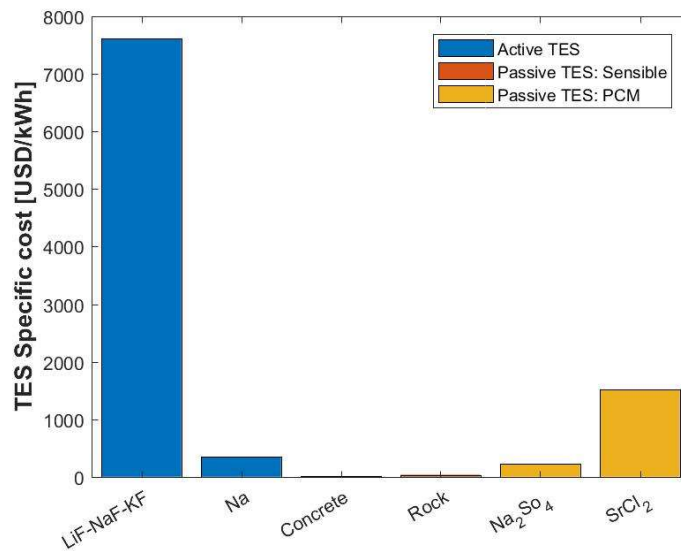


Figure 4.9: Results about TES specific cost, considering different storage configuration

On the contrary both sensible and latent passive TES solution offer different advantages to the STBC plant, in according to the natural heat transfer mechanism involved and their physical-chemical proprieties as well. Surely PCM used as storage medium has very high energy density which leads to smallest space required among all studied technologies, for the same energy cumulation amount. Na<sub>2</sub>SO<sub>4</sub> and SrCl<sub>2</sub> need less than 100 volume litres with a weight less than 200 kg. This can be favourable from a layout point of view, since the placing can occur on the support of tracking system, very close to the other plant components. This optimum configuration allows to obtain a very complex plant and a minimisation of the heat losses. Furthermore, the losses of this kind of system are less than a sensible one thanks to the lower temperature reached during the storage process (melting temperature is constant during the phase change). On the other hand, PCM technology requires a great economical investment: the specific cost for Na<sub>2</sub>SO<sub>4</sub> is of 215 USD/kWh while the

$\text{SrCl}_2$  requires 1500 USD/kWh. But the main disadvantage for the latent storage is surely the chemical instability of which PCM suffers at high temperature, leading to a progressive deterioration of the material properties.

Passive TES option with sensible medium is characterized by a lower energy density of the material, not allowing the optimum placing of the storage, owing to the enormous weight predicted of about 1500 kg. In this way the TES should be placed on the ground, so far from the turbine and the other plant components. Surely this is the cause of great heat losses and pressure drops owing to the tank size and longer piping required, with an increasing of the layout complexity. Anyway, it is a very cheap technology: being under the 50 USD/kWh the specific cost of this technology is negligible compared to the other ones, through employing conventional materials of construction, easily manufacturable. Beside they have very high chemical stability. Table 4.5 summarizes the main features proper of sensible and latent technology.

Table 4.5: Summary of advantages for latent and sensible TES technology

Aspects	Sensible	Latent
Energy density	Low	High
Volume	High	Low
Heat Losses	High	Low
Chemical Stability	High	Low
Costs	Negligible	Medium-High
Manufacturing	Simple	Complex

This study continues with a more detailed investigation about the passive TES configuration using the sensible material. This is way aspects like economical convenience, simplicity of material involved, and long-term work life are fundamental for a new technology developing. Beside this analysis represents the first investigation about the integration of TES in the STBC plant, so that it can be considered a more conceptual and starting analysis rather than design one. Obviously in the future a more detailed CFD analysis about passive TES storage with PCM can be conducted, favouring the plant practical aspect.

## 4.2 Plant layout

For the STBC application two plant layout options are proposed, where the TES is placed in series and parallel way. The Figure 4.10 shows a scheme of the series layout where the air path is underlined during idle, charging and discharging cycle.

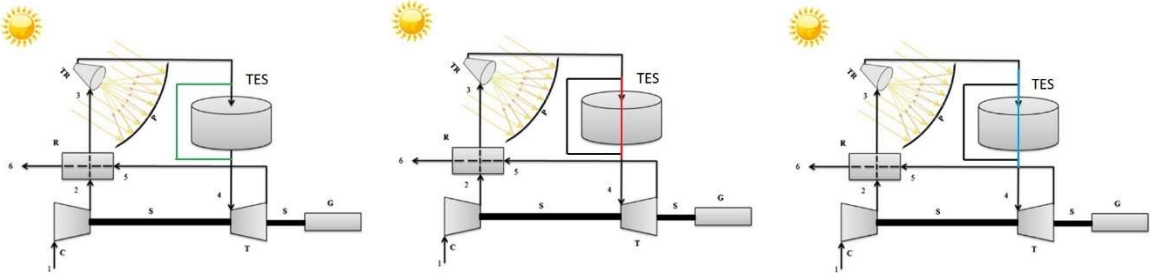


Figure 4.10: Series Layout: air path during idle, charging, discharging phases

Surely this is a very simple plant solution, easy to build, cheap with less temperature and pressure drops. But it needs to have a negligible temperature stratification of the TES packed-bed after the charging. The air flows through the storage in the same direction during charging and discharging, so in case of considerable temperature difference in the TES height, the heat exchange could occur in low quality.

To overcome this last issue, the layout in Figure 4.11 is introduced. The heat is exchanged efficiently during the discharging. On the other hand, the plant is very complex, and great temperature and pressure drops occur, since longer pipes have to be gone through.

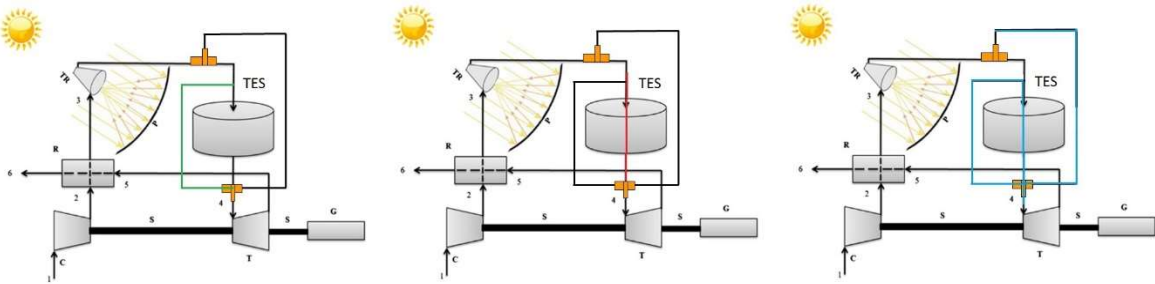


Figure 4.11: Parallel Layout: air path during idle, charging, discharging phases

Anyway, this is the layout selected for the plant configuration in this research: it has been chosen to pay major attention to the quality heat exchange aspect, considering that this study is still at conceptual stage which is so far from the practical one.

An alternative parallel layout is shown in the Figure 4.12. It can be considered when the passage through the receiver during the discharging phase has to be avoided. This situation occurs when the irradiance is too low and  $\dot{Q}_{net, receiver}$  is a negative term. It means that the just heat losses occur passing through it.

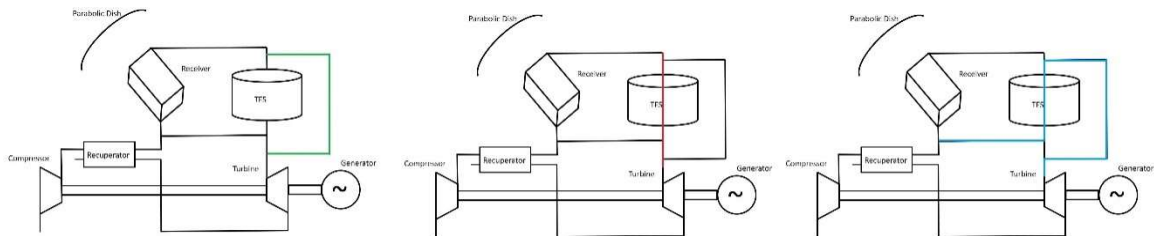


Figure 4.12: Alternative parallel layout: idle, charging, discharging



## 5. Sensible Packed-bed TES analysis

### 5.1 Literature review

---

Among the various strategies to thermally store energy, the most suitable for the STBC application is the passive storage technology, which is the cheapest one, as the previous results show. In this system TES the HTF can provide/absorb energy flowing through the storage material, which can store/release it in a sensible or latent form. The most common passive TES configuration is the packed-bed one: it represents not only a valuable alternative to the most commonly exploited two-tank configuration in conventional CSP plants, but also an interesting energy storage facility in high-temperature industrial processes and compressed air energy storages (CAES). A lot of authors have worked on the modelling of packed bed thermal energy storages, whereby modelling shall support the design of the thermal energy storage and also its integration into the energy system or the industrial plant under investigation. Sensible heat storage is still dominating in practical applications of high-temperature TES. Allen [29] has presented a cost-optimum method useful to determine the particle size and bed length of a rock bed, by fixing the Biot number, Anderson [30] has used simplified one-equation thermal model for the behaviour to simulate a packed bed  $\alpha$ -alumina as solid storage material and air as the heat transfer fluid, successfully predicting the thermocline behaviour over time. Zanganeh [31] has studied thermal storage unit immersed in the ground contained by a conical shape tank, which experimentally demonstrated can generate thermocline. Then it has been coupled with a round-the-clock concentrated solar power plant, simulating a multiple 8 h-charging/16 h-discharging cycles.

Anyway, significant research is also done on packed bed TES applying PCM: Felix Regin et al. [32] have developed a packed-bed storage model using the fundamental equations similar to those of Schumann, except that the phase change phenomena of PCM inside the capsules, analysed through the enthalpy method. The equations have been numerically solved in order to simulate a thermal performance analysis of both charging and discharging processes. Differently Pakrouh [33] has considered paraffin wax as the PCM, while water plays the role of HTF, investigating both various inlet temperatures, and capsules' diameter. Another solution is presented by Peng [34] with molten salt as HTF with phase change material (PCM) capsules as the filler. While the phase change phenomena of PCM inside the capsules is analysed by using enthalpy method, the model developed uses the concentric dispersion equations.

### 5.2 Main features

---

Of special interest is becoming the use of a packed bed of rocks as sensible heat storing material and air as heat transfer fluid, such a storage concept which can be incorporated in solar power plants such as STBC. The main advantages are:

- Applicability in a wide temperature range, with limiting temperatures given by the rock's melting point;
- No degradation or chemical instability;
- Very low operating pressure, avoiding the need for complex sealing;
- Direct heat transfer between working fluid and storage material;

- Employing conventional materials of construction that means significantly lower fabrication costs than those for existing storage systems based on molten salts and steam;
- No safety concerns;
- Elimination of chemicals and corrosive materials.

On the other hand, the disadvantages are associated with the larger air mass flow rates and surface area needed due to the lower volumetric heat capacity and thermal conductivity of air as compared to those of the other generic HTF fluid.

### 5.3 Ait-Baha pilot plant:

The rock packed-bed TES is the most common passive TES strategy to cumulate energy in a solar plant. The first industrial-scale CSP pilot plant has been constructed at the Cimar's site (Italcementi group) in Ait Baha (Morocco) is reported as a practical example. This plant has the aim of producing electricity from the waste heat recovery system of the cement factory. The CSP pilot plant is composed of three parabolic trough collectors, characterized by a length of about 200 m, for a total useful aperture area of 6159 m<sup>2</sup>. The CSP plant provides power for 3.9 MW<sub>th</sub> peak to the air-to-diathermic oil heat exchanger of the organic Rankine cycle (ORC) for 2 MW<sub>e</sub> power generation. A 100 MWh<sub>th</sub> TES unit, based on a packed bed of rocks, is exploited to increase the CSP plant capacity factor. A plant scheme is shown in Figure 5.1.

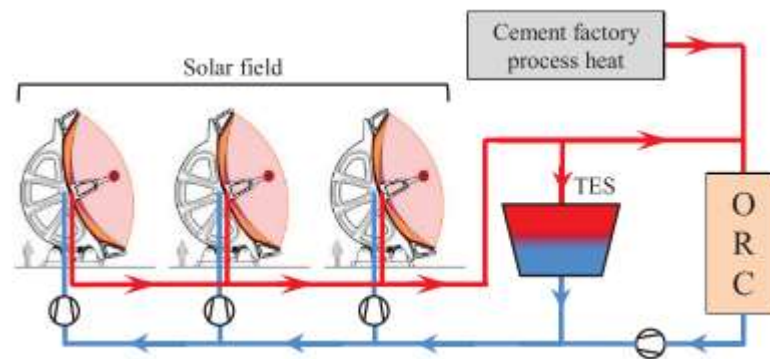


Figure 5.1: Ait-Baha CSP pilot plant layout scheme, from [35]

The HTF, which is air at ambient pressure, enters the solar field at 270°C leaving it at 570°C. A fraction of this high-temperature HTF is fed through the TES while, the remaining part is sent to the power block. The TES unit is designed for daily operating conditions of 10 h of charging followed by 4.5 h of discharging and 9.5 h of idle. To effectively store the resulting amount of thermal energy, a total volume of 381.2 m<sup>3</sup> of sedimentary rocks were positioned into the truncated cone-shaped TES tank, as Figure 5.2 represents.

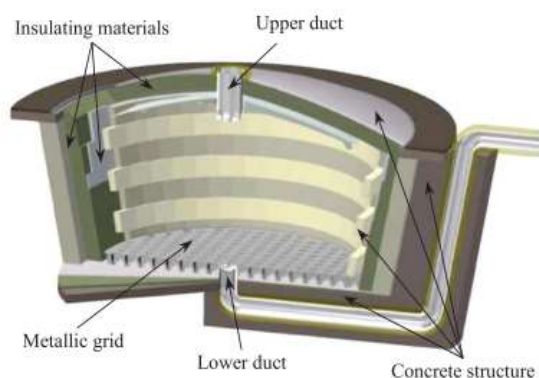


Figure 5.2: Ait-Baha TES 3D CAD model and actual TES unit

It is easy understanding how far this plant is from the STBC application involved in this research. Firstly, the Ait-Baha pilot plant is a large-scale system, since it generates electricity in the MW range, through a wide extension of parabolic linear collector area. So, the TES required is very large, promoting energy cumulation for hundred MW amount. On the contrary, STBC plant in this analysis is a small-scale system, useful to provide power for small communities isolated from the main grid. This is the reason why the power and energy levels involved, can't be compared at all. Furthermore, the coupling with storage occurs indirectly for the former system: air flows through solar collectors and the charging/discharging of packed-bed TES occurs through just a less spillage. Another heat exchanger is used to absorb/release energy from/to the working fluid in the power-block which is oil. Differently, in the STBC application air works as HTF in the TES sub-system and working fluid in Brayton plant as well, leading to a more compact solution without the intermediate heat exchanger. Besides, the spillage of air-flow rate is not allowed in the latter plant, since the current worked by compressor has to be the same of the turbine one, being an only-shaft system. Anyway, the Ait-Baha pilot plant is the actual demonstration of how the packed bed of rocks is a very promising technology to boost the power production of a solar plant, when air is employed like HTF.

## 5.4 Modelling methodology

Concerning the model building, the research work of Hänchen et al. [35] has been considered as starting point. Here 1D two-phase energy conservation equations for combined convection and conduction heat transfer have been formulated and solved numerically in order to simulate charging/discharging cycles. Then a parameter study of the packed bed dimensions, particle diameter, fluid flow rate, and solid phase material has been carried out to estimate the charging/discharging characteristics, overall thermal efficiency, daily cyclic operation, and capacity ratio.

The domain consists of the inside of a cylindrical tank, which is divided into a solid part, a packed bed of particles, and the fluid flowing through the void space surrounding the particles. In this analysis a

two-phase transient model is formulated, considering convection heat transfer and heat losses. The assumption made are:

- solid and fluid phases;
- conduction heat transfer among solid particles neglected;
- 1D Newtonian plug flow;
- constant solid heat capacity of uniformly packed bed;
- temperature gradient in radial direction neglected;
- uniform temperature particles, as justified by  $Bi \leq 1$ ;
- no mass transfer;
- no internal heat generation;

The governing unsteady energy conservation equations are:

- For the fluid phase:

$$\frac{\partial T_a}{\partial t} + \frac{G}{\rho_a c_a} \frac{\partial T_a}{\partial x} = \frac{h_v}{\rho_a c_a \varepsilon} (T_s - T_a) + \frac{UD\pi}{\rho_a c_a \varepsilon A} (T_{inf} - T_a) \quad 5.1$$

- For the solid phase:

$$\frac{\partial T_s}{\partial t} = \frac{h_v}{\rho_s c_s (1 - \varepsilon)} (T_a - T_s) \quad 5.2$$

In these equations, some terms present the subscripts  $a$  or  $s$  which are respectively referring to air and rocks conditions.

Overall the terms are:

- Temperature,  $T$  [K];
- Density,  $\rho$   $\left[\frac{kg}{m^3}\right]$ ;
- Specific heat,  $c$   $\left[\frac{J}{kg-K}\right]$ ;
- Air flow-rate,  $G$   $\left[\frac{kg}{s}\right]$ ;
- Void friction,  $\varepsilon$  [–];
- Surrounding temperature,  $T_{inf} = 293$  [K];
- Volumetric heat transfer coefficient between fluid and particles,  $h_v$   $\left[\frac{W}{m^3K}\right]$  defined:

$$h_v = 6 \frac{1 - \varepsilon}{d_p} \alpha_p \quad 5.3$$

as a function of the particle to fluid convective heat transfer coefficient  $\alpha_p$   $\left[\frac{W}{m^2K}\right]$ , equal to:

$$\alpha_p = \frac{700}{6(1 - \varepsilon)} G^{0.76} d_p^{0.24} \quad 5.4$$

- Overall heat transfer coefficient through the wall,  $U \left[ \frac{W}{m^2 K} \right]$ , supposed constant for simplicity, following data from [35]:

$$U = U(T = 523 \text{ K}) = 0.678 \left[ \frac{W}{m^2 K} \right] \quad 5.5$$

The initial conditions for the single charge cycle are:

$$T_a(t = 0) = T_s(t = 0) = T_{inf} \quad 5.6$$

The boundary conditions are:

- for the fluid phase:

$$T_a(x = 0) = T_{in} \quad 5.7$$

$$\frac{\partial T_a(x = H)}{\partial x} = 0 \quad 5.8$$

- for the solid phase:

$$\frac{\partial T_s(x = 0)}{\partial x} = \frac{\partial T_s(x = H)}{\partial x} = 0 \quad 5.9$$

## 5.5 Computational settings

The governing equation 5.1 and 5.2 require a combinations of space-time discretization to be solved. Time discretization has been obtained dividing the whole analysis period in M time instants, through the time step value  $\Delta t$ . Similarly, space discretization consists of N layers of the tanks, resulting from the spatial division through  $\Delta x$ . To clarify the concept, the space discretization is shown in Figure 5.3.

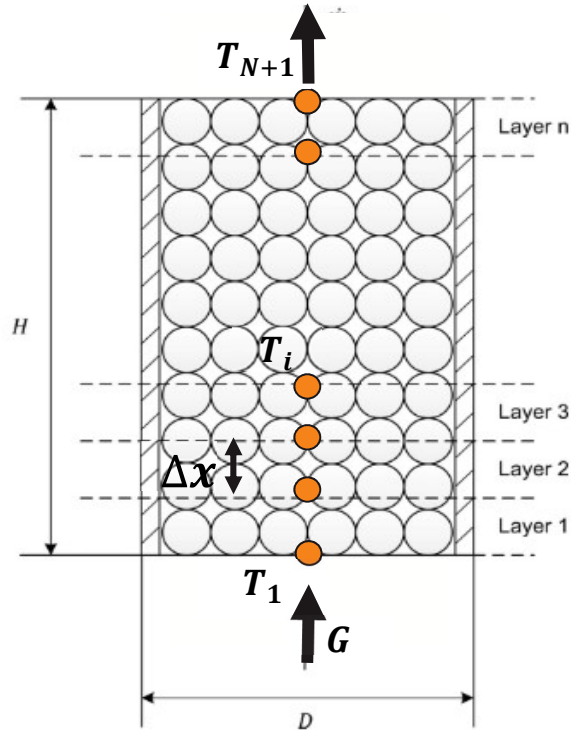


Figure 5.3: Spatial discretization of the storage for modelling

The equations have been discretized by applying the explicit-forward difference scheme in time and the upwind difference scheme in space. Considering this solving strategy, the air temperature for each  $j$ -th time and each  $i$ -th layer  $T_a(i, j)$  has been evaluated as a function of the temperature at same time but at previous layer  $T_a(i - 1, j)$  and the temperature at the same layer but at previous time  $T_a(i, j - 1)$ . For the solid phase temperature for each  $j$ -th time and each  $i$ -th  $T_s(i, j)$  is just function of the one at same layer but at previous time  $T_s(i, j - 1)$ . The flow chart about computational procedure adopted it is available in Figure 5.4.

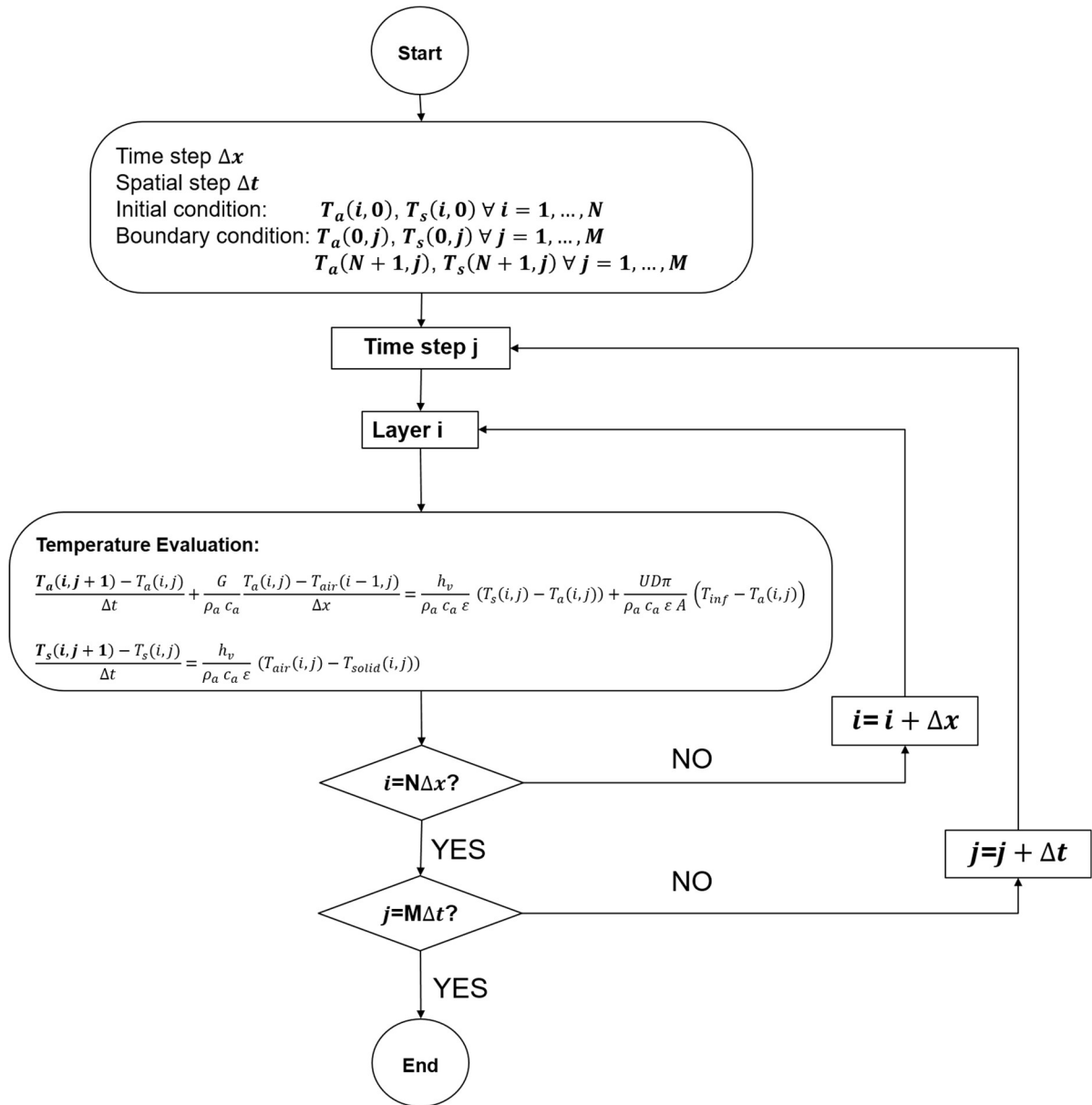


Figure 5.4: Flow chart of computational procedure to solve TES modeling equation

## 5.6 Results about validation of TES model

The validation of the present numerical model is performed by comparing the results with Hänchen et al. [35] research. The model adopted is the same of the reference one, except for the heat losses evaluation: the former estimates the losses using a constant value of the overall heat transfer coefficient through the wall  $U$ , for simplicity. In the latter Hänchen et al. [35] have defined it as function of inner/outer convective heat transfer coefficient ( $\alpha_i$ ,  $\alpha_{ao}$ ) and stratification of TES tank, in terms on material conductivity ( $\lambda_j$ ) :

$$\frac{1}{U} = \frac{1}{\alpha_i} \frac{d_r}{D} + \frac{D}{2} \sum_{j=1}^n \frac{1}{\lambda_j} \ln \frac{d_{j+1}}{d_j} + \frac{1}{\alpha_{ao}} \frac{d_r}{d_{n+1}} \quad 5.10$$

Furthermore the literature study [35] haven't neglected the conduction phenomena among the solid rock particles, which is expressed from the second term in the right-side equation:

$$\frac{\partial T_s}{\partial t} = \frac{h_v}{\rho_s c_s (1 - \varepsilon)} (T_a - T_s) + \frac{k_{s,eff}}{\rho_s c_s (1 - \varepsilon)} \frac{\partial^2 T}{\partial x^2} \quad 5.11$$

The model validation has been carried out through the simulation of the charging process, considering various duration. The results are shown in Figure 5.5 and Figure 5.6 in terms of air and solid temperature, with the estimation of percentage error, particularly of mean and maximum one:

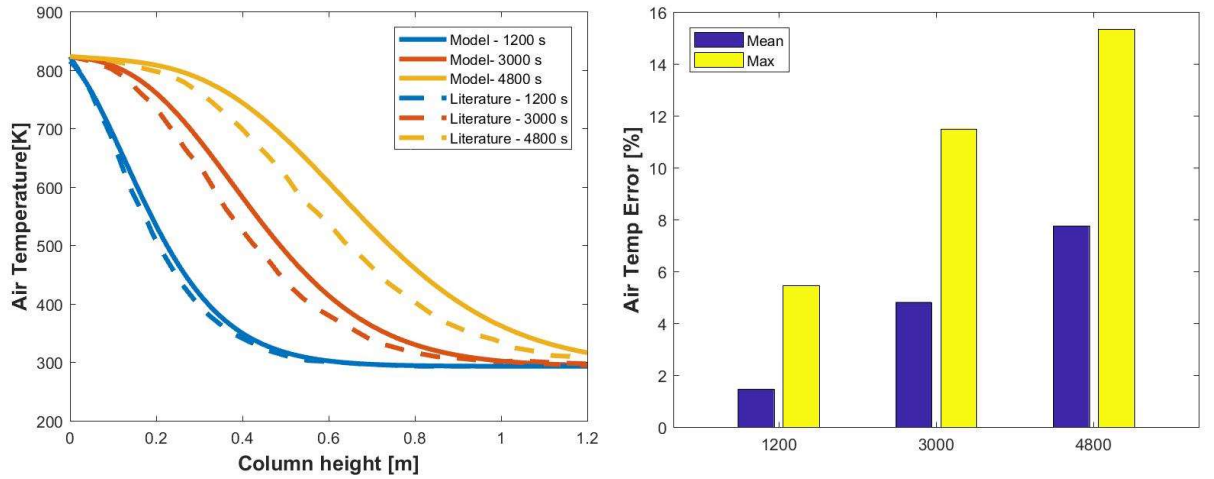


Figure 5.5: Validation results about air temperature and percentage relative error

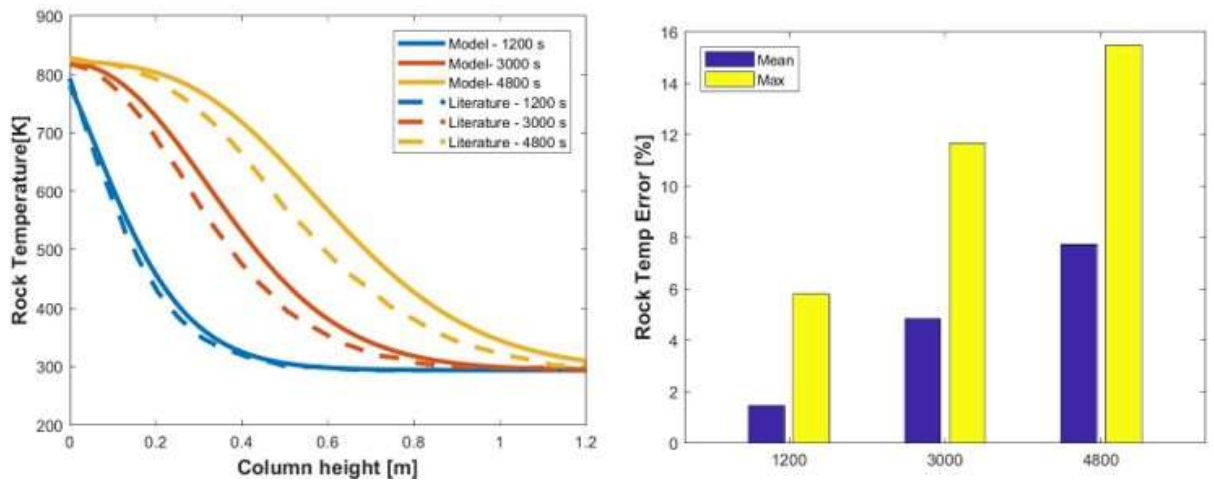


Figure 5.6: Validation results about rock temperature and percentage relative error

As it is possible to notice, the built model performs different results from literature at the increasing of the charging process duration, owing to all the simplifications made for more simplicity. Anyway, the percentage error is very low: on average it is under the 10% and its maximum is equal to 16% in the worst case. So, the model has been considered a good tool for a more detailed analysis about the integration of TES in the STBC plant, able to produce reliable and realistic results.



## 6. Introduction of rocks packed-bed TES in the STBC plant

---

The investigation about the TES functioning in the STBC plant has been carried out basically adding the storage sub-model in the plant one. This operation has been not a simple “copy & paste” work, since both the models have been built using different software. Anyway, the link between MatLab and EES has been set through the EES Macro file (.emf). A macro is a set of instructions to EES that are read from an ASCII file or from the EES Macro Window, useful to instruct EES to automatically open a file and solve the equations system. So, using MatLab as basic platform, EES can be started and directed to run a predefined macro file, calling the plant model. This starting concept about the communication between the two programs has been progressively improved. Dynamic Data Exchange (DDE) function has been used to start/close the linking channel, and clipboard function has been fundamental to manage the data input/output exchange.

### 6.1 Starting hypothesis and inputs for the model

---

Similarly, to the previous study about the best control strategy definition (see section 3.3), a quasi-steady-state analysis is performed, considering the time variation as a sequence of consecutive steady-states. Transitory effects are neglected.

Concerning the solar power input varying during the day, the actual Pretoria’s irradiance trend considered is the same of the preliminary study. It is again depicted in Figure 6.1, for reader convenience.

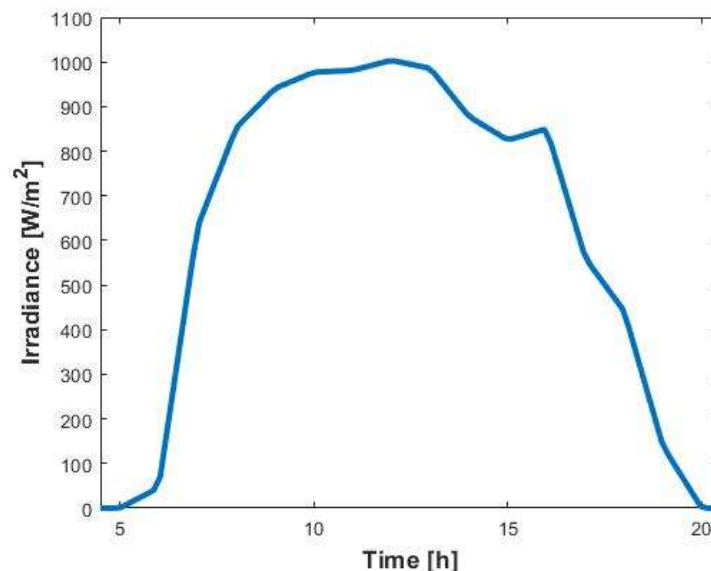


Figure 6.1: Actual daily irradiance measured in Pretoria on 22nd January 2019

In terms of pressure and temperature, the common surrounding conditions of Pretoria are supposed:

Table 6.1: Pretoria's surrounding conditions

Environment	Data
$p_1$ [Pa]	86000
$T_1$ [K]	300.2

The plant inputs for the model are listed in Table 3.5, divided for each component. They have been chosen from some previous works in the literature, as it has been well explained in Section 3.

Table 6.2: Input for STBC plant model

Receiver:	Data
Cavity geometry [ $m^2$ ]	0.25 x 0.25
Depth Receiver $h_{rec}$ [m]	0.5
Steel Tube Emissivity [-]	0.7
Collector:	Data
Diameter [m]	4.8
$\eta_{optical}$ [-]	0.95
$\eta_{reflec}$ [-]	0.85
Recuperator:	Data
Width [m]	0.5
Length [m]	0.6
Height channel [m]	0.002
Number of channel pairs [-]	40
Thickness plate [m]	0.001
Operating Condition:	Data
Air flow rate G [kg/s]	0.06
$\beta_{compressor}$ [-]	1.5
$\beta_{turbine}$ [-]	1.5
Turbocharger Group	Data
$\eta_{is,compressor}$ [-]	0.62
$\eta_{is,turbine,MAX}$ [-]	0.62
$\eta_{mech,compr}, \eta_{mech,turb}$ [-]	0.97
Rotor speed [rpm]	180000

TES model needs some input too, which are available on Table 6.3. Talking about storage sizing, the value of diameter D and height H have been selected in according to the results of the previous analysis (see section 4.1.3):

$$V_{TES} \approx 800 [l] \quad 6.1$$

and the practical rule, through which:

$$\frac{H}{D} \approx 3 \quad 6.2$$

While the proprieties of storage material are the Steatite's ones, which is a type of metamorphic rock, particularly suitable for the heat cumulation. The particles diameter  $d_p$  as well as the void friction  $\varepsilon$  values have been inspired by Hänchen's research [35].

Table 6.3: Input for TES sub-model

TES sizing	Data
$D$ [m]	2
$H$ [m]	0.75
$V$ [l]	883
Storage material	Data
$cp_s$ [J/kg-K]	2680
$\rho_s$ [kg/m <sup>3</sup> ]	1068
$d_p$ [m]	0.02
$\varepsilon$ [-]	0.4

Concerning the initial condition of storage packed bed, a certain stratification across the TES height has been supposed, which is depicted in Figure 6.2. It is known that the TES performance is enhanced by thermal stratification. Stratification in the storage tank results from buoyancy effects cause by density differences in the storage. The hotter fluid rises to the top and the colder fluid falls to the bottom. Thus, a thermal gradient exists between the top and the bottom of the storage tank and the region between these two regions should be kept at a minimal possible thickness in order to improve efficiency of the systems.

Hence, the study has been conducted as if the storage had reached the cyclic steady state condition, obtained at the end of the charging period, after a series of charge and discharge cycles. The situation of a charging starting from a tank initially at ambient temperature, has been neglected.

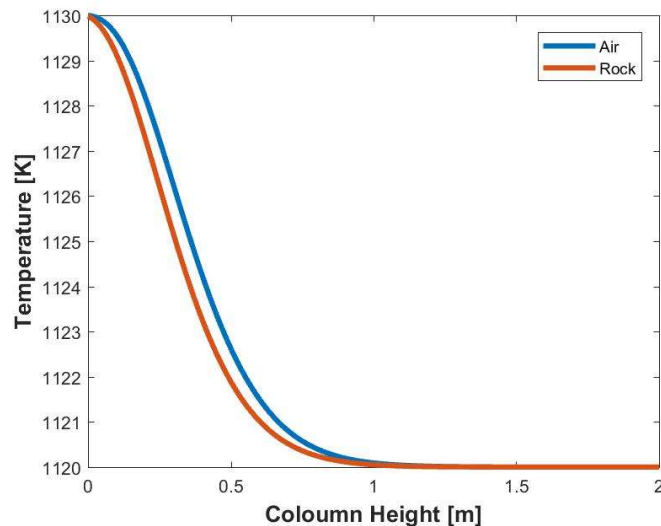


Figure 6.2: Initial condition of the TES model: a storage packed-bed stratification

About the computational settings, mesh and time-step independence for the model have been found by systematically decreasing values for each of the mesh size and time step until the solution

minimally changes and can be performed independently of each other. The Courant–Friedrichs–Lewy (CFL) condition provides a guide for choosing a timestep in an implicit solution by evaluating cell size and local velocity to ensure a fluid element does not pass through more than one element ( $C = u \Delta t / \Delta x$ ). This is a minimum requirement for explicit CFD solutions. All these considerations have led the following values:

$$\Delta x = 0.013 [m] \quad 6.3$$

$$\Delta t = 0.01 [s] \quad 6.4$$

## 6.2 Results

---

The functioning of the STBC plant with rock packed-bed TES integration has been simulated over the time and this section will present results and some discussions. Overall, the reader has to consider that this investigation leads to the analysis of the TES performance working through not so common conditions. Particularly, the storage charging and discharging phases will occur through a variable inlet temperature. This is due to the choice of keeping constant the air flow rate in the plant, to promote the steady-state working condition for the turbocharger group, while the heat input due to the available daily irradiance, is surely variable. This is a condition which has not widely analysed in the literature so far, since the greater part of TES modelling studies as well as experimental activities, use to consider an unvarying temperature. Hence, this analysis is even more interesting since allows the understanding of how this variation influences the TES performance, in terms of stratification temperature of packed-bed.

Two scenarios will be presented. In the first one the heat losses through the wall have been neglected, in order to focus the investigation just on the convective heat transfer mechanism between air and particles of rock. So that Equation 5.1, regarding the energy balance for the fluid phase becomes:

$$\frac{\partial T_a}{\partial t} + \frac{G}{\rho_a c_a} \frac{\partial T_a}{\partial x} = \frac{h_v}{\rho_a c_a \varepsilon} (T_s - T_a) \quad 6.5$$

In the second scenario heat losses are considered, making the analysis more realistic: the TES works at very high temperature, so that the losses will surely occur. So that Equation 5.1 is modelled, using a constant value of overall heat transfer coefficient through the wall  $U$ :

$$U = 0.2 \left[ \frac{W}{m^2 K} \right] \quad 6.6$$

## 6.2.1 1<sup>st</sup> Scenario: Heat losses neglected

### 1<sup>st</sup> Design phase

As it has been previously modelled (see Section 3.3), the so-called “Design Phase” occurs when the available irradiance is included by the extreme allowable values. These are:

$$Irr_{design,MIN} = 640 \left[ \frac{W}{m^2} \right] \quad 6.7$$

in correspondence of that value, the plant can generate positive mechanical power ( $P_u > P_{ass}$ ), ensuring a certain electricity amount for the user. This moment happens in the first hours of morning (at 7:00 am) and it indicates the start of STBC plant functioning. On the other hand, the end of this phase happens at 8:20 am, when the bottom extreme irradiance value is reached:

$$Irr_{design,MAX} = 900 \left[ \frac{W}{m^2} \right] \quad 6.8$$

Since the inlet turbine temperature becomes higher than the allowed value, the charging of TES must start, in order to allow the continuous functioning of STBC plant, without any damages of the turbocharger group. Obviously, during the Design Phase the TES is in idle mode.

### Charging

The charging phase of TES is the best control strategy for the plant. It promotes its continuous functioning during the overload phase keeping the turbine inlet temperature near the design value, without any waste of the surplus energy. In the simulation, the charging starts at 8:30 a.m., when:

$$Irr > Irr_{design,MAX} \quad 6.9$$

and so, the STBC model has been run with the TES one. This phase continues until the value of energy stored in each time step is positive, which means that the air flow rate is still able to provide energy for the cumulation. Energy stored on the generic  $j$ -th is evaluated like:

$$Energy\ stored\ (j) = \int \rho_s c_s (1 - \varepsilon) A (T_s(j) - T_s(j - 1)) dx \quad 6.10$$

Considering the spatial discretization, Eq. 6.10 becomes:

$$Energy\ stored\ (j) = \sum_{i=1}^{N+1} \rho_s c_s (1 - \varepsilon) A (T_s(i, j) - T_s(i, j - 1)) \quad 6.11$$

The cumulative energy stored in the storage is depicted in Figure 6.3.

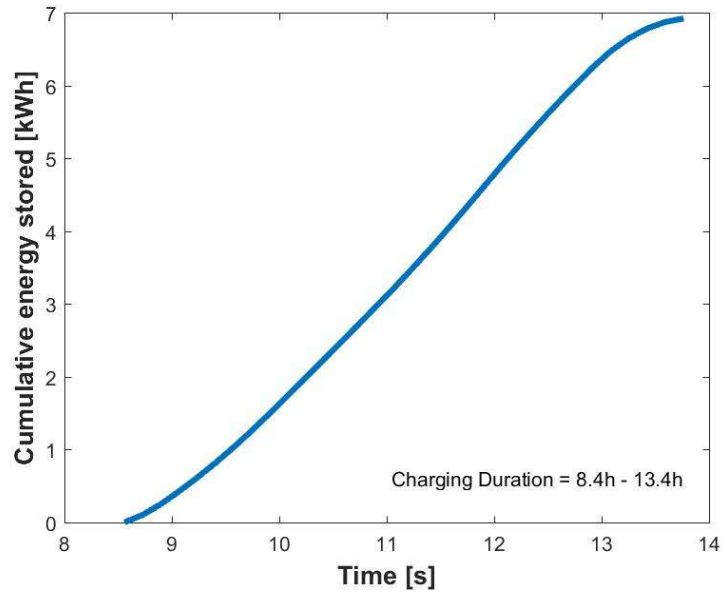


Figure 6.3: Cumulative energy store in TES during the charging process

overall, the amount of cumulated energy is:

$$Energy\ stored_{tot} = 6.9 [kWh] \quad 6.12$$

As it was expected, the turbine inlet temperature and the power generation keep a constant value: observing the results in Figure 6.4, the values are:

$$T_7 = [1120 \div 1137] [K] \quad 6.13$$

$$P_u = [998 \div 1058] [W] \quad 6.14$$

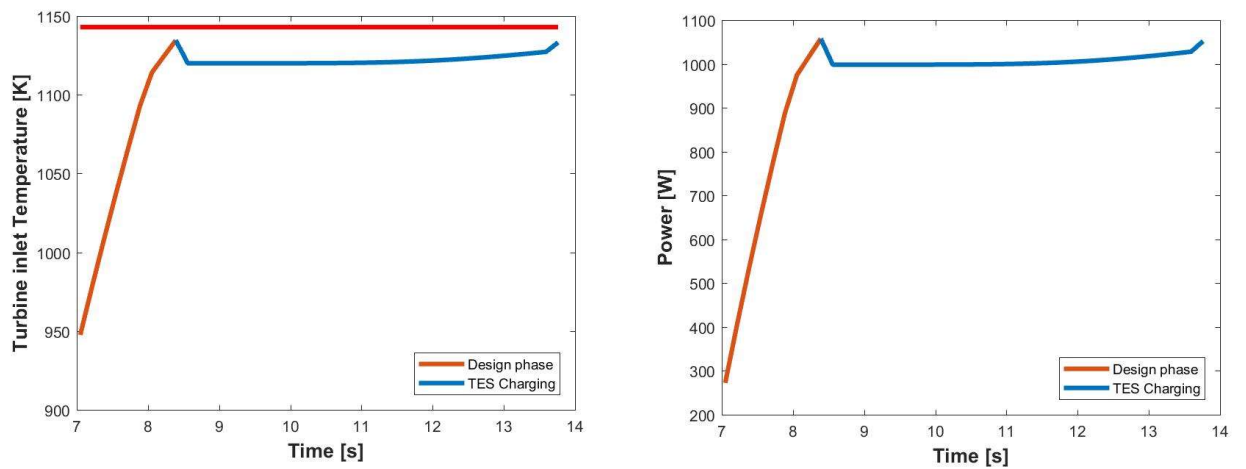


Figure 6.4: Turbine inlet temperature and power production during the design and charging phase

Results about the temperature stratification in the rock packed-bed is presented in Figure 6.5.

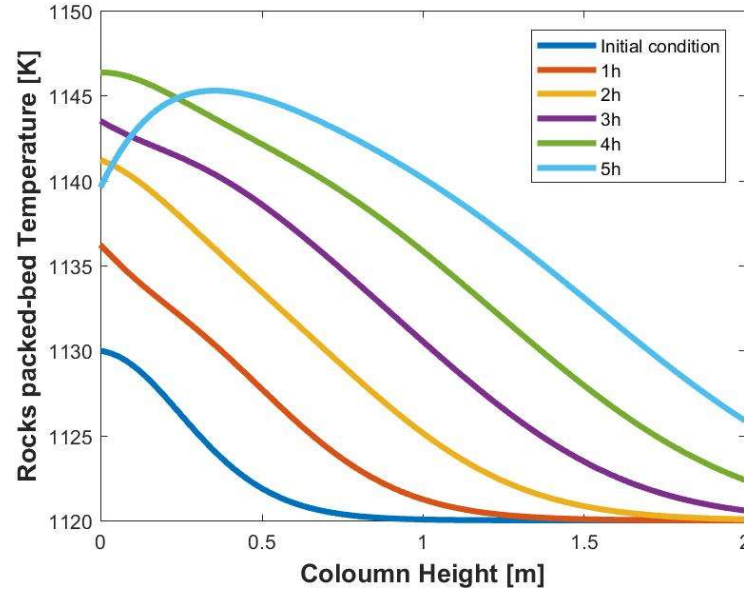


Figure 6.5: Temperature stratification in the rock packed bed during the charging

Here it is possible to notice the effects of a varying inlet temperature in the storage during the charging. The extreme values of the stratification are not constant, too: during the first four hours of process they progressively increase, while during the last one the temperature trend undergoes a relevant variation. Due to the decreasing of the inlet temperature occurring after the maximum irradiance value available during the day, the first layers of storage decrease their temperature. On the whole the storage is able to cumulate energy, even if the stratification shows this instable behavior, which negatively influences the TES performance.

## 2<sup>nd</sup> Design Phase

After the charging, the STBC functions without the flowing of air flow-rate through the TES, since the irradiance available is still high enough. Concerning the duration of this second Design Phase, it depends on the adopted power production strategy, in according to the user requirements. There are many options which basically consist of the beginning of the next discharging process. In the case of a user who doesn't admit the power generation decreasing, even it occurs during the design time range. Otherwise, there is the possibility to accept a lower production, choosing the best DNI value from what starts the discharging, leading to a greater increasing of the plant working hours. In this research, the criteria chosen to indicate the discharging start has been given in terms on power production:

$$P_{u,Design\ Phase} < P_{u,design} * 0.9 = 900 [W] \quad 6.15$$

So, when the power generated during the 2<sup>nd</sup> Design Phase decreases by 90 percent compared to the design value, the discharging starts. In this way, the power production is kept almost constant, for most of the time.

## Discharging

The discharging process starts at the end of the 2<sup>nd</sup> Design phase and it is considered finished when the energy cumulated in the storage is totally used. This is visible in Figure 6.6

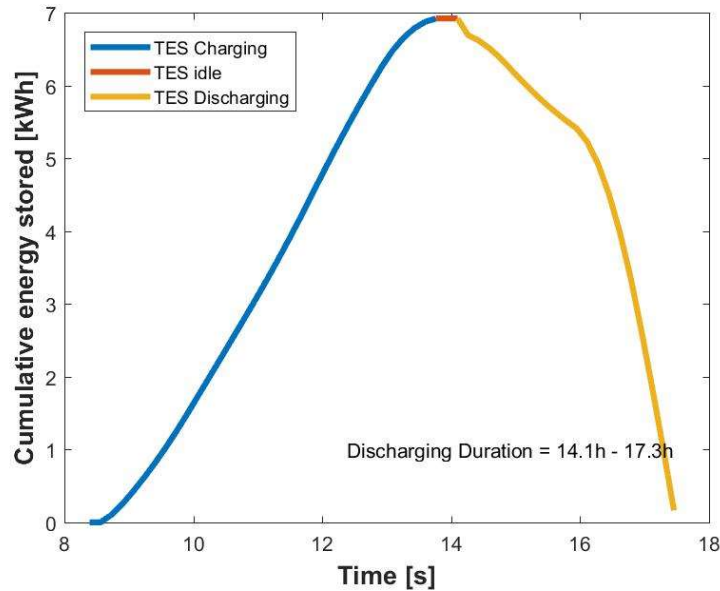


Figure 6.6: Cumulative energy in the storage during the working hours

The discharging process is 3 hours long. The air flow rate flows in the opposite direction through the tank compared to the one occurred during the charging, promoting the best heat exchanger between fluid and particles. Obviously, it is only possible adopting a parallel plant layout.

The power production and the inlet turbine temperature trend are shown in Figure 6.7.

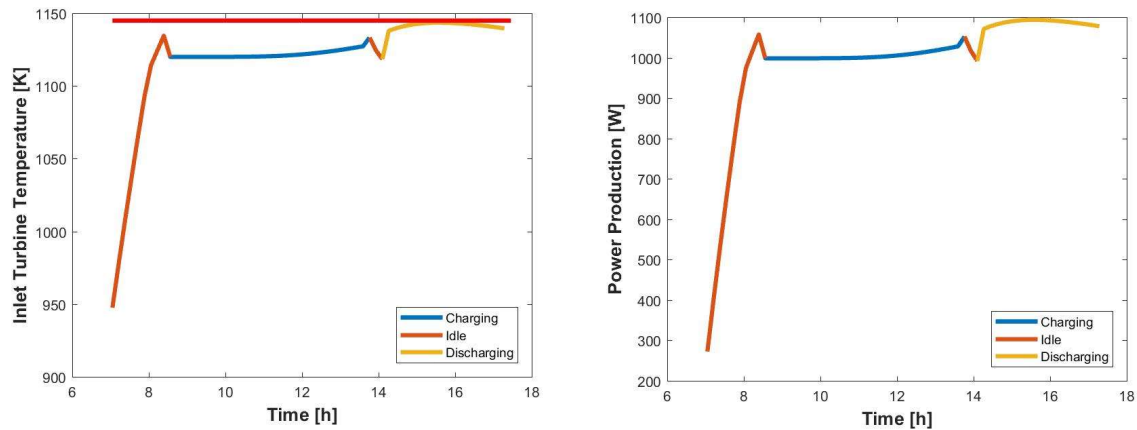


Figure 6.7: Turbine inlet temperature and power production during the all working hours

The power generation increasing is directly linked to the higher temperature at TES outlet, which is the same of the inlet turbine. That increasing is mainly due to the previous charging phase, when there has been a progressively increasing of the first layer temperature in the tank. Anyway, the maximum limit is never passed over.

Concerning the temperature stratification of the particles, the results are shown for the first two-hours discharging (Figure 6.8) and for the last one (Figure 6.9).



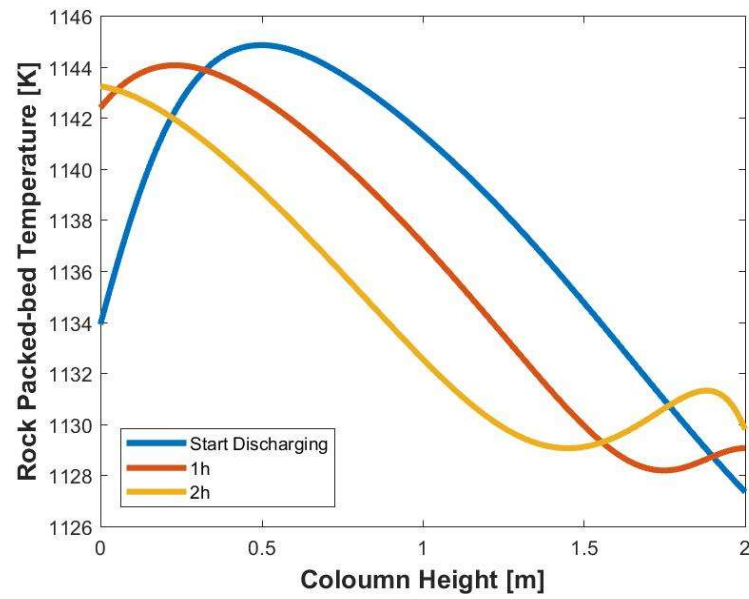


Figure 6.8: Temperature stratification in the rock packed bed during the first two discharging hours

For the first two discharging hours, the packed-bed temperature decreases following an almost regular trend, mainly provided by a translation of the starting one. This is since the inlet TES temperature is quite constant at the end layer. There are just some fluctuations at the end layers, which are perfectly expected considering the fluctuations on the first ones. The situation suddenly changes during the last discharging hour, when there is a sharp decreasing of the air temperature, leading to the depicted trend:

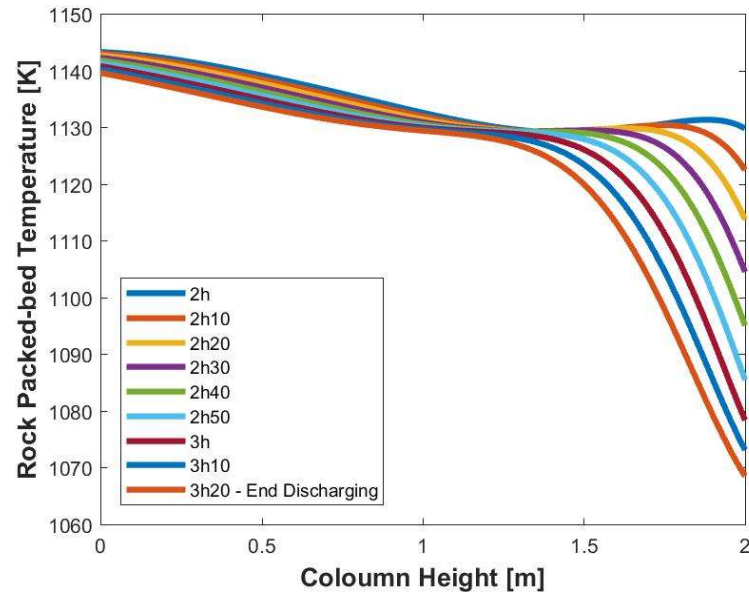


Figure 6.9: Temperature stratification in the rock packed bed during the last discharging hour

The end discharging curve should be the starting one for the next charging-process. In the future research could be very interesting investigate about the stratification temperature evolution for a series of multiple charging-discharging processes.

As it is possible to notice in Figure 6.10, the plant efficiencies trends are the expected one.

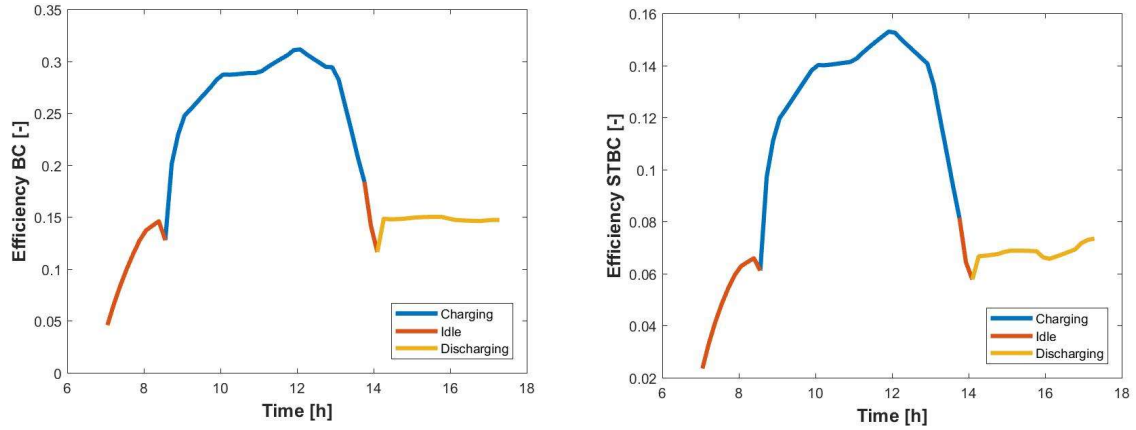


Figure 6.10: Plant efficiencies during the all working hours

The increasing recorded during the charging is due to the total exploiting of the surplus sun power available, useful to charge the TES, while the power production is constant, near the design value. During the discharging the lack of irradiance is filled by the energy extracted from the storage, promoting a constant power production.

All the analysed phases are reported here, with their features:

Table 6.4: Summary about the various phases of the whole STBC plant daily cycle, neglected the heat losses

Phase	h start	h finish	Irr [W/m <sup>2</sup> ]	Power [W]	$T_7$ [K]	$\eta_{STBC}$ [%]
1 <sup>st</sup> Design	7:00	8:30	[640÷902]	[272÷998]	[948÷1135]	[2.3÷6.1]
Charging	8:40	13:40	[902÷1002]	[998÷1058]	[1120÷1137]	[8.1÷15.1]
2 <sup>nd</sup> Design	13:50	14:00	[872÷885]	[992÷1017]	[1184÷1124]	[6.4÷5.8]
Discharging	14:10	17:30	[486÷864]	[1071÷1094]	[1120÷1143]	[6.5÷7.3]

## 6.2.2 2<sup>st</sup> Scenario: Heat losses considered

### 1<sup>st</sup> Design phase

For this phase, all previous considerations have been adopted.

#### Charging

The cumulative energy stored in the storage is depicted in Figure 6.11.

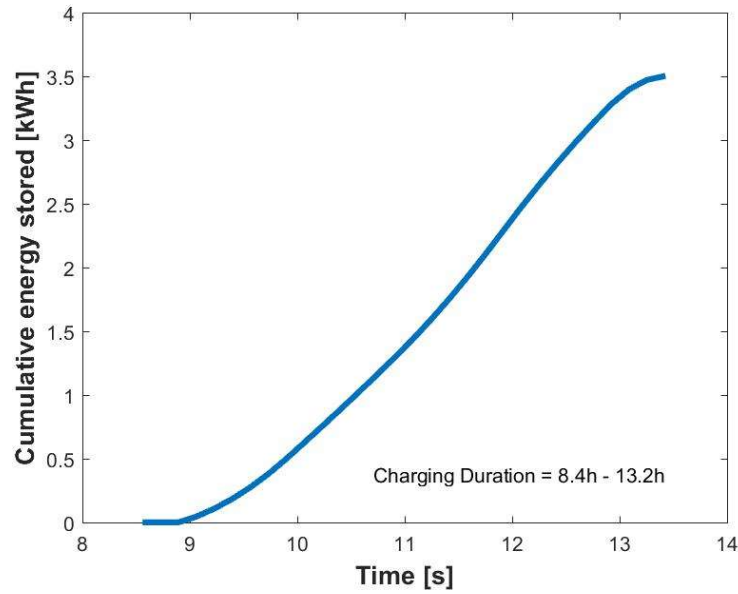


Figure 6.11: Cumulative energy store in TES during the charging process

The amount of cumulated energy is almost halved, compared to the ideal case:

$$Energy\ stored_{tot} = 3.5 [kWh] \quad 6.16$$

Furthermore, it is possible to notice that for the about the first 30 minutes from charging start, there isn't an energy cumulation. This is due to the heat losses presence which makes insufficient the energy amount brought from the air flow rate during that time range. This is true also for the last 20 minutes of this phase, which aren't considered useful for the charging.

As it was expected, the turbine inlet temperature and the power generation keep a constant value: observing the results available in Figure 6.12, the values are:

$$T_7 = [1115 \div 1119] [K] \quad 6.17$$

$$P_u = [978 \div 996] [W] \quad 6.18$$

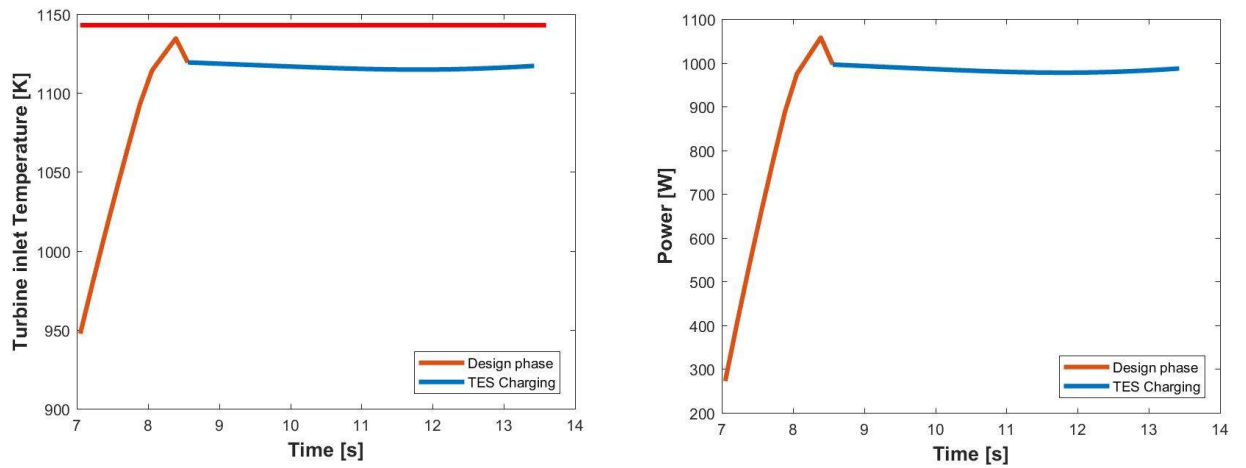


Figure 6.12: Turbine inlet temperature and power production during the design and charging phase

The results about the temperature stratification in the rock packed-bed is presented in Figure 6.13.

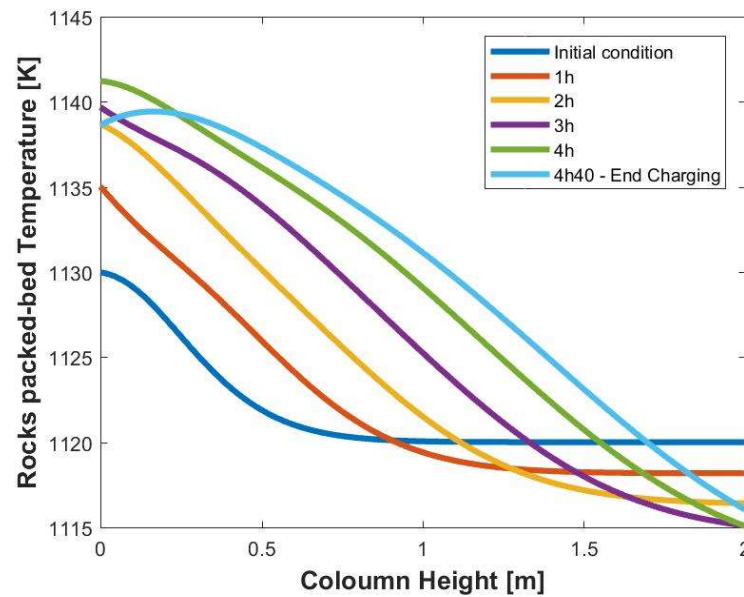


Figure 6.13: Temperature stratification in the rock packed bed during the charging

The picture shows not only the effects of a varying inlet temperature for the storage charging, which is the same of the already discussed case, but also the influence of the heat losses. In fact, these cause the decreasing of rocks temperature on the last layers for all charging hours. This is the reason why the amount of energy of the air flow rate is not always enough to make the charging possible.

## 2<sup>nd</sup> Design Phase

For this phase, all previous considerations have been adopted.

## Discharging

The discharging process starts at the end of the 2<sup>nd</sup> Design phase and it is considered finished when the energy cumulated in the storage is totally used. This is visible in Figure 6.14.

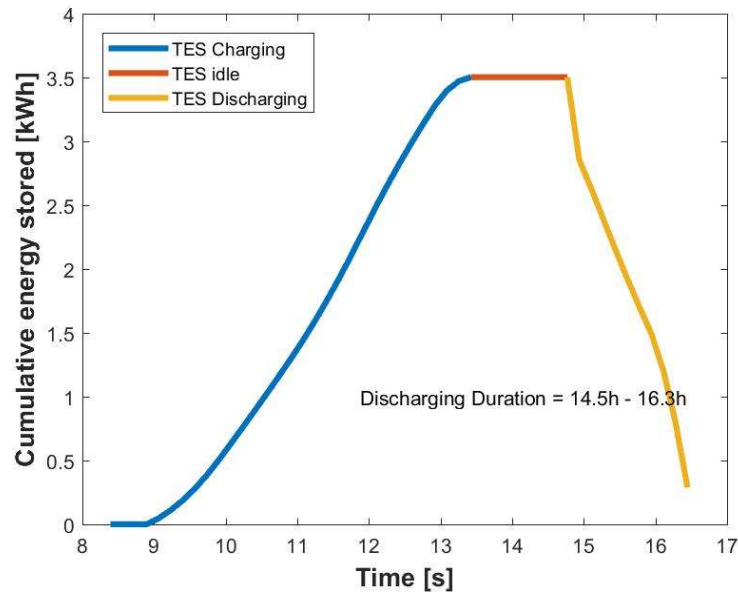


Figure 6.14: Cumulative energy in the storage during the working hours

On one hand the 2<sup>nd</sup> Design phase increases its duration, thanks to the stop of TES charging occurred at relatively greater irradiance. On the other hand, the discharging process is helped, since it is less than half past hour long.

The power production and the inlet turbine temperature trend are shown in Figure 6.15.

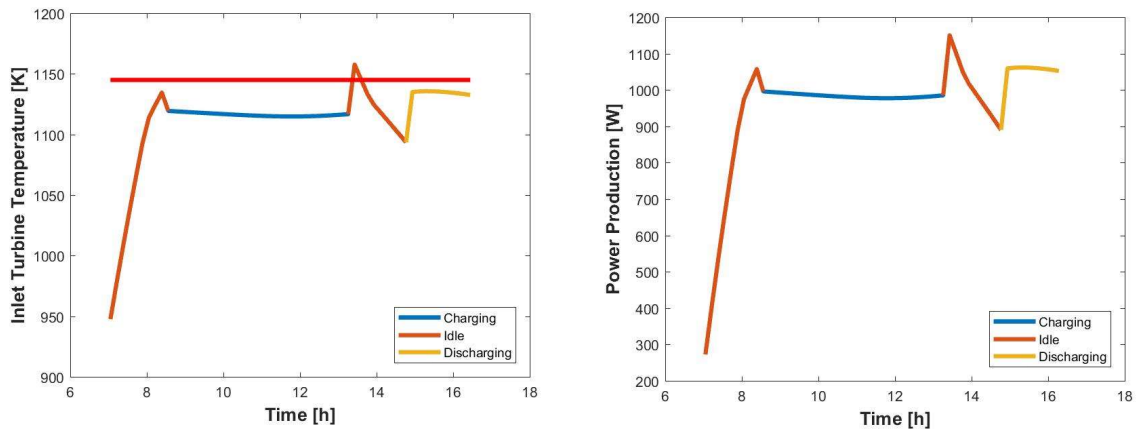


Figure 6.15: Turbine inlet temperature and power production during the all working hours

The stop of charging during the overload phase leads to have an increasing of the turbine inlet temperature, over the maximum value allowable. This fact can be considered acceptable at this study stage, since the main goal of the analysis is the investigation about TES performance. Anyway, the reader has to consider that the overheating of working fluid causes the decreasing of the turbine working-life and not an immediate break.

Concerning the temperature stratification of the particles, the results are shown for the first hour discharging (Figure 6.16) and for the last one (Figure 6.17).

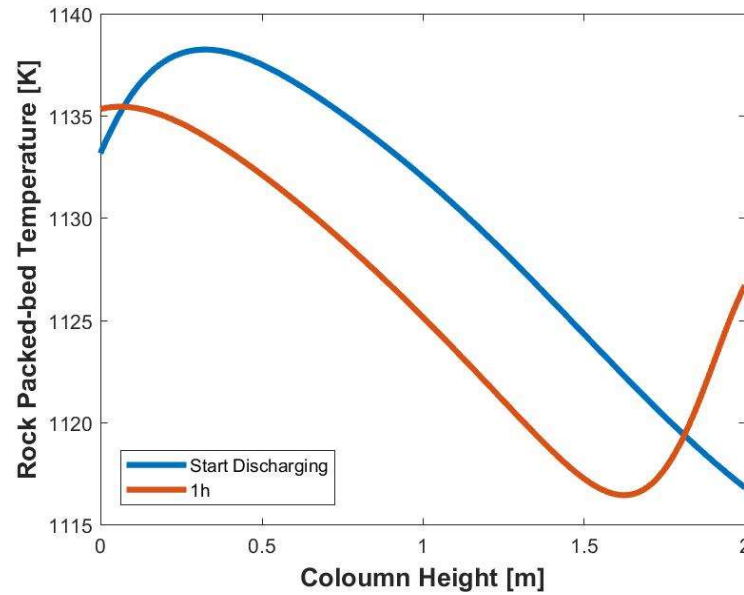


Figure 6.16: Temperature stratification in the rock packed bed during the first two discharging hours

Similarly, to the previous case, the first discharging hour, is characterized by a decreasing regular trend of the packed-bed temperature, as it is provided by a translation of the starting one. The fluctuations at the end layers, are evident, here too. The situation suddenly changes during the last discharging hour, when there is a sharp decreasing of the air temperature, leading to the depicted trend:

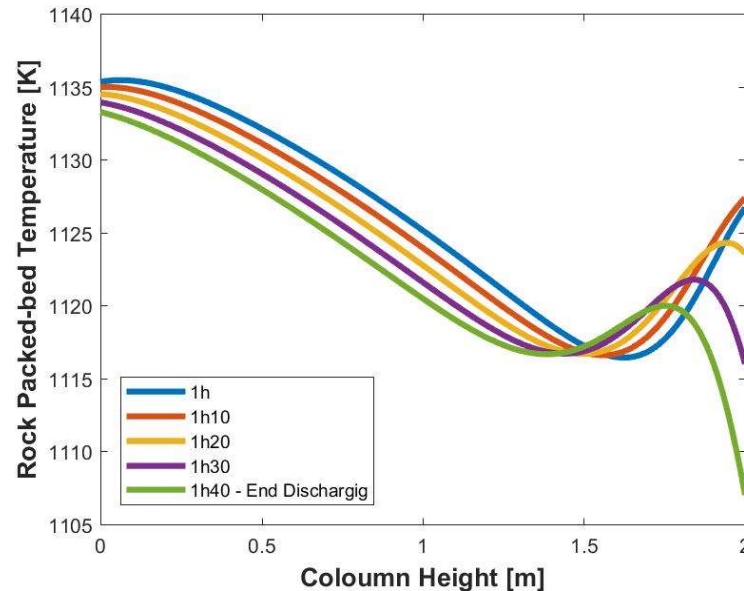


Figure 6.17: Temperature stratification in the rock packed bed during the last discharging hour

Concerning the plant efficiencies, the results are available in Figure 6.18.

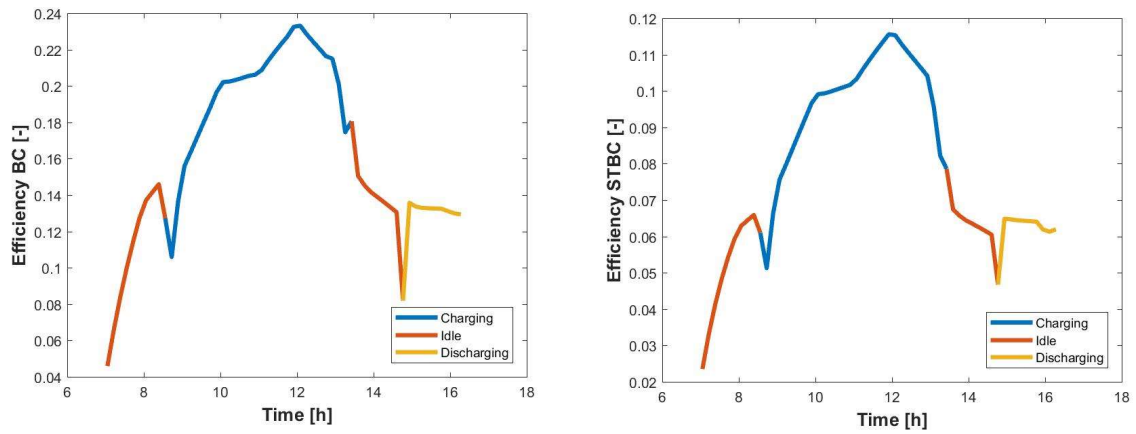


Figure 6.18: Plant efficiencies during the all working hours

These values are lower compared to previous ones, which means that the heat losses badly influence the TES performance.

The summary of all analysed phases features is in Table 6.5

Table 6.5: Summary about the various phases of the whole STBC plant daily cycle, considered the heat losses

Phase	h start	h finish	Irr [W/m <sup>2</sup> ]	Power [W]	$T_7$ [K]	$\eta_{STBC}$ [%]
1 <sup>st</sup> Design	7:00	8:30	[640÷902]	[272÷1058]	[948÷1135]	[2.3÷6.1]
Charging	8:40	13:20	[902÷1002]	[977÷996]	[1115÷1119]	[5.1÷11.5]
2 <sup>nd</sup> Design	13:30	14:40	[872÷885]	[890÷1150]	[1094÷1158]	[4.7÷7.8]
Discharging	14:50	16:30	[486÷864]	[1049÷1062]	[1120÷1143]	[6.2÷6.5]

## 7. Conclusions

---

In response to the increasing demand of worldwide society to overcome the environmental pollution issue, the Solar Thermal Brayton Cycle (STBC) plant provides a good technology for the power production, exploiting the solar energy. Among all the Concentrated Solar Power (CSP) solutions it is certainly the best performing, thanks to the higher operating temperature reachable and the greater concentration ratio as well. Particularly, the small-scale dish-mounted STBC plant (1-20 kW) with recuperator has an advantage in terms of mobility and cost, offering an off-grid electricity solution to the people of the water-scarce southern Africa, who live in small villages and isolated communities. Actually, this technology is still at demonstration stage, so that there are infinite possibilities about its functioning, which have been totally unexplored so far. This is the reason why the overall objective of this thesis was to investigate some conceptual idea about the STBC plant working methods, with some update to improve its performance. This was achieved through the development and validation of numerical tools that simulate the main physical phenomena involved. Concerning the evolution over the time of the STBC plant, the analysis has requested the definition of a control strategy in order to run the dish-Brayton system continuously and generate power efficiently during the overload period, when the irradiance exceeds the design value, without any turbine overheating. Among the all proposed, the introduction of a Thermal Energy Storage (TES) has shown the best results since it allows to keep constant the value of the turbine inlet temperature, without any waste of the surplus solar energy available: it is stored as thermic form, to be released when an irradiance lack will occur, promoting a certain plant dispatchability. So that the TES introduction in the STBC plant has been conceptually studied, for the first time in the literature. The choice about the most suitable TES configuration has been based on some design criteria which are important in terms of plant practical construction and feasibility: costs, sizing and volume. Favouring the economical aspect, the rock-packed bed solutions has been selected, thanks also to its simple manufacturing and its chemical stability at high temperature. A more detailed analysis about TES introduction in the STBC has been carried out through a numerical model, which have been built and validated on the basis of previous researches available on literature. This study has led to the investigation of the TES performance which is fed by a varying temperature inlet air flow rate. Just considering the convective heat transfer between the air and the rocks particles, there is a continuously variation of temperature stratification through the packed-bed. During the charging process, the inlet temperature slightly changes, promoting a quite regular stratification, resulted by a translation of the initial one. The situation changes during the discharging, where the rapid decreasing of that temperature causes a more unstable trend. Although TES performance are not the best one, its presence improves a lot the STBC functioning, increasing the plant working hours and promoting a quite constant power generation, which would be not possible given the variability of the irradiance. The same results have been carried out when the heat losses through the wall tank have been considered in the simulation, making the analysis more realistic since the components work at very high temperature. In this last case the energy amount of the air flow rate has to be greater to make possible the charging, since the heat losses cause an overall decreasing of packed temperature.



## 8. References

---

- [1] International Energy Agency, "World Energy Outlook - Special Report Energy and Air Pollution," *World Energy Outlook - Spec. Rep.*, p. 266, 2016.
- [2] V. Ramanathan and Y. Feng, "Air pollution, greenhouse gases and climate change: Global and regional perspectives," *Atmos. Environ.*, vol. 43, no. 1, pp. 37–50, 2009.
- [3] H. Shi and J. Chen, "How to meet the increasing demands of water , food and energy in the future ? How to meet the increasing demands of water , food and energy in the future ?," no. April, 2017.
- [4] Y. Tian and C. Y. Zhao, "A review of solar collectors and thermal energy storage in solar thermal applications," *Appl. Energy*, vol. 104, pp. 538–553, 2013.
- [5] K. M. A. Pi and S. L. S. Pm, "Heat Transfer Phenomena in Concentrating Solar Power Systems," no. November, 2016.
- [6] M. Liu *et al.*, "Review on concentrating solar power plants and new developments in high temperature thermal energy storage technologies," *Renew. Sustain. Energy Rev.*, vol. 53, pp. 1411–1432, 2016.
- [7] S. Kuravi, J. Trahan, D. Y. Goswami, M. M. Rahman, and E. K. Stefanakos, "Thermal energy storage technologies and systems for concentrating solar power plants," *Prog. Energy Combust. Sci.*, vol. 39, no. 4, pp. 285–319, 2013.
- [8] U. Pelay, L. Luo, Y. Fan, D. Stitou, and M. Rood, "Thermal energy storage systems for concentrated solar power plants," *Renew. Sustain. Energy Rev.*, vol. 79, no. May, pp. 82–100, 2017.
- [9] R. Chacartegui, L. Vigna, J. A. Becerra, and V. Verda, "Analysis of two heat storage integrations for an Organic Rankine Cycle Parabolic trough solar power plant," *Energy Convers. Manag.*, vol. 125, pp. 353–367, 2016.
- [10] S. Turrini, M. Bettonte, M. Eccher, M. Grigiante, A. Miotello, and R. S. Brusa, "An innovative small-scale prototype plant integrating a solar dish concentrator with a molten salt storage system," *Renew. Energy*, vol. 123, pp. 150–161, 2018.
- [11] W. G. Le Roux, T. Bello-Ochende, and J. P. Meyer, "Optimum performance of the small-scale open and direct solar thermal Brayton cycle at various environmental conditions and constraints," *Energy*, vol. 46, no. 1, pp. 42–50, 2012.
- [12] E. Jansen, T. Bello-Ochende, and J. P. Meyer, "Integrated solar thermal Brayton cycles with either one or two regenerative heat exchangers for maximum power output," *Energy*, vol. 86, pp. 737–748, 2015.
- [13] R. P. Merchán, M. J. Santos, A. Medina, and A. Calvo Hernández, "Thermodynamic model of a hybrid Brayton thermosolar plant," *Renew. Energy*, vol. 128, pp. 473–483, 2018.
- [14] W. G. Le Roux, T. Bello-Ochende, and J. P. Meyer, "Operating conditions of an open and direct solar thermal Brayton cycle with optimised cavity receiver and recuperator," *Energy*, vol. 36, no. 10, pp. 6027–6036, 2011.
- [15] A. M. Daabo, S. Mahmoud, R. K. Al-Dadah, and A. Ahmad, "Numerical investigation of pitch value on thermal performance of solar receiver for solar powered Brayton cycle application," *Energy*, vol. 119, pp. 523–539, 2017.
- [16] E. Abbasi-Shavazi, G. O. Hughes, and J. D. Pye, "Investigation of Heat Loss from a Solar Cavity Receiver," *Energy Procedia*, vol. 69, pp. 269–278, 2015.
- [17] W. G. Le Roux, T. Bello-Ochende, and J. P. Meyer, "The efficiency of an open-cavity tubular solar receiver for a small-scale solar thermal Brayton cycle," *Energy Convers. Manag.*, vol. 84, pp. 457–470, 2014.
- [18] W. Gabriel, "THERMODYNAMIC OPTIMISATION AND EXPERIMENTAL COLLECTOR OF A DISH-MOUNTED SMALL-SCALE SOLAR THERMAL BRAYTON CYCLE by," p. p.41, 2015.
- [19] H. Li, W. Huang, F. Huang, P. Hu, and Z. Chen, "Optical analysis and optimization of parabolic

- dish solar concentrator with a cavity receiver," *Sol. Energy*, vol. 92, no. August, pp. 288–297, 2013.
- [20] T. M. Wolff, W. G. Le Roux, and J. P. Meyer, "ANALYSIS OF A PARABOLIC DISH SOLAR COLLECTOR VIA LUNAR FLUX MAPPING."
  - [21] K. E. Dellar, W. G. Le Roux, J. P. Meyer, A. Engineering, and S. Africa, "Experimental Testing of a Small-Scale Solar Thermal Brayton Cycle Recuperator," pp. 1–8, 2018.
  - [22] J. P. Le Roux, W.G.; Bello-Ochende, T. & Meyer, "Optimisation of an Open Rectangular Cavity Receiver and Recuperator Used in a Small-Scale Solar Thermal Brayton Cycle With Thermal Losses," no. July, pp. 499–507, 2014.
  - [23] Y. A. Cengel, "Heat Transfer Apractical Approach," p. 874, 2003.
  - [24] W. G. Le Roux and J. P. Meyer, "Modeling the small-scale dish-mounted solar thermal Brayton cycle," *AIP Conf. Proc.*, vol. 1734, no. 2016, 2016.
  - [25] W. Wang, A. Malmquist, and B. Laumert, "Comparison of potential control strategies for an impinging receiver based dish-Brayton system when the solar irradiation exceeds its design value," *Energy Convers. Manag.*, vol. 169, no. March, pp. 1–12, 2018.
  - [26] R. Sioshansi and P. Denholm, "The value of concentrating solar power and thermal energy storage," *IEEE Trans. Sustain. Energy*, vol. 1, no. 3, pp. 173–183, 2010.
  - [27] L. Heller, "Literature review on heat transfer fluids and thermal energy storage systems in CSP plants," *Lit. Rev. heat Transf. fluids Therm. energy storage Syst. CSP plants*, 2013.
  - [28] M. M. Kenisarin, "High-temperature phase change materials for thermal energy storage," *Renew. Sustain. Energy Rev.*, vol. 14, no. 3, pp. 955–970, 2010.
  - [29] K. G. Allen, T. W. Von Backström, and D. G. Kröger, "Packed rock bed thermal storage in power plants: Design considerations," *Energy Procedia*, vol. 49, pp. 666–675, 2013.
  - [30] R. Anderson, L. Bates, E. Johnson, and J. F. Morris, "Packed bed thermal energy storage: A simplified experimentally validated model," *J. Energy Storage*, vol. 4, pp. 14–23, 2015.
  - [31] G. Zanganeh, A. Pedretti, S. Zavattoni, M. Barbato, and A. Steinfeld, "Packed-bed thermal storage for concentrated solar power - Pilot-scale demonstration and industrial-scale design," *Sol. Energy*, vol. 86, no. 10, pp. 3084–3098, 2012.
  - [32] A. Felix Regin, S. C. Solanki, and J. S. Saini, "An analysis of a packed bed latent heat thermal energy storage system using PCM capsules: Numerical investigation," *Renew. Energy*, vol. 34, no. 7, pp. 1765–1773, 2009.
  - [33] R. Pakrouh, M. J. Hosseini, A. A. Ranjbar, and R. Bahrampoury, "Thermodynamic analysis of a packed bed latent heat thermal storage system simulated by an effective packed bed model," *Energy*, vol. 140, pp. 861–878, 2017.
  - [34] H. Peng, H. Dong, and X. Ling, "Thermal investigation of PCM-based high temperature thermal energy storage in packed bed," *Energy Convers. Manag.*, vol. 81, pp. 420–427, 2014.
  - [35] M. Hänchen, S. Brückner, and A. Steinfeld, "High-temperature thermal storage using a packed bed of rocks - Heat transfer analysis and experimental validation," *Appl. Therm. Eng.*, vol. 31, no. 10, pp. 1798–1806, 2011.

## 9. Webography

---

- I. <https://www.epa.gov/ghgemissions/global-greenhouse-gas-emissions-data>
- II. <https://www.ecotricity.co.uk/our-green-energy/energy-independence/the-end-of-fossil-fuels>
- III. <https://www.isep.or.jp/en/statistics>
- IV. <https://www.renewableenergyworld.com/ugc/articles/2013/03/how-solar-pv-is-winning-over-csp.html>
- V. <https://solarpaces.nrel.gov/by-technology/dish-engine>
- VI. <http://www.sauran.net/ShowStation.aspx?station=148>